machines

MDPI

Review

A Review on In-Situ Monitoring in Wire Arc Additive Manufacturing: Technologies, Applications, Challenges, and Needs

Mohammad Arjomandi, Jackson Motley, Quang Ngo, Yoosuf Anees, Muhammad Ayaan Afzal and Tuhin Mukherjee *

Department of Mechanical Engineering, Iowa State University, Ames, IA 50011, USA; mohi@iastate.edu (M.A.); motley05@iastate.edu (J.M.); qngo1705@iastate.edu (Q.N.); yoosuf02@iastate.edu (Y.A.); mayaan31@iastate.edu (M.A.A.)
* Correspondence: tuhinm@iastate.edu

Abstract

Wire Arc Additive Manufacturing (WAAM), also known as Wire Arc Directed Energy Deposition, is used for fabricating large metallic components with high deposition rates. However, the process often leads to residual stress, distortion, defects, undesirable microstructure, and inconsistent bead geometry. These challenges necessitate reliable in-situ monitoring for process understanding, quality assurance, and control. While several reviews exist on in-situ monitoring in other additive manufacturing processes, systematic coverage of sensing methods specifically tailored for WAAM remains limited. This review fills that gap by providing a comprehensive analysis of existing in-situ monitoring approaches in WAAM, including thermal, optical, acoustic, electrical, force, and geometric sensing. It compares the relative maturity and applicability of each technique, highlights the challenges posed by arc light, spatter, and large melt pool dynamics, and discusses recent advances in real-time defect detection and control, process monitoring, microstructure and property prediction, and minimization of residual stress and distortion. Apart from providing a synthesis of the existing literature, the review also provides research needs, including the standardization of monitoring methodologies, the development of scalable sensing systems, integration of advanced AI-driven data analytics, coupling of real-time monitoring with multi-physics modeling, exploration of quantum sensing, and the transition of current research from laboratory demonstrations to industrial-scale WAAM implementation.

Keywords: wire arc additive manufacturing; 3D printing; wire arc deposition; welding; gas metal arc; high-speed imaging; pyrometer; infrared; acoustic; quantum sensing

Check for updates

Academic Editor: Gianni Campatelli

Received: 14 November 2025
Revised: 12 December 2025
Accepted: 18 December 2025
Published: 22 December 2025

Copyright: © 2025 by the authors. Licensee MDPI, Basel, Switzerland. This article is an open access article distributed under the terms and conditions of the Creative Commons Attribution (CC BY) license.

1. Introduction

Wire Arc Additive Manufacturing (WAAM) or Wire Arc Directed Energy Deposition (WA-DED) is an additive manufacturing process that uses an electric arc as the heat source and a metal wire as the feedstock to build near-net-shape metallic components layer by layer [1–4]. WAAM offers high deposition rates, cost-effective material utilization, and scalability for large structures [5–11]. Because of its high productivity and compatibility with various metals such as titanium, aluminum, steel, and nickel alloys, WAAM has gained significant attention in the aerospace, marine, and energy sectors [12–33]. However, the process is characterized by complex thermal and fluid dynamics, resulting in residual

stresses, porosity, uneven bead geometry, and distortion. These issues can degrade mechanical performance and limit industrial adoption. Therefore, in-situ monitoring plays a crucial role in understanding and controlling the process. Real-time sensing enables the detection of thermal anomalies, geometric deviations, and defect formation during deposition, allowing the users to control them [34]. The integration of monitoring systems into WAAM is thus essential for achieving high-quality components for various manufacturing applications.

Compared to other metal additive manufacturing processes, such as laser powder bed fusion (LPBF) and laser-directed energy deposition (LDED), in-situ monitoring in WAAM is growing faster [35,36]. A quantitative assessment of the literature based on the Web of Science database (as illustrated in Figure 1) shows a significant disparity in research. LPBF dominates the field, particularly in the use of infrared cameras, high-speed imaging, and acoustic emission monitoring, each with several hundred studies. LDED also exhibits strong research coverage. Because of these reasons, several review papers exist on in-situ monitoring in LPBF [37–41] and LDED [42–45]. In contrast, the number of studies focused on in-situ monitoring in WAAM is currently lower across almost all sensing modalities. This discrepancy arises from the unique challenges it poses, including the large melt pool size, spatter, arc light interference, safety concerns with the electric arc, and dynamic bead surface. These factors complicate sensor calibration and data interpretation. The limited but growing literature [46–50] on in-situ monitoring in WAAM highlights the need for a dedicated review that consolidates existing research, compares sensing strategies, identifies current challenges, and provides future research directions for reliable process monitoring.

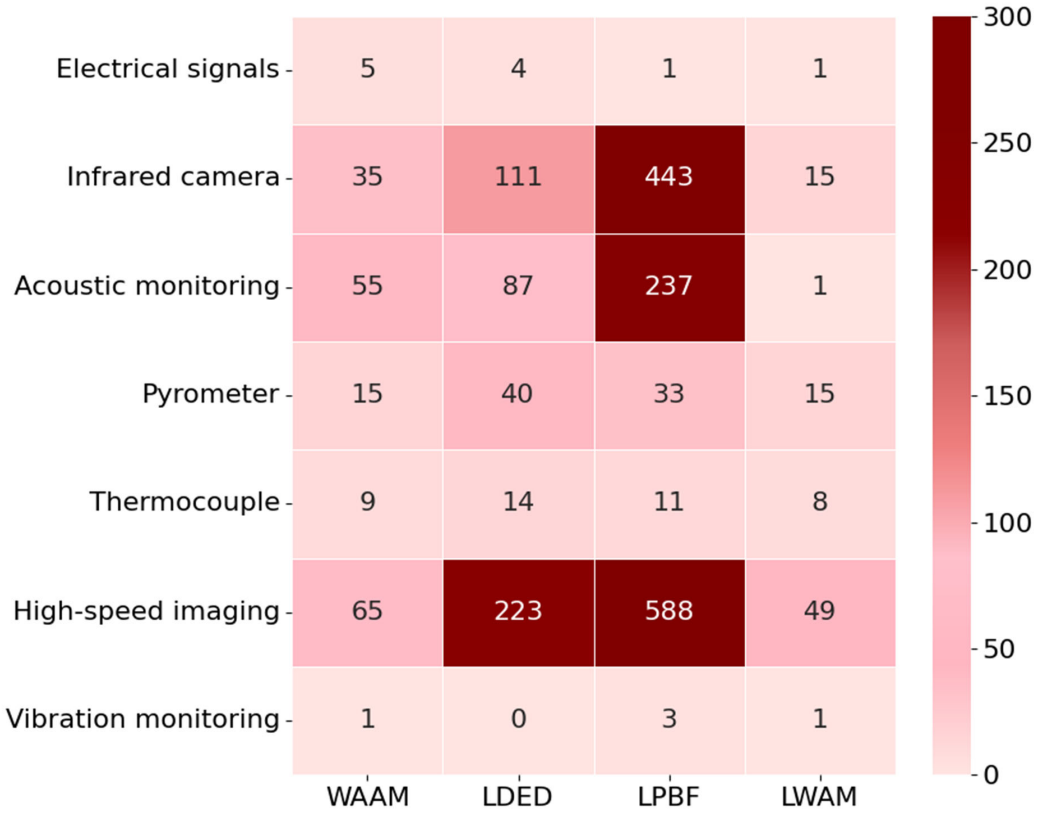


Figure 1. Literature data analysis using a heatmap based on Web of Science all database search on 3 November 2025. The heatmap includes data on the number of papers on various in-situ monitoring methods for wire arc additive manufacturing (WAAM), laser directed energy deposition (LDED), laser powder bed fusion (LPBF), and laser wire additive manufacturing (LWAM). This heatmap shows that, compared to LDED and LPBF additive manufacturing, literature on in-situ monitoring of WAAM is growing, which justifies the need for this review paper.

In-situ monitoring in WAAM can be broadly classified into several categories (Figure 2) based on the sensing principle and measurement objective [51]. Thermal monitoring methods, such as infrared cameras, pyrometers, and thermocouples, capture temperature distribution. Geometric and surface monitoring using optical systems enables real-time tracking of bead height, width, and layer uniformity. Acoustic and vibration-based sensors record transient mechanical signals associated with arc stability, droplet transfer, and defect formation. Electrical signal monitoring, including voltage and current analysis, offers valuable process signatures that reflect variations in arc energy and material transfer dynamics.

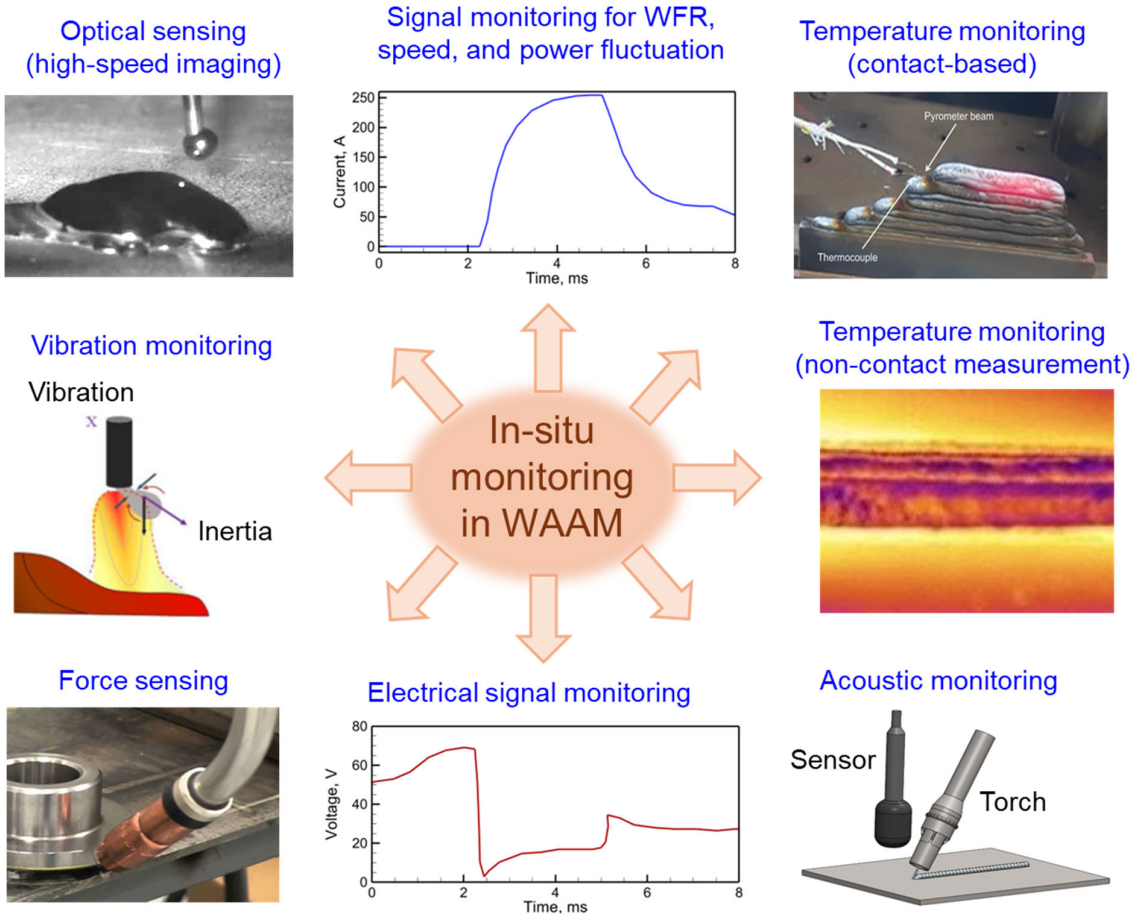


Figure 2. Various in-situ monitoring systems in WAAM. Sub-figures are taken from [52–55].

This review provides a comprehensive synthesis of the current state of in-situ monitoring in WAAM, emphasizing both sensing technologies and their practical applications. The review first introduces the principles and measurement capabilities of various monitoring methods used in WAAM, followed by detailed discussions on their implementation, data analysis strategies, and correlation with process characteristics such as temperature field, geometry, and defect formation. Challenges associated with sensor robustness, signal interference, and real-time integration are analyzed to highlight limitations that impede industrial deployment. The review also identifies emerging trends, including machine learning-assisted monitoring, sensor fusion, and closed-loop feedback systems that are driving the development of self-adaptive WAAM. Unlike previous reviews on LPBF [37–41] and LDED [42–45] monitoring, this work uniquely addresses WAAM's distinct monitoring requirements, where high heat input, arc-based energy deposition, and wire feeding dynamics create fundamentally different challenges compared to the other AM processes.

In addition, unlike existing reviews on laser-based systems, this work comprehensively examines monitoring techniques tailored to arc-based phenomena, including acoustic metal transfer signatures, electrical arc stability analysis, and thermal management for WAAM's characteristically larger melt pools. By organizing existing knowledge and outlining key research needs, this review aims to provide a foundation for future development of reliable, intelligent, and autonomous WAAM systems.

2. Overview of In-Situ Monitoring in WAAM

WAAM is susceptible to various defects, including porosity, lack of fusion, distortion, and inconsistent bead geometry, that can compromise the structural integrity and mechanical properties of fabricated components [56]. These defects arise from the complex interplay of process parameters such as heat input, travel speed, and shielding gas flow, which create highly dynamic thermal conditions during deposition. In-situ monitoring is essential because it enables real-time detection and correction of defects as they form, allowing for immediate parameter adjustments that prevent defect propagation and reduce costly post-process repairs or part rejection. Early diagnosis and mitigation of process-induced defects are possible through the continuous recording of data and the real-time analysis of signals [57]. This section begins with the goals of real-time monitoring, then summarizes various monitoring sensors used in online inspection in WAAM. Finally, a brief description of employing different strategies for online data collection in wire arc deposition is provided.

2.1. Goals of In-Situ Monitoring

Various sensors utilized in WAAM to enable the accurate and reliable detection of process features are summarized in Table 1. Optical and vision-based monitoring uses high-speed cameras, CCD (Charge-Coupled Device), CMOS (Complementary Metal-Oxide-Semiconductor), and spectrometers to capture melt pool geometry and arc stability, detecting defects like humping and bead irregularities through image processing. Acoustic and sound-based monitoring analyzes sound emissions during WAAM, where acoustic signature variations indicate arc instability, spatter, and porosity in a non-intrusive manner. Electrical signal monitoring tracks current and voltage waveforms to characterize arc behavior, with deviations signaling issues like short circuits or inconsistent wire feed. Thermal and temperature monitoring employs infrared cameras and pyrometers to measure temperature distributions and cooling rates, controlling thermal gradients and preventing hot cracking and distortion. Force and vibration monitoring uses accelerometers and load cells to detect mechanical disturbances, revealing wire feeding irregularities, tip wear, and issues affecting dimensional accuracy.

Controlling the dynamic behavior of the molten pool has a direct impact on improving the quality of the deposited bead during deposition [58]. Integrating advanced sensors into the WAAM system enhances arc stability and ensures process reliability during deposition [59–62]. To reduce deposition deviation in WAAM, a real-time inspection system is required to act as an adaptive feedback unit, adjusting process parameters based on in-situ measurements of signal changes [63]. In addition to process parameters, dwell time has a strong impact on geometrical accuracy [64]. Insufficient cooling time between layers increases the temperature gradient, causing part distortion [64]. Moreover, the build-up strategy is another crucial step in fabricating complex structures [65]. By using tool path planning with the COBOT-assisted WAAM system, continuous deposition minimizes arc instabilities, thereby reducing residual stresses [66]. Although real-time monitoring allows for the detection of process-induced defects, the high brightness of the arc and the increased temperature environment in WAAM introduce significant sensing errors [67]. Filtering melt

pool signals without losing important data is a significant challenge, as it is a crucial step in capturing precise data on melt pool behavior [61,68]. The upcoming section provides a brief explanation of the various sensing techniques for real-time monitoring of WAAM.

Table 1. Selected examples of various real-time monitoring methods in WAAM.

Various in-Situ Monitoring	Equipment	Measurable Parameters	Measurement Approach	Ref.
Optical and vision-based monitoring	IR camera	Thermal (infrared) intensity	The infrared camera detects radiative energy from the molten pool and its surrounding area to generate thermal intensity maps, which show temperature variations during the WAAM process.	[69]
	CMOS sensor	Nozzle-to-work distance	They measure the nozzle to work distance indirectly by measuring the wire that sticks out through semantic segmentation, and add it to a hidden length of wire in the nozzle	[58]
	CCD camera	Melt-pool contact angles and arc radius	Processing of the captured images of the melt pool to extract its boundary profile. The melt pool edge is then fitted with tangent lines at specific points using a geometric fitting algorithm	[70]
	CMOS sensor	Molten pool region	A CMOS sensor captures the optical emission from the molten pool. It detects molten pool signals by using pixel-intensity tracking. The captured image sequence is analyzed over time to determine how quickly droplets change and how stable the arc remains.	[55]
	CMOS sensor	Light intensity distribution from the melt pool	Droplet size and detachment frequency are extracted through image-processing techniques applied to the light-intensity distribution captured in successive frames.	[71]
Acoustic and sound-based monitoring	Acoustic sensor	Acoustic pressure signal emitted by the arc	The sound signal goes through FFT analysis to obtain frequency-domain features that include dominant frequency and spectral power, and bandwidth measurements, which link to metal transfer stability and weld quality.	[72]
	Shure SM57 dynamic microphone	Acoustic pressure fluctuation emitted by the welding arc	The microphone converts sound pressure waves into electrical signals, which become digital data for stability feature and defect indicator analysis through wavelet coefficients.	[73]
	Microphone	Sound waveform	The microphone records the acoustic pressure waveform from the welding arc. The kurtosis value of this sound signal, which stems from the time-domain waveform, helps evaluate arc stability and forecast metal deposition performance.	[74]
Electrical signal monitoring	Current/voltage signal acquisition system	Welding current and arc voltage	The recorded electrical signals received wavelet denoising and time-domain analysis to extract average, RMS, and peak values. Variation in recorded signals affects the molten pool droplet behavior and arc stability.	[75]
	Lincoln Power Wave software 2025	Welding current and voltage	Arc stability and droplet transfer behavior can be deduced by analyzing current and voltage in short-circuit and pulsed transfer operations	[55]
Thermal and temperature monitoring	Passive infrared thermography camera	Infrared radiance map	The measurement process is performed with online thermograph acquisition, then image analysis helps to detect thermal irregularities (hotspots and non-uniform cooling patterns), which indicate weld defects.	[76]
	Thermocouple and IR pyrometer	Inter-layer temperature	Two measurement approaches, the Upper Pyrometer and Sideward Pyrometer measurement techniques, are used through sensor placement at set arc distances, followed by emissivity calibration, to determine their effectiveness for temperature control between layers.	[52]
Force and vibration monitoring	Force Torque sensor	Contact force	A force sensor monitors the contact force between the dry-coupled ultrasonic roller probe and the WAAM surface. The robotic controller performs Z-axis adjustments to the probe in real time for stable contact pressure maintenance, which allows reliable in-process ultrasonic data acquisition during layer-by-layer inspection.	[62]
	Vibration sensor/acceleration sensor	Acceleration amplitude/frequency	By measuring the acceleration amplitude/frequency, and combining with imaging of the arc, the arc morphology, and droplet transition behavior can be analyzed.	[54]

2.2. Types of Signals and Parameters Measurable in WAAM

Various sensing modalities have been developed to monitor the complex physical phenomena occurring during WAAM, each capturing different aspects of the process dynamics. These monitoring signals range from optical emissions and acoustic signatures to electrical parameters, thermal profiles, and mechanical vibrations, providing complementary information about process stability and part quality. The integration of multiple signal types enables comprehensive process characterization, facilitating early defect detection and closed-loop control strategies for improved manufacturing reliability. In addition, real-time monitoring of the deposition formation leads to better dimensional accuracy, which can be controlled by optical monitoring. However, spatter generation by molten pool instability during the arc deposition process can distort optical signals and may reduce the accuracy of the reported data [77,78]. Another method is to use an acoustic emission sensor during the deposition process, which provides a better understanding of the melt pool behavior and the internal material properties of the deposited beads. Arc-sound monitoring is sensitive to arc instability, but it cannot reliably identify or localize all defect types [73]. Thermography, like an IR camera, can provide non-contact temperature measurements; however, the measurement accuracy is influenced by the surface condition [79]. Electrical signal monitoring is a technique used to understand arc fluctuations and droplet transfer through changes in current and voltage [75]. In addition to electrical sensing, a force and vibration sensor can measure dynamic mechanical responses. Various sensing approaches for in-situ monitoring in WAAM are categorized based on their interaction with the process, which is discussed in the subsequent section.

2.3. Monitoring Strategies: Direct vs. Indirect, Intrusive vs. Non-Intrusive

Various monitoring methods are used in WAAM; some of them measure the variable directly, like strain gauges. Piezoresistive thin-film gauges measure strain through resistance changes, which produce measurable voltage signals for affordable in-situ strain monitoring of small-scale objects [80]. However, the operating conditions in WAAM make conventional piezoelectric sensors unsuitable [81]. Elevated temperatures can cause element depolarization and bonding deterioration, while intense electromagnetic interference from the arc requires specialized shielding and isolation to protect the signal-conditioning electronics [81]. The protection thickness can vary, depending on the deposition conditions [81]. This method of signal monitoring is intrusive and can be embedded in the fabrication part. Some intrusive in-situ monitoring systems are easy to install and offer accurate measurements in the specific location. However, as they need to be installed on the substrate surface, such as thermocouples, they may not display the data immediately and may interfere with the WAAM process, as shown in Figure 3. Moreover, temperature acquisition in WAAM is prone to uncertainty because electromagnetic emission and radiant heat from the arc and molten pool can contaminate the sensor reading [52]. Contactless and non-intrusive real-time monitoring systems rely on indirect signal measurement, which is preferred because they are less constrained by the substrate geometry [52]. However, as they achieve their data through monitoring the surface, some defects, such as oxidation and contamination, can cause data acquisition errors [82]. Moreover, for non-contact thermal measurements, such as those obtained using a pyrometer in Figure 3, a sharp fluctuation in arc brightness can introduce significant measurement error [52]. Therefore, the choice of in-situ monitoring strategy depends on the respective advantages and limitations of each method. The subsequent sections provide a detailed review of those monitoring strategies.

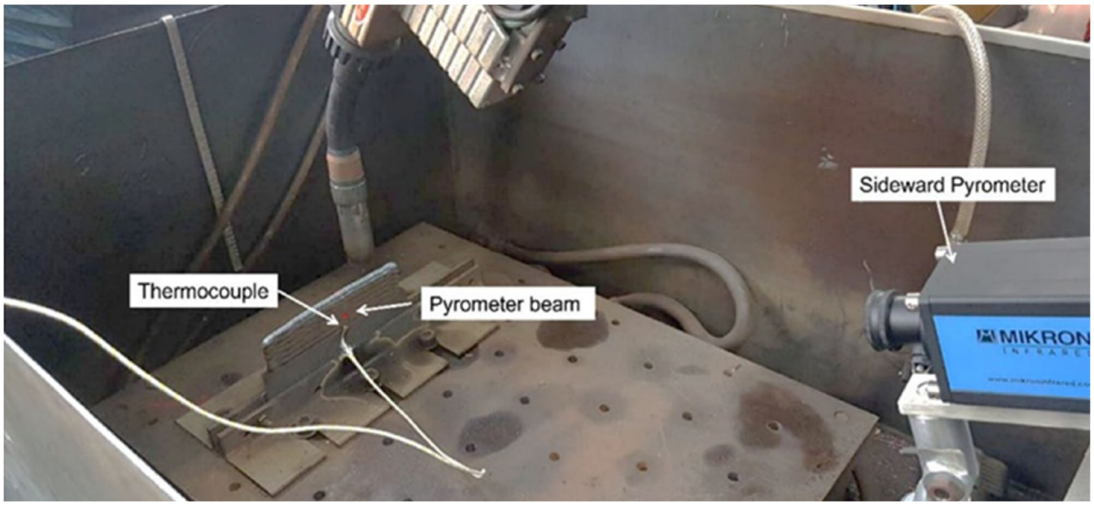


Figure 3. Location of thermocouple and sideward pyrometer for interlayer temperature measurement in the multilayer deposition process in WAAM [52].

3. Optical and Vision-Based Monitoring

The quality of WAAM parts depends on the behavior of the molten pool, and vision-based sensing offers the most direct means of capturing its dynamics [83]. High-speed cameras capture rapid events during WAAM at frame rates exceeding 1000 fps, enabling visualization of droplet transfer and melt pool behavior invisible to conventional imaging. CCD (Charge-Coupled Device) and CMOS (Complementary Metal-Oxide-Semiconductor) systems are solid-state sensors converting optical signals to electrical data, with CMOS offering faster readout and lower power consumption while CCD provides superior low-light image quality. Infrared imaging measures temperature distributions and thermal gradients across deposited material without physical contact. In this section, these monitoring methods are reviewed. Additionally, methods for extracting the molten-pool geometry, bead shape, and surface condition from these images are presented.

3.1. High-Speed Cameras, CCD/CMOS Systems

The process reliability of WAAM improves through vision-based monitoring, which minimizes the total amount of accumulated deviations that occur during each layer of deposition [84–87]. The optical monitoring system operates in two real-time stages. In the first stage, an optical system captures the dynamic behavior of the melt pool to characterize the evolution of the bead geometry and surface topography [88]. In the second stage, the recorded data are analyzed using image processing techniques to extract quantitative information about the melt pool and deposition quality [88]. Processing the image begins with acquiring data from the designated area, followed by analyzing the image by differentiating it from nearby objects [89,90]. Through image segmentation, image clarity increases, and by removing noise from the area of interest, the required feature becomes clearer than the surrounding region [91,92]. Figure 4 illustrates the use of a CCD camera as a vision-based monitoring method [70]. Using the force balance estimation method can predict pool stability from measuring contact angles and analyzing the geometry of the molten pool through using deep learning algorithms in fabricating a suspended rod, shown in Figure 4 [70,89,93]. Transferring the acquired data to the controller enables real-time optimization of process parameters, which reduces molten metal sagging and improves the structural integrity of the near-suspended geometry [70]. Therefore, the process requires constant observation of the melt pool behavior to prevent rod collapse, which can result in damaged structures [70]. If the droplet detachment force is excluded from force-balance

equations, the method becomes less accurate under dynamic metal transfer conditions, particularly when measuring the transient effects of droplet impact and arc fluctuation.

A vision-based monitoring system tracks pool variation through calibrated machine vision to adjust process parameters in real-time [94]. Both CCD and CMOS sensors have been used for WAAM vision monitoring [95]. For high-speed imaging of metal transfer and melt-pool dynamics, CMOS is preferred due to its reading speed and higher frame-rate capability [95]. A COBOT integrated WAAM with Cavitar C300 as a high-speed camera used to monitor for droplet transfer in real time [55]. In this approach, different metal transfer modes were employed to consider the effect of gravity on deposition quality [55]. By using short-circuit mode in the deposition direction against gravity, as shown in Figure 5 [55], capturing the droplet transition provides a better understanding of the deposition process. Figure 5a shows the onset of the molten droplet formation. Then, the Electromagnetic pinch transfers the droplet from the wire tip into the weld pool, as shown in Figure 5b. However, due to the gravitational effect, the droplet enters the pool with a deviation from its intended path, which affects the final deposition shape, as shown in Figure 5c. Delay in droplet detachment and arc instability result in droplet enlargement, as shown in Figure 5d. Gravity enhances droplet sagging when the substrate is held vertically (at a 90-degree angle to the horizon), which promotes insufficient fusion. Finally, the melt pool flows downward, as shown in Figure 5e. Since there is no supporting bead for the first part of the deposition, the bulge is shaped [55]. The lack of stability during the process leads to disrupting the deposition consistency. By tracking those changes during arc deposition in real-time, process parameter adjustments based on vision-based monitoring provide a better quality in WAAM [55]. Optical-based monitoring utilizes visible light to detect process-induced defects, whereas accurate temperature distribution measurement relies on infrared radiation, which is mentioned in the next section.

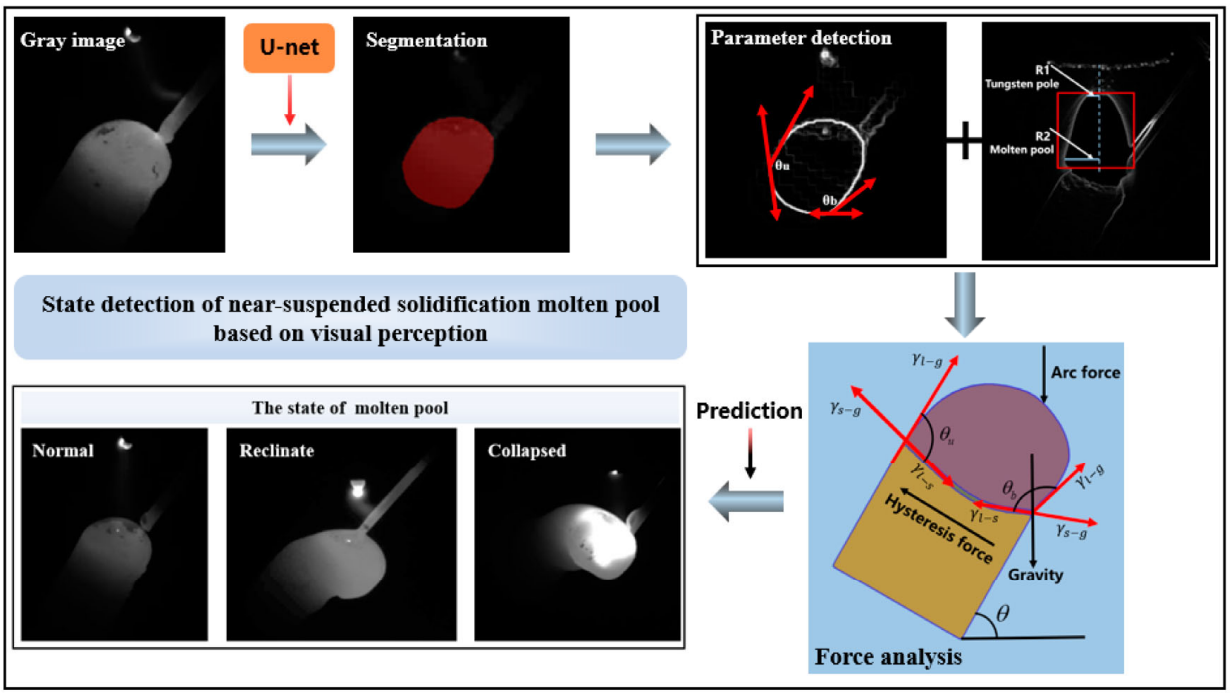


Figure 4. An example of the application of a CCD (Charge-Coupled Device) camera as a vision-based monitoring system in fabricating nearly suspended geometry using WAAM. Vision-based, deep-learning segmentation of the melt pool on high-speed camera frames to estimate melt-pool force balance and predict collapsing states in the unsupported rod [70].

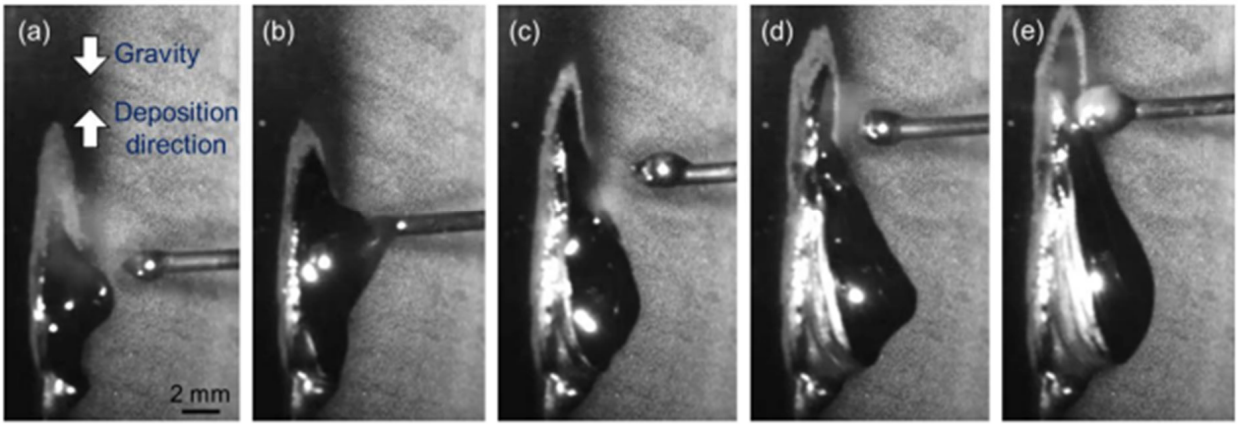


Figure 5. The use of high-speed imaging of deposition on a vertical plate against gravity by using the short-circuit transfer mode during bottom-to-top deposition. (**a**) It begins with a droplet forming at the tip of the wire; (**b**) gravity pulls it downward, causing it to goes off its intended deposition path; (**c**) the size of droplet increased as a result of delayed detachment and arc instability; (**d**) downward force prevents proper fusion and causes sagging; and finally, (**e**) droplet detaches, resulting in bulging at the lower region of the bead and reducing the deposition uniformity. This figure is owned by the authors.

3.2. Infrared Cameras

An infrared (IR) camera system enables the visualization and detection of thermal fluctuations and bead irregularities during the welding process. These anomalies cause inconsistent deposition in the WAAM system [96]. Some inconsistencies occur in the deposited bead during arc initiation and extinction, which can be detected through an IR system. Figure 6 [97] illustrates an experimental setup that comprises a camera for monitoring the molten pool behavior and an IR system for capturing the spatial temperature variation during deposition. This in-situ monitoring technique provides a clear image of the molten pool geometry, which is less affected by the arc brightness during the process [98]. Therefore, integrating an IR camera for online inspection provides real-time feedback on process conditions, allowing for parameter adjustments, which in turn provides a better understanding of process stability [98]. During WAAM, the emitted infrared radiation from the molten pool is recorded as raw pixel intensities in the thermal image [98]. By applying an emissivity value, the thermographic system converts these pixel intensities into a temperature field. However, obtaining accurate temperature data during deposition is highly related to the accuracy of the emissivity used, which makes emissivity calibration a critical source of uncertainty in IR-based temperature measurements [99]. Wire stick-out, defined as the distance between the contact tip and the arc, influences arc stability and the resulting bead quality [100]. In addition, the deposited track width reflects deposition consistency and can be adjusted through sensor-based feedback control [100]. Therefore, identifying the arc flame to measure the wire stick-out length is plausible by using a fast object detection deep learning algorithm [100], which is used for RGB images. The application range of infrared-based welding defect detection can be expanded through the integration of 3D imaging techniques that complement those employed with RGB cameras [100]. Optical imaging and infrared cameras, which are reviewed in the last two sections, can provide insight into monitoring molten pool geometry, bead shape, and surface morphology, as discussed in the following section.

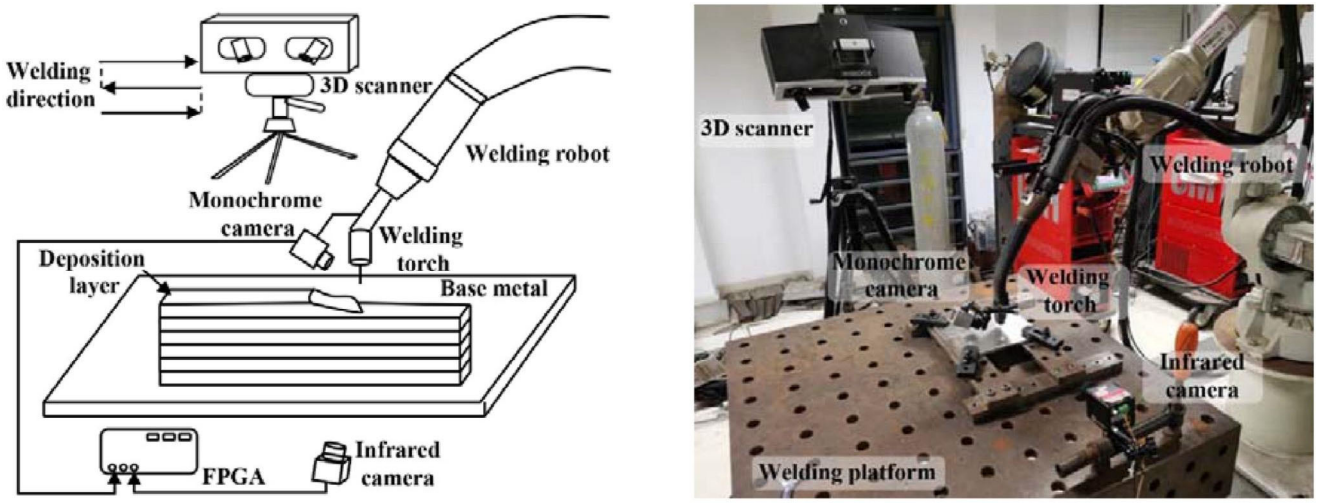


Figure 6. Experimental setup for in-situ monitoring in WAAM with the help of a robotic system: (**a**) schematic and (**b**) welding system [97].

3.3. Molten Pool Geometry, Bead Shape, and Surface Condition Monitoring

Maintaining arc stability during the WAAM process results in less spatter, smoother droplet transfer, improved bead formation, and high-quality deposition [101]. However, reaching that target requires understanding the arc morphology and its relation to process parameters to mitigate defect formation [101]. Real-time monitoring of crucial process parameters, combined with feedback adjustment, ensures that an acceptable forming quality is maintained during WAAM [102,103]. High-speed in-process imaging during deposition against gravity offers the possibility of tracking the behavior of the molten pool across different substrate angles [55]. As shown in Figure 7 [55], pulse transfer mode provides more consistent beads by increasing droplet transfer velocity and reducing heat input, thereby mitigating gravity-induced arc destabilization [55]. Figure 7a shows droplet formation at the wire tip [55]. In Figure 7b, the current peak drives a decisive electromagnetic pinch-off [55]. In Figure 7c detached droplet enters the pool with little gravitational deflection, and in Figure 7d, it fused smoothly into the weld pool [55].

A structured-light laser and a high-speed camera were integrated to capture molten pool and bead formation in the active visual sensing framework for WAAM based on CMT [104]. To separate the useful regions representing the laser stripes and the molten pool from the background noise caused by arc-light interference, the obtained pictures underwent pre-processing using range of interest (ROI) segmentation and filtering [104]. Direct assessment of pool geometry during deposition was made possible by measuring the molten pool width and height by tracking the pool boundary and wire location. As the wall height in multilayer deposition is increased layer by layer, the sensing system records changes in the shape of the beads and surface morphology [104].

Optical and vision-based monitoring has emerged as the most widely adopted in-situ sensing approach in WAAM due to its ability to provide rich, non-contact information about critical process features, including melt pool dynamics, bead geometry evolution, and surface quality characteristics. The complementary nature of visible-spectrum imaging (capturing arc behavior, droplet transfer, and geometric features in Section 3.1) and infrared thermography (revealing thermal distributions in Section 3.2) enables comprehensive process characterization that correlates directly with final part quality, making multi-modal optical systems particularly effective for defect prediction and control. The external quality of deposition is accessed through vision-based monitoring, whereas acoustic sensing

provides insight into the underlying process dynamics of WAAM, which are described in the next section.

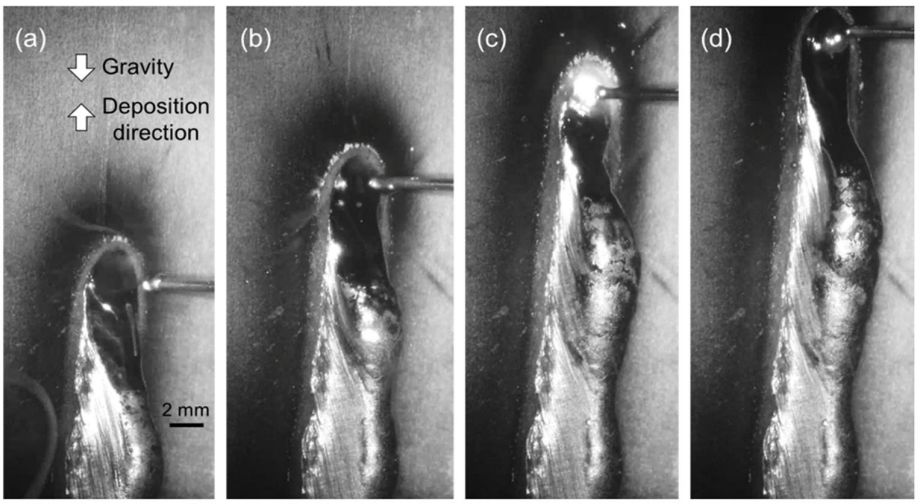


Figure 7. High-speed imaging of deposition against gravity: (**a**) droplet formation at the wire tip during the base current, (**b**) pulse peak induces electromagnetic pinch and detachment, (**c**) detached droplet enters the molten pool under pulse force, and (**d**) the droplet impinges and fuses. This figure is owned by the authors.

4. Acoustic and Sound-Based Monitoring

Acoustic and sound-based monitoring are common non-destructive inspection methods used to detect geometric inconsistencies in large and complex parts fabricated by WAAM [73]. Fumes, bright arcs, and oxidation are environmental conditions in WAAM that may make vision-based online defect detection less reliable [82]. Acoustic and sound-based monitoring is an effective technique for controlling deposition consistency in real-time, thereby optimizing the chosen process parameters [105]. Acoustic emission sensors detect high-frequency stress waves generated by microstructural changes, crack formation, and material deformation during WAAM, providing early warning of defects at frequencies typically ranging from 100 kHz to several MHz. Arc sound monitoring captures audible acoustic signals produced by arc plasma oscillations and metal transfer, where variations in sound frequency and amplitude correlate with process stability, shielding gas effectiveness, and defect formation. These sensors are reviewed here.

4.1. Acoustic Emission Sensors

The process of real-time acoustic monitoring for arc deposition consists of three stages, which include background noise suppression from raw signals, extraction of stability indicators from processed acoustic data, and real-time WAAM monitoring through online indicator tracking [73]. Figure 8 [73] shows the WAAM system with a Shure SM57, a dynamic cardioid microphone serving as the acoustic sensor, which is installed on the welding torch to maintain a consistent distance from the arc. Three thin walls, each with a different contaminant (chalk, oil, and sand) considered to create arc instability in the same way as the practical WAAM situation, which is prone to penetration of contaminants [106]. Those contaminations are created in the specific location by drilling a hole, as shown in Figure 9 [73]. Based on Figure 9(a1), the chalk powder makes the arc unstable by disrupting the argon gas, which results in inconsistent deposition with thickness changes along the track, as shown in Figure 9(a3) [73]. Through the raw acoustic signal, the chalk contamination is clearly visible, as indicated by the green section in Figure 9(a2) [73]. However, detecting a pore at the end of the track in the raw acoustic signal is not possible [73]. In Figure 9(b1), since the

boiling point of the used oil is less than the molten pool temperature, the contamination not only disrupts the shielding gas but also creates large pores, as shown in Figure 9(b3). As shown in Figure 9(b2), the background noise makes it hard to separate arc instability and defect formation from the rest of the raw acoustic signals. In Figure 9(c1), the higher density of sand in comparison to other contaminants does not disturb the shielding gas and the arc stability, as the hole is not big enough to prevent the arc from moving. Based on Figure 9(c2,c3), the individual perception of the acoustic signal and the track shows fewer flaws compared to the previous contaminations. The method cannot identify the specific defect; it only flags that the arc behavior is abnormal [73]. The monitoring system of arc sound detects airborne signals produced in the arc area, providing better sensitivity to process disturbances that affect arc behavior through metal transfer and changes in arc stability, and thus better reveals shielding-gas-related irregularities, which are described in the next section.

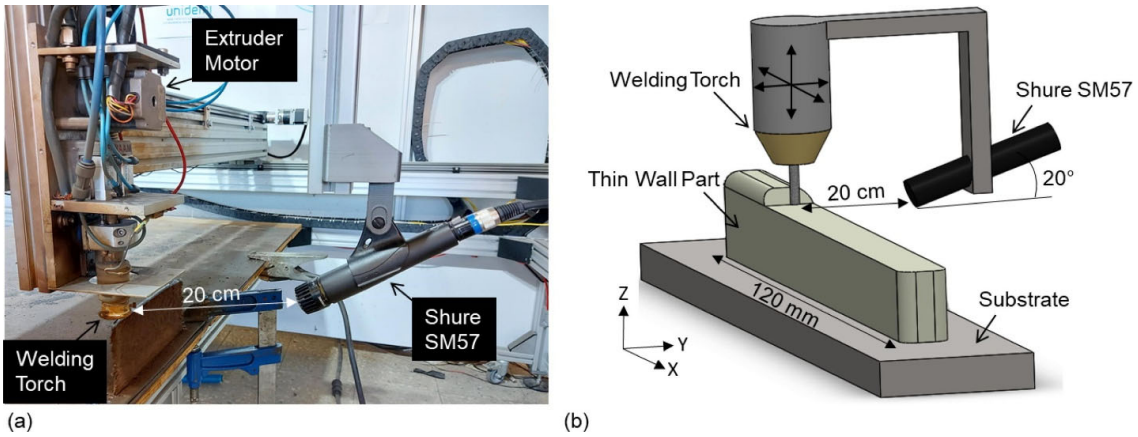


Figure 8. (**a**) WAAM system with Shure SM57 as an acoustic sensor; (**b**) schematic of the experimental setup with specifying the exact location of the sensor [73].

4.2. Arc Sound Monitoring for Defect Detection

Although industrial background noise can impede the accurate analysis of welding acoustics, effective noise suppression enables acoustic monitoring to outperform many in situ techniques for detecting process instabilities [107]. The raw welding sound enables researchers to extract two essential metrics, including root mean square (RMS) for metal transfer intensity measurement and kurtosis for evaluating the sharpness of the arc sound signal [72]. Under constant-voltage conditions, the quantity of spatter and the dynamics of metal transfer are the principal variables that correlate with arc acoustic pressure [108]. As the welding speed increases and the arc power decreases, the sound pressure of the arc decreases [108]. By considering the changes in process parameters on the arc sound, a clear understanding of the relationship between defect formation and arc sound can be achieved. When more material is deposited due to increased wire feed rate, the RMS values of the arc sound also increase. However, at the very low feed rate, the RMS is higher, which might be caused by increased spatter during deposition [72].

Acoustic monitoring offers a cost-effective and non-intrusive alternative to optical methods (Section 4.1), with the unique capability to detect subsurface defects such as porosity, cracking, and lack of fusion that are invisible to camera-based systems through high-frequency acoustic emission analysis. Arc sound monitoring (Section 4.2) in the audible frequency range provides real-time feedback on process stability and shielding gas effectiveness, where characteristic sound signatures correlate strongly with metal transfer modes and arc disturbances, enabling rapid defect detection without the line-of-sight limitations or calibration complexities associated with vision-based approaches. The

behavior of the arc can be monitored by analyzing its sound; however, several monitoring methods exist to obtain the features of the arc by monitoring the electrical signal, such as current and voltage, which is described in the next section.

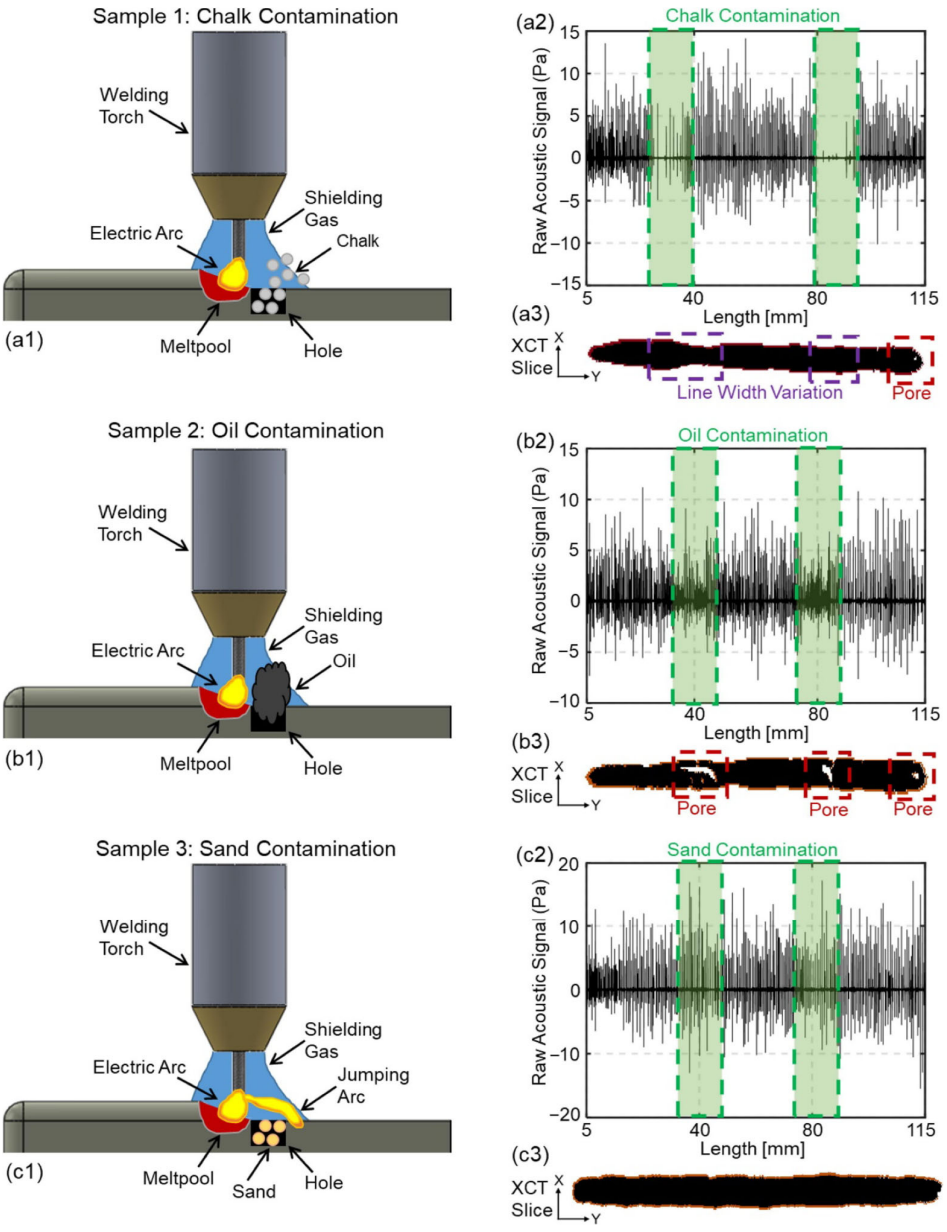


Figure 9. Schematic of the location of the defect in regard to the welding torch: (**a1**) introduction of chalk contamination, and (**a2**) its signature in the raw acoustic trace. (**a3**) Corresponding track-width variations aligned to the contamination site. (**b1**) Introduction of oil contamination. (**b2**) Raw acoustic signal at the same defect location. (**b3**) Track-width changes mapped to the oil-contaminated region. (**c1**) Sand contamination. (**c2**) Raw acoustic signal shows no obvious change. (**c3**) Defects are not visually discernible in the track for this case [73].

5. Electrical Signal Monitoring

Another real-time inspection technique in WAAM is tracking electrical signals by monitoring current and voltage [75]. Arc voltage and current sensing monitors real-time electrical parameters to characterize energy input and arc stability, with deviations indicating short circuits, arc length variations, or heat input inconsistencies. Wire feed rate and travel speed monitoring tracks material deposition rates and torch movement to ensure

consistent bead geometry, while power fluctuation detection identifies instabilities in the power source that can cause defects like lack of fusion or excessive penetration.

5.1. Arc Voltage and Current Sensing

The monitoring of key WAAM parameters through continuous observation of current and voltage facilitates the determination of defects during fabrication [103]. By providing real-time adjustments during the deposition process, parts with minimal variability and improved forming quality will be produced [102]. The WAAM system, as shown in Figure 10, consisted of a Trans Plus Synergic 4000 CMT (manufactured by Fronius, Pettenbach, Austria) power source, which operated with a KUKA KR10R 1420 C4 robot (produced by KUKA company, a manufacturer of industrial robots, headquarters is in Augsburg, Germany), a VR1500 4R/F++ROBOTER as a wire feeder, a current and voltage acquisition unit, and an AcutEye high-speed camera(developed by Hunan Kotianjian Optoelectronics Technology Co., Ltd. (Changsha, China) [75]. The electrical monitoring system consisted of three main components: a current–voltage acquisition unit, a signal processing module, and a computer [75]. The acquisition unit maintained a connection to the CMT power source, allowing for the monitoring of waveforms as they occurred in real-time. The monitoring system tracks two signals that measure current and voltage. The periodic changes in arc length and circuit resistance, caused by droplet transfer and arc formation, result in corresponding variations in current and voltage. Electrical signal behavior enables the detection of arc interruption and extinction, facilitating the evaluation of arc stability [75]. The relationship between current/voltage signals and droplet transfer is shown in Figure 11 [75]. Figure 11a shows that when a short-circuit transfer happens, the current becomes less than 60 A and the voltage decreases to 0.5–0.8 V, while the wire feed direction reverses and both signals decrease to zero [75]. In Figure 11b, the current and voltage rise again as the arc re-ignites [75]. As shown in Figure 11c,d, the signals remain almost constant for roughly 40 ms during the peak-current stage as the droplet grows and its neck contracts under electromagnetic force [75]. Finally, in Figure 11e, both current and voltage slightly decrease as the wire feeds downward and the arc narrows, until contact with the molten pool triggers another short-circuit transfer (Figure 11f).

Analyzing a single cycle of the metal transfer process allows for a clearer identification of the correlation between waveform variation and molten pool behavior. Figure 12a–f [55] shows synchronized electrical waveform and high-speed imaging of the molten pool for deposition on the vertical substrate in pulsed WA-DED. The current and voltage traces in Figure 12a,b span a single transfer cycle. As the cycle begins, a droplet nucleates at the low current shown in Figure 12c [55]. Then, by increasing the current in Figure 12d, the droplet grows, and when it reaches its peak in Figure 12e, the electromagnetic pinch force drives the droplet to the weld pool, and finally, in Figure 12f, the droplet traverses to the pool, and the cycle repeats [55]. Compared to against-gravity deposition, depositing along the gravity reduces gravity-driven pool disturbance and lowers the impact of process-induced surface defects. However, it can exacerbate the lack of fusion unless the process parameters and metal transfer mode are adjusted properly. The primary electrical signals in WAAM consist of instantaneous current and arc voltage measurements, which directly come from the power source to show the physical changes in arc length and short-circuit occurrences and transfer stability [101]. However, the secondary voltage/current indicators for arc stability and metal transfer behavior are mathematically derived from these waveforms through power, RMS, and kurtosis calculations [101]. Electrical signals during WAAM are not only associated with the generation of current and voltage but are also influenced by the wire feed rate. Since the generation of the arc and its stability in WAAM depend on

the wire feed rate, in-situ monitoring of the wire feed rate is crucial for ensuring process reliability, as described in the next section.

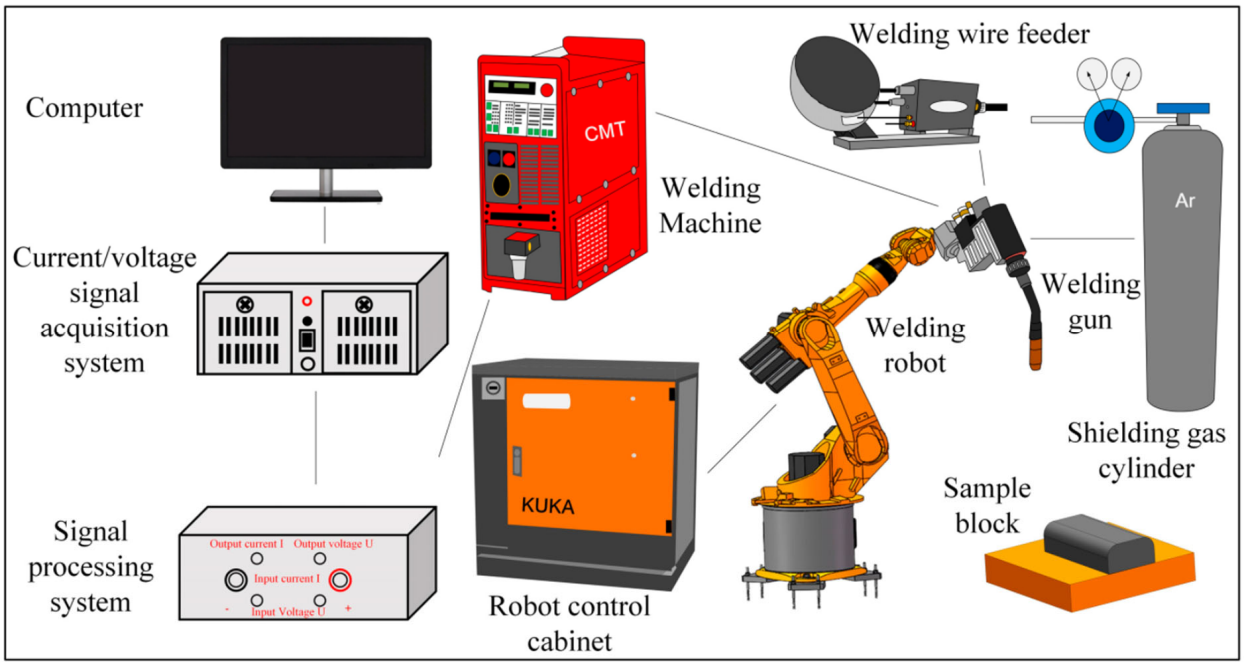


Figure 10. Schematic of the WAAM system with equipment for monitoring the current and voltage in the online system inspection [75].

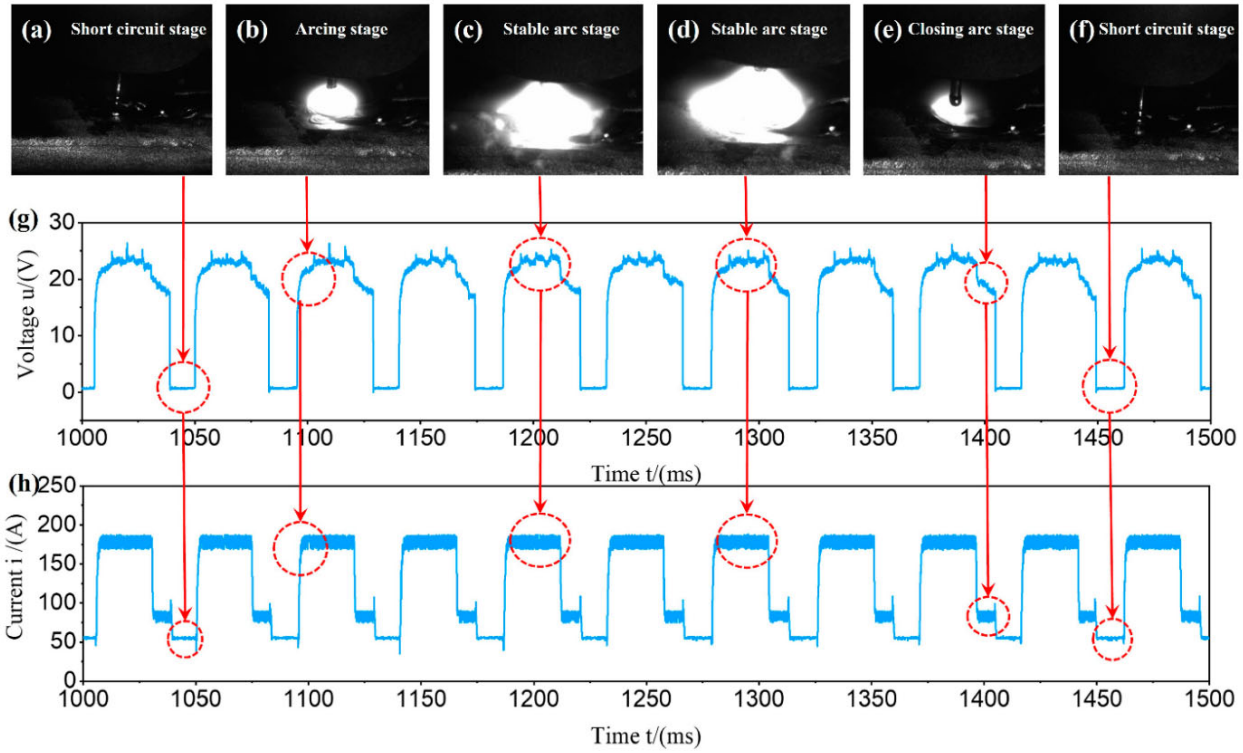


Figure 11. The correlation between droplet transfer behavior and current/voltage waveforms in WAAM is illustrated through the following stages: (**a**) short-circuit phase, (**b**) arcing phase, (**c**,**d**) stable arc period, (**e**) arc-ending phase, (**f**) return to short-circuit, along with (**g**) the corresponding voltage evolution and (**h**) the associated current variation over time [75].

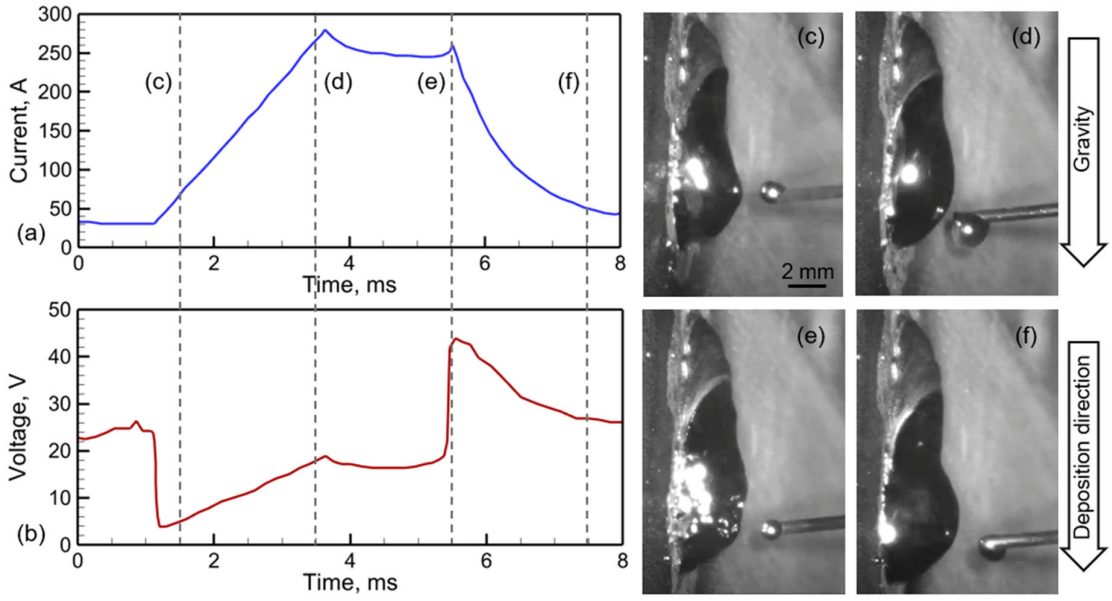


Figure 12. High-speed imaging of pool behavior with waveform monitoring on a vertical substrate toward gravity: (**a**) Current and (**b**) voltage monitoring for pulse metal transfer. (**c**) shows that the droplet nucleates and grows at the wire tip, (**d**) rising current enlarges the droplet, (**e**) peak current drives pinch-off, and (**f**) droplet fuses with substrate. This figure is owned by the authors.

5.2. Wire Feed Rate, Travel Speed, and Power Fluctuations

In WAAM, the behavior of molten droplets at the wire tip determines the stability of the arc, the efficiency of heat transfer, and the overall integrity of the deposited beads [101]. Since every short-circuit transfer induces disturbances in current, voltage, and acoustic response, the morphology of the droplet influences the transient behavior of the arc, which is recorded by an in-situ monitoring system [109]. Parameters such as wire feed rate and travel speed determine the amount of heat delivered per unit length, thereby controlling how quickly the droplet grows and detaches [109]. This relationship is very evident in Figure 13 [75]. As the welding speed increases, the droplets become smaller. This is because the arc stays over a certain spot for a shorter time, the heat input per unit length decreases, and the droplet has less time to expand before it breaks. As the travel speed decreases, the heat input increases, leading to larger droplet formation and a prolonged necking stage before detachment. As a result, the recorded voltage, current, and acoustic signals exhibit altered periodic patterns during the deposition process. For larger droplets, the cycles are slower and have a greater amplitude, whereas for small droplets, the cycles are faster and more uniform [75]. Therefore, the visual droplet evolution in Figure 13 not only represents a physical phenomenon but also explains the distinct responses observed in electrical, acoustic, and vision-based in-situ monitoring systems.

While electrical signal monitoring provides valuable real-time data on arc behavior and energy input characteristics, and the consistency of the deposition process can be significantly improved through optimization of related parameters such as wire feed rate, travel speed, and power fluctuations, these electrical signatures offer limited insight into the thermal consequences and material behavior resulting from energy deposition. Temperature-based monitoring techniques, discussed in the following section, complement electrical measurements by providing direct and accurate information about heat transfer mechanisms, thermal accumulation effects, cooling behavior, and the thermal conditions that govern phase transformations and defect formation, thereby enabling more comprehensive process understanding and control strategies.

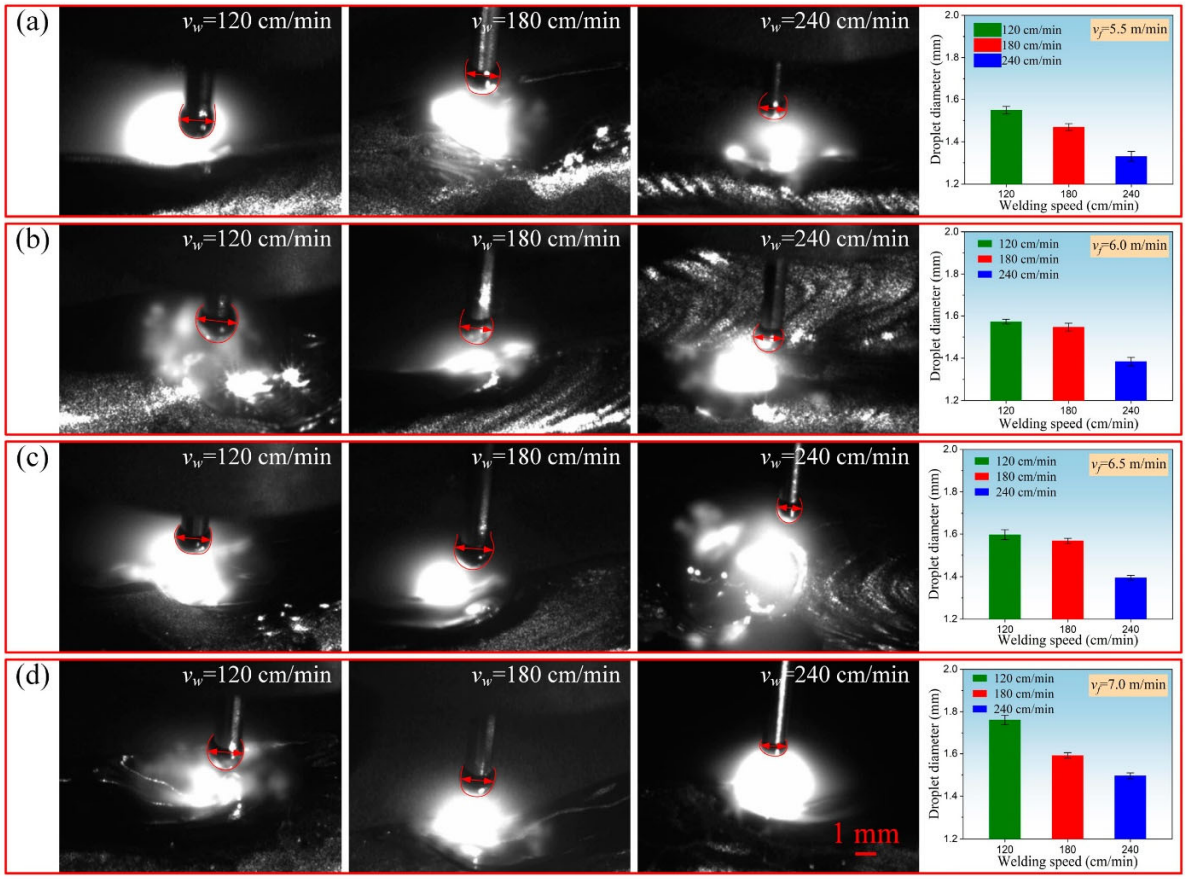


Figure 13. Droplet morphology under different welding speeds at a fixed wire feed rate during WAAM of AA 2319 [75]. υ_w is a travel speed, and υ_f shows the wire feed rate. (**a**) At a wire feed rate of 5.5 m/min, increasing travel speed produces smaller droplets prior to detachment. (**b**) At υ_f = 6 m/min, the droplet diameters at 120 and 180 cm/min become comparable. (**c**) At a wire feed rate of 6.5 m/min, the same trend persists, with higher travel speeds generating finer droplets. (**d**) By increasing the wire feed rate to 7 m/min, the lowest travel speed yields the largest droplets, while faster travel speeds continue to promote smaller droplet formation. The droplet size at the wire tip is indicated by the red double-headed arrow.

6. Thermal and Temperature Monitoring

Thermocouples function as an affordable piece of equipment, commonly used for measuring local temperature [110,111]. However, thermocouples are a contact-based measurement approach that cannot monitor the molten pool temperature. Since this measurement technique has been extensively used in the literature, it is not reviewed in this section. Instead, non-contact temperature measurement methods, such as an IR camera and a pyrometer, and their importance in predicting the temperature variations and cooling rate are described in the following sections. Infrared thermography provides two-dimensional temperature field mapping across the workpiece surface using thermal cameras. Pyrometers are point-measurement devices that determine temperature at specific locations by detecting emitted thermal radiation.

6.1. Infrared Thermography

Thermal imaging, or infrared thermography, is a method of visualizing heat by creating an image of surface temperatures and their fluctuations using infrared light [112]. Within the weld block, a temperature gradient forms due to the reheating and cooling cycles of successively deposited layers in WAAM [113]. The thermographic image shown in Figure 14, captured by an infrared camera, reveals the temperature distribution in the

uppermost deposited layer during multilayer deposition [113]. An increase in heat input enlarges the heat-affected zone (HAZ), leading to greater heat accumulation within the material. Heat accumulation in the deposited beads has a significant impact on the disruption of the geometrical precision of the next layer [114,115]. This deviation alters the distance between the melt pool and the welding wire, thereby affecting arc stability during deposition. Monitoring the interlayer temperature is a promising approach to reducing geometric deviation in the upper layers, which is caused by insufficient cooling time in the lower layers [114,115]. This temperature is defined as the surface temperature of the previously deposited layer before the start of the new layer [116]. Several variables influence the measurement of the temperature distribution. Three main factors in thermographic measurements are welding conditions, suitable emissivity, and transmittance. The welding atmosphere in the building environment and the generated fumes affect the accuracy of thermographic measurements during WAAM [116]. Substrate temperature and its coloration are both factors that impact emissivity [117,118], while transmission is related to atmospheric variables such as temperature and humidity. Moreover, the location of the camera relative to the surface is another variable that affects both transmission and emissivity [116–118]. For measuring emissivity, an infrared camera and thermocouples can be used [111]. However, unreliable results may be achieved in a rapid transient environment in WAAM, as process interface and signal delay can decrease measurement accuracy [79,119].

Infrared cameras cannot be affected by the contact measurement problem, as they monitor the surface from a distance. Their main problem is their dependence on emissivity [52]. Therefore, any sort of surface contamination affects emissivity and thus causes a deviation in measurement [82]. Another issue during in-situ monitoring of arc deposition is the increased light and electromagnetic radiation during deposition, which makes it difficult for the pyrometer to detect infrared radiation [120]. However, covering the high radiance of the arc during deposition and measuring the temperature is feasible using pyrometers [121]. Figure 15 shows the location of the IR camera regarding the part [122]. To minimize the effect of arc brightness on temperature measurement during welding, a region of interest (ROI) is defined, located at a fixed offset from the molten pool on the most recent layer [122]. Each technique has its own pros and cons. However, some errors can still occur due to welding conditions, their temperature dependence, and the lack of calibrated instruments, which necessitates the use of a pyrometer as an accurate measurement approach for in-situ monitoring in WAAM [123].

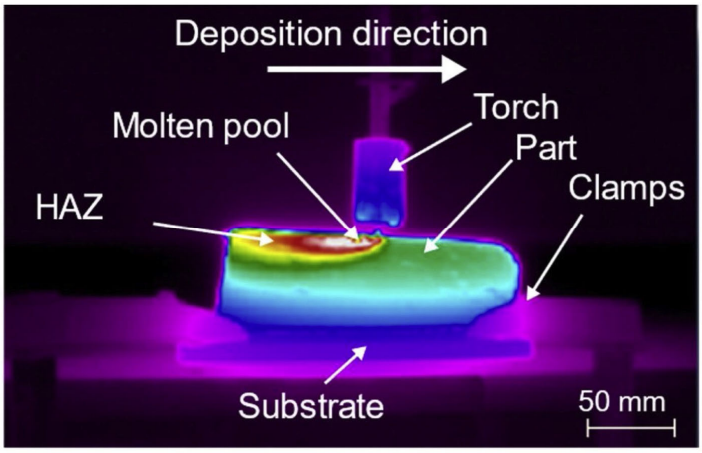


Figure 14. IR thermographic image of the last deposited bead in multilayer WAAM [113].

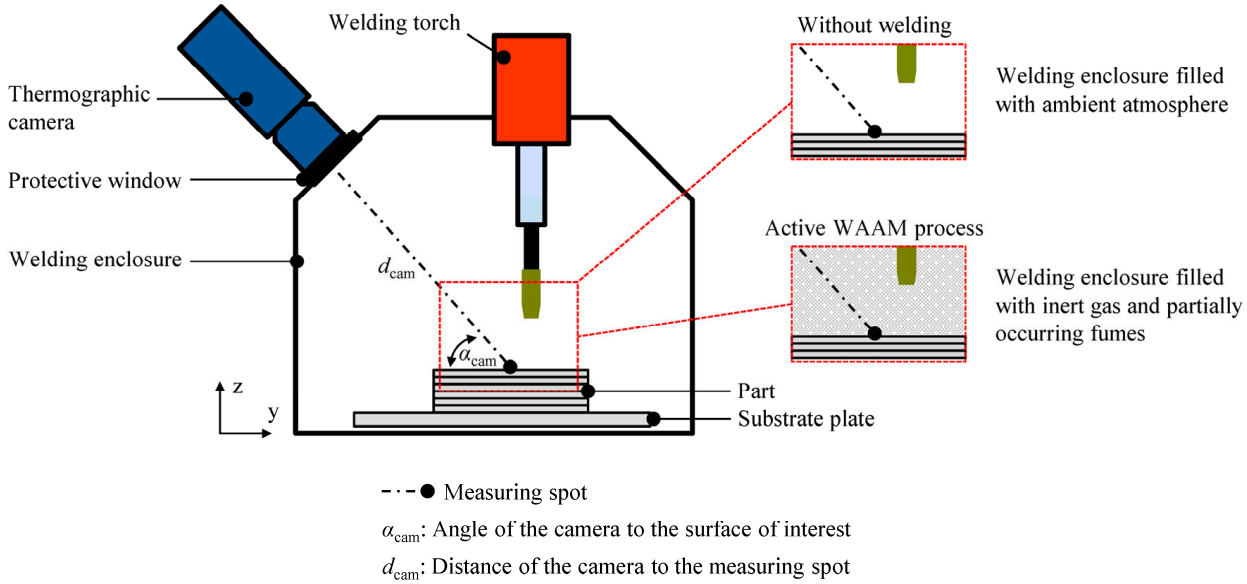


Figure 15. Schematic of the WAAM thermography setup (camera location, protective window) used to calibrate emissivity and transmittance to acquire absolute interlayer temperatures [122].

6.2. Pyrometers

The interlayer temperature (IT) in WAAM represents the temperature measurement at specific points on the newly deposited layer before the start of the next pass, which can be measured using pyrometers. There are two pyrometric strategies for capturing IT in WAAM, as shown in Figure 16 [52]. The first is the upper-pyrometer approach. The sensor views downward onto a spot on the top surface just ahead of the melt pool. The measurement location near the pool surface enhances the detection of pool dimensions, bead shape, and thermal history [110,124,125]. The pool requires a minimum offset L to avoid operational problems, and L functions as a critical parameter as it determines both the reduction in arc influence and the precision of temperature measurement. The arc heating effect on reading values increases with shorter L values, but longer L values result in less accurate readings. The schematic and experimental setup of the ratio pyrometer, mounted above the deposition area, is shown in Figure 17a–c [126]. A ratio pyrometer determines the molten pool temperature by taking the radiation intensities at different reference wavelengths [126]. To minimize the impact of the arc glare, two narrowband optical filters are mounted and tuned to the desired wavelength range. This setup enables non-contact temperature measurement of the molten pool. In Figure 17d,e, two synchronized infrared images of the weld pool are captured through narrowband optical filters and then converted into a temperature map [126]. From this map, the melt pool shape and size can be identified based on regions exceeding the melting temperature [126].

The second IT strategy, which is not common in WAAM, utilizes a sideward pyrometer to monitor a point on the wall located below the melt pool [52]. Since the dominant heat flow is along the build (Z) direction, arc heating influences this lateral measurement regardless of the offset distance (L). The target point will approach a near-equilibrium region with homogenized heat flow when L becomes very large, which makes the signal less useful for maintaining layer stability [52]. Both IR cameras and pyrometer methods are used to measure temperature, with the broader objective of predicting cooling rates and controlling the microstructure, as discussed below.

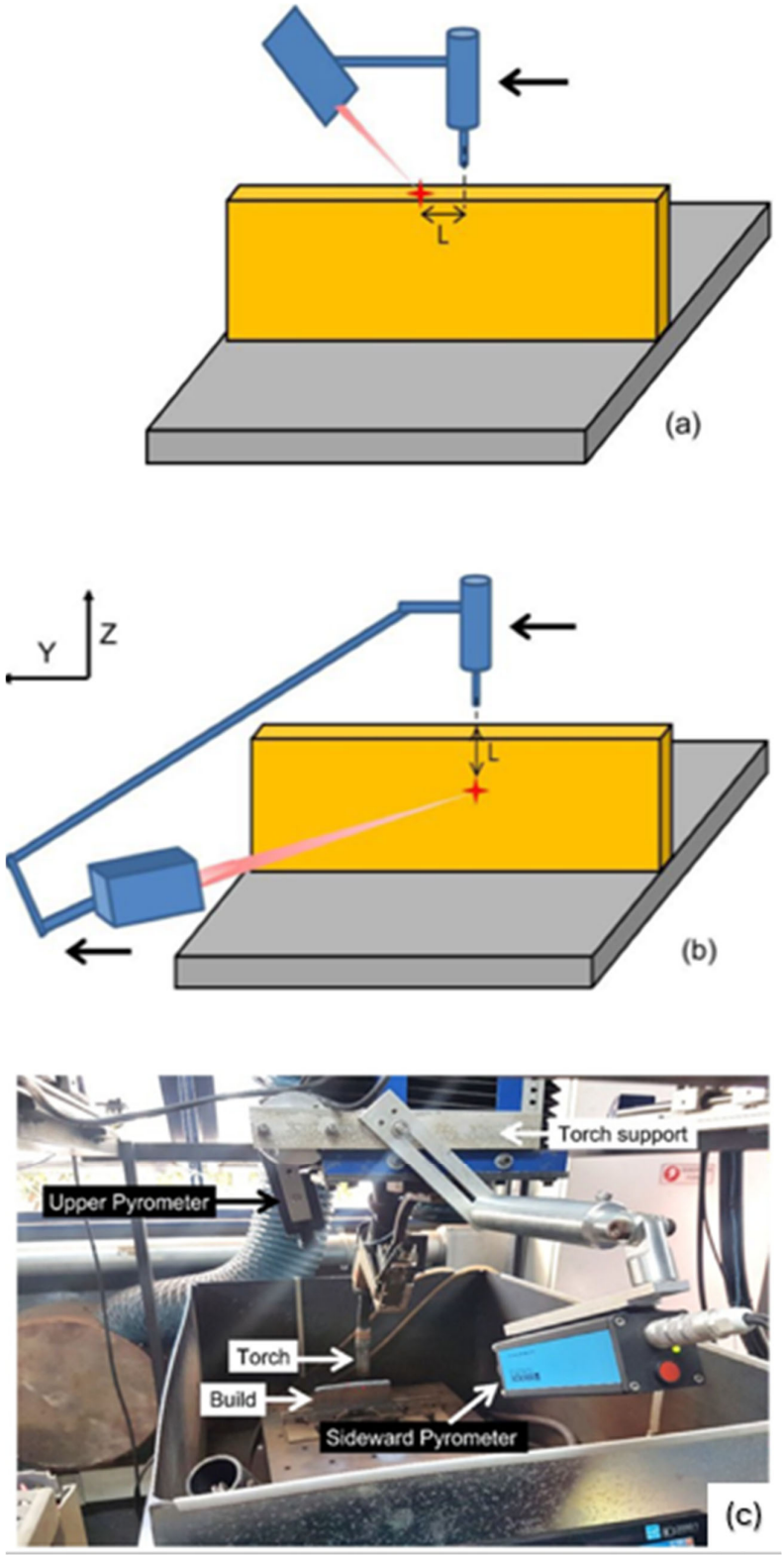


Figure 16. Measuring interlayer temperature (IT) in thin wall WAAM: (**a**) upper pyrometer, (**b**) sideward pyrometer, and (**c**) experimental system for measuring with both upper and sideward pyrometers [52].

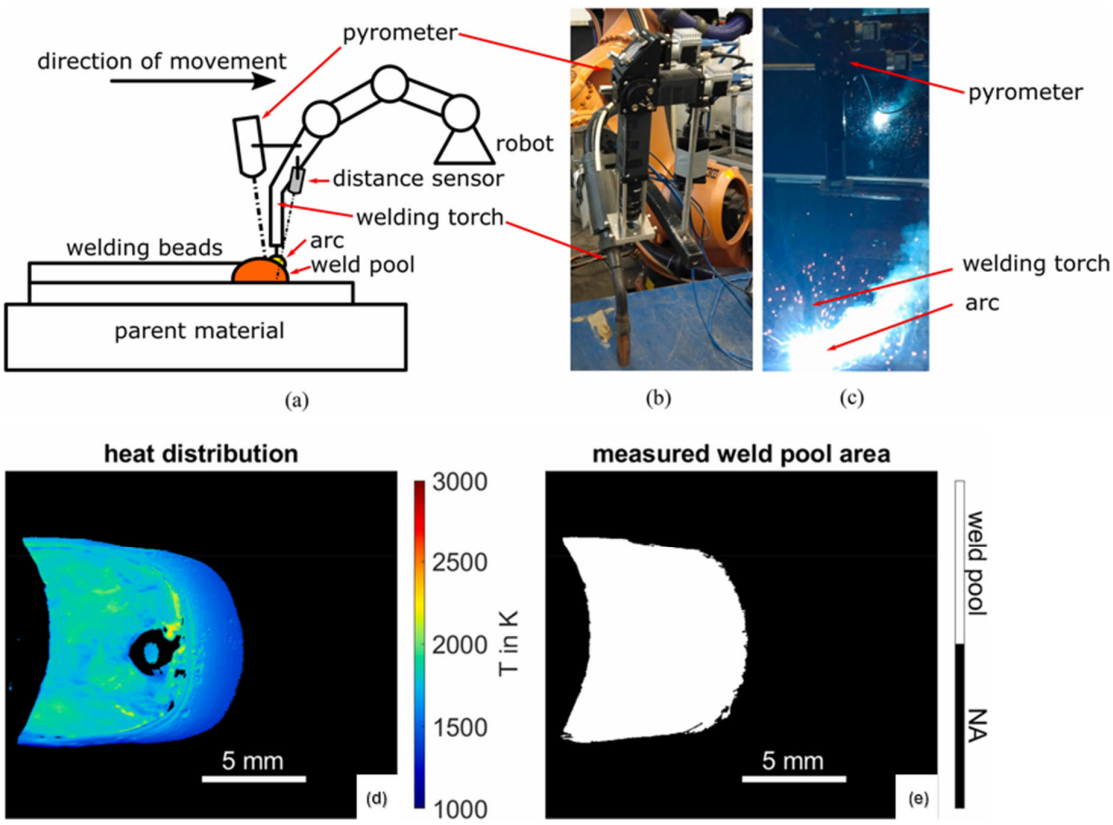


Figure 17. (**a**) Schematic and (**b**,**c**) experimental setup of the ratio pyrometer installed on a robotic arc deposition: (**d**) shows the heat distribution, and (**e**) shows the pool region measurement [126].

6.3. Cooling Rate and Solidification Control

Online inspection enables the observation of the cooling rate, which is the principal determinant of solidification rates and variations in grain size [127]. In WAAM, the cooling rate is often estimated indirectly using microstructural parameters like secondary dendrite arm spacing or directly from temperature-time data collected from in-situ thermal measurements [128]. High-speed pyrometers, IR cameras, and thermocouples all can provide direct, time-resolved measurements of the thermal history during deposition, from which the cooling rate of deposited beads can be accurately derived [129]. By combining two X-ray imaging approaches, the secondary arm can be observed by capturing two images with only a 21-s gap between them, which can be an effective approach for real-time monitoring of the solidification process [130,131].

Thermal monitoring is critical for WAAM process control as temperature history directly governs microstructural evolution, residual stress formation, and dimensional accuracy of fabricated components. Infrared thermography (Section 6.1) provides spatial temperature field mapping, enabling inter-layer dwell time optimization and distortion prediction, while pyrometers (Section 6.2) offer high-speed point measurements suitable for real-time control of heat input, together forming the foundation for thermal management strategies that balance productivity with metallurgical quality requirements. Multilayer deposition in WAAM is characterized by transient temperature variation caused by the reheating and cooling cycles. These thermal anomalies can be reduced by using a multi-axis robot or a CNC system that utilizes force and vibration sensors, enabling adaptive control to minimize thermally induced geometric deviations, as described below.

7. Force and Vibration Monitoring

In WAAM, force and torque sensors play a critical role in regulating normal contact forces between the torch and substrate, compensating for surface irregularities and geometric variations, and ensuring robust probe connection and consistent standoff distance throughout the deposition process [62]. These sensors provide feedback for adaptive control strategies that maintain optimal process conditions despite workpiece imperfections. Additionally, accelerometers mounted on the robotic manipulator or welding torch can detect mechanical vibrations and oscillations that may indicate instability during arc ignition, metal transfer, or droplet detachment [54]. To maintain the arc stability and bead shape during on-site WAAM, it is essential to detect and compensate for vibrations caused by external disturbances [54]. Both methods are reviewed as in-situ monitoring techniques in WAAM in the subsequent sections.

7.1. Force Sensors on Deposition Head

The deposition head integration of force sensing technology enables the direct measurement of mechanical interactions between the torch and the growing wall, which directly affects bead height errors and lack-of-fusion problems [62]. Force measurements are more effective than visual or thermal inspection methods when optical viewing becomes impossible due to arc light and fume interference [59]. The force feedback system in thin-wall WAAM detects minor changes in stiffness and heat input before any surface defects become visible [62]. The local contact stiffness changes due to variations in bead morphology and reinforcement height, which produce force signatures that serve as early indicators of geometric divergence during multi-layer buildup. As shown in Figure 18, a force-torque sensor integrated into the KUKA industrial robot detects deviations between the as-built surface and the designed geometry, and the controller compensates for these deviations in real-time [62]. Force sensing contributes to maintaining process stability by monitoring contact interactions; however, dynamic disturbances such as vibration require additional control strategies, which are introduced in the next section.

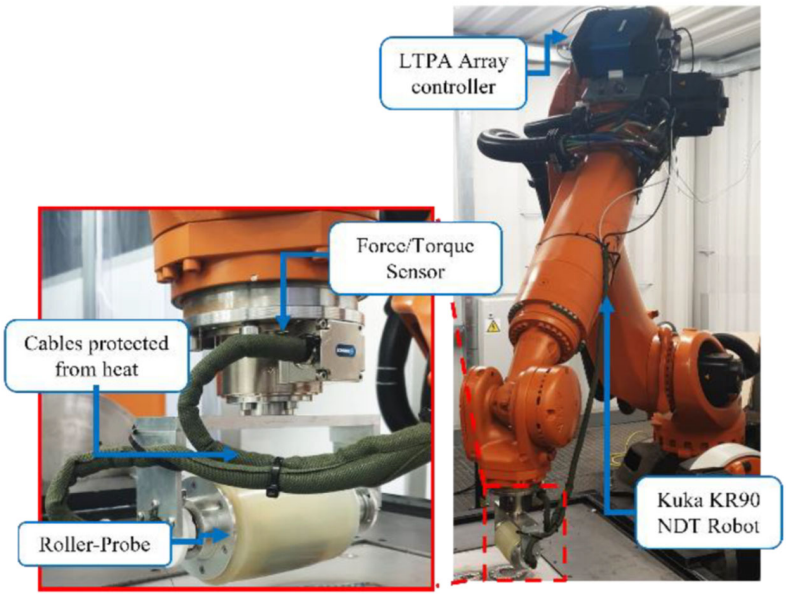


Figure 18. An FT sensor (FTN-GAMMA-IP65 SI-130-10, Schunk, Germany) is mounted on the end effector of the KUKA KR90 (KUKA Robotics Corporation, Augsburg, Germany). The Large-Channel Time-Domain Phased Array (LTPA) array controller functions as an ultrasonic phased-array acquisition system, controlling the transducer while acquiring ultrasonic signals to detect internal defects that occur during or after the deposition process [62].

7.2. Vibration Analysis for Stability Monitoring

As shown in Figure 19, a real example of vibration can be observed during 3D printing on a ship, which is impacted by the swing motion of the environment [132]. To track the effects of vibration on part quality during the WAAM process, a real-time monitoring system consists of a high-speed camera with a frame rate of 1500 frames per second and a vibration measurement setup. The entire system, featuring a MIG welding machine integrated with a DOBOT SR4-2, which is positioned on a vibration platform, simulates ship-induced vibration, as illustrated in Figure 20 [54]. To investigate the effect of external vibration on arc stability in the on-site WAAM process, discrete vibration frequencies at 2, 5, 10, 15, 20, and 25 Hz were applied, each lasting 0.2 s [54].

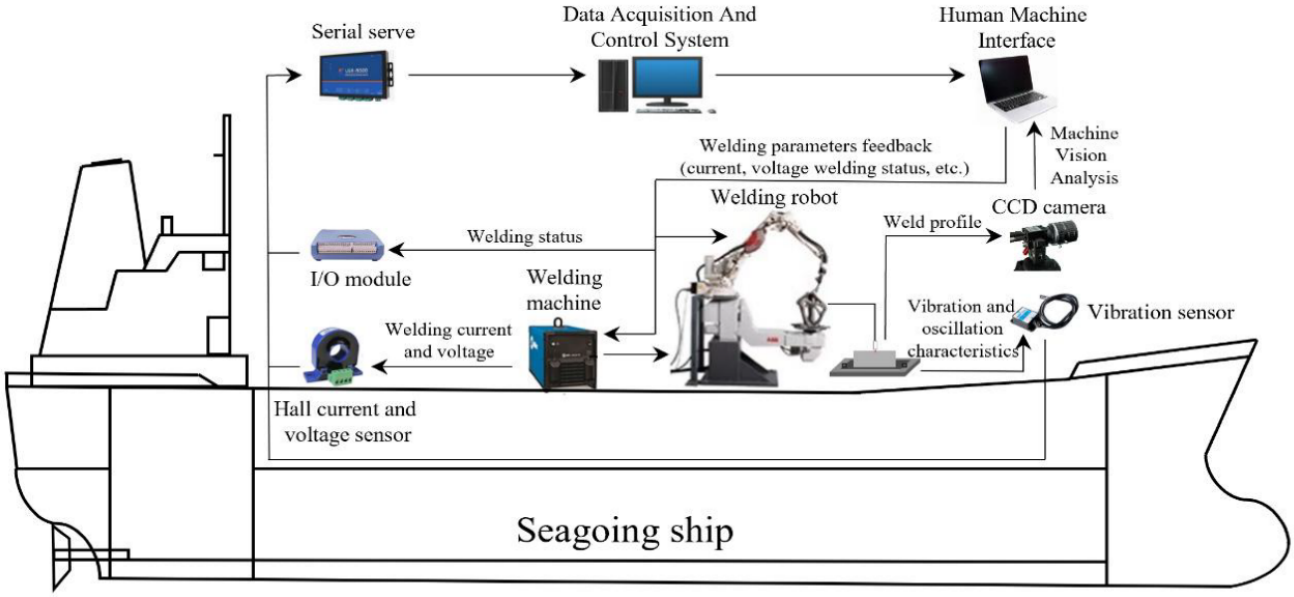


Figure 19. Schematic of an onboard WAAM system for naval applications [132].

The arc instability during the WAAM process is caused by the unstable ship environment, which affects on topography of deposited beads [54]. The effect of vibration on the arc torch and the base plate can be measured through the acceleration curves shown in Figure 21. Due to the different structure and materials of those two parts, the vibration behavior is different for each of them [132]. Moreover, the permanent change in distance between the weld torch and the substrate affects the topography of the deposited bead and the arc shape during the process [132]. In Figure 22, a longer distance of the arc torch to the substrate caused by vibration in the Z direction, changing the arc shape from the bell jar in the steady state to the horn shape, which causes a tendency for excessive spatter or, in extreme cases, arc extinction [54]. However, if the distance is reduced, the arc becomes fan-shaped, resulting in inadequate arc burning and a narrowed weld path, which increases the likelihood of short-circuit contact [54]. Moving the arc in the X-direction creates an ellipse shape, while vibrating in the Y-direction creates an irregular shape [54]. The surface quality of samples produced under vibration conditions stayed poor, but the cross-sections showed full density without any signs of porosity or lack of fusion [54]. The results indicate that WAAM can withstand significant vibrations, making it suitable for shipboard applications [54]. Sections 3–7 discuss various sensors used for in-situ monitoring in WAAM. However, due to the diverse requirements of process monitoring, a single sensor is often insufficient. Simultaneous measurement of multiple variables through multi-sensor fusion is commonly employed, which is reviewed in the next section.

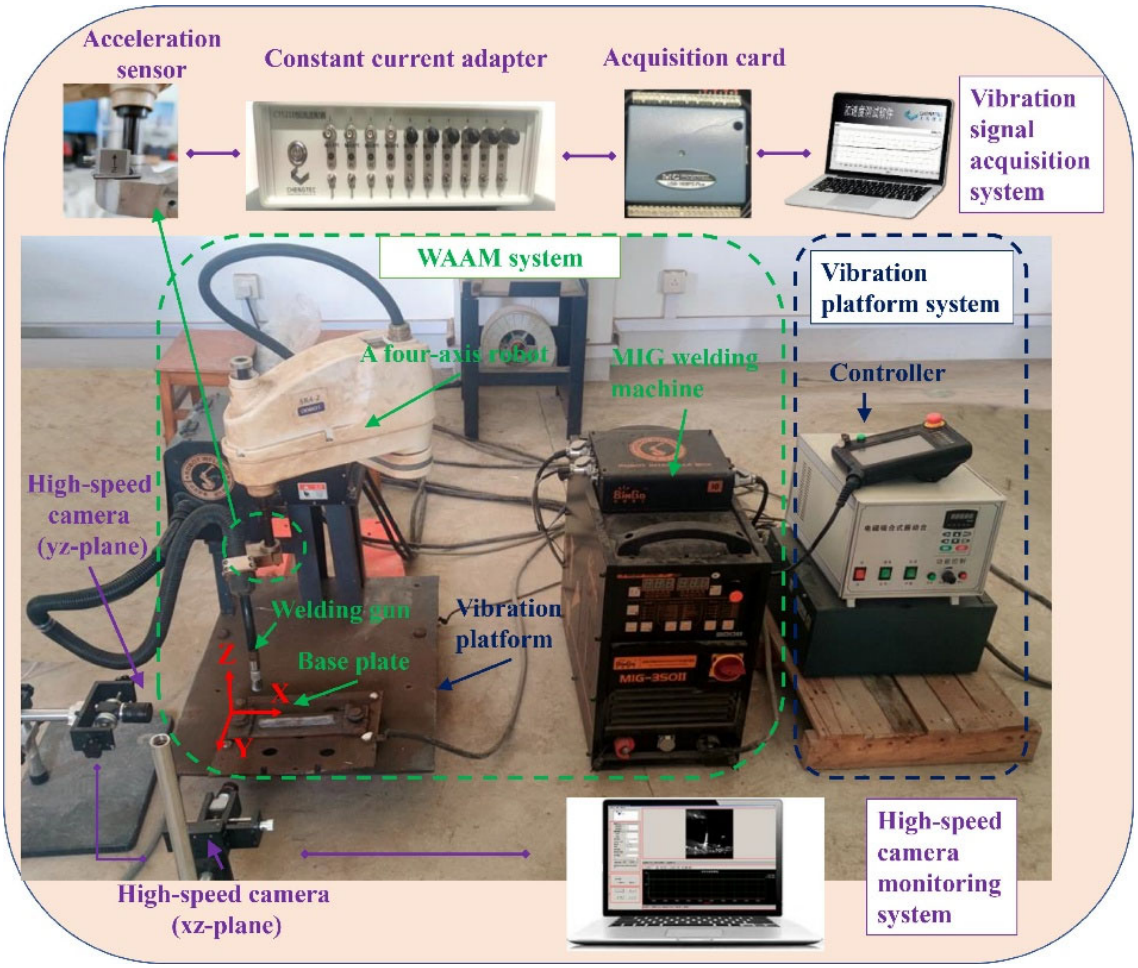


Figure 20. Experimental setup in the WAAM system, which consists of an acceleration sensor, a high-speed camera with a frame rate of 1500 f/s, a welding robot (DOBOT SR4-2), and a metal inert gas (MIG) welding machine [54].

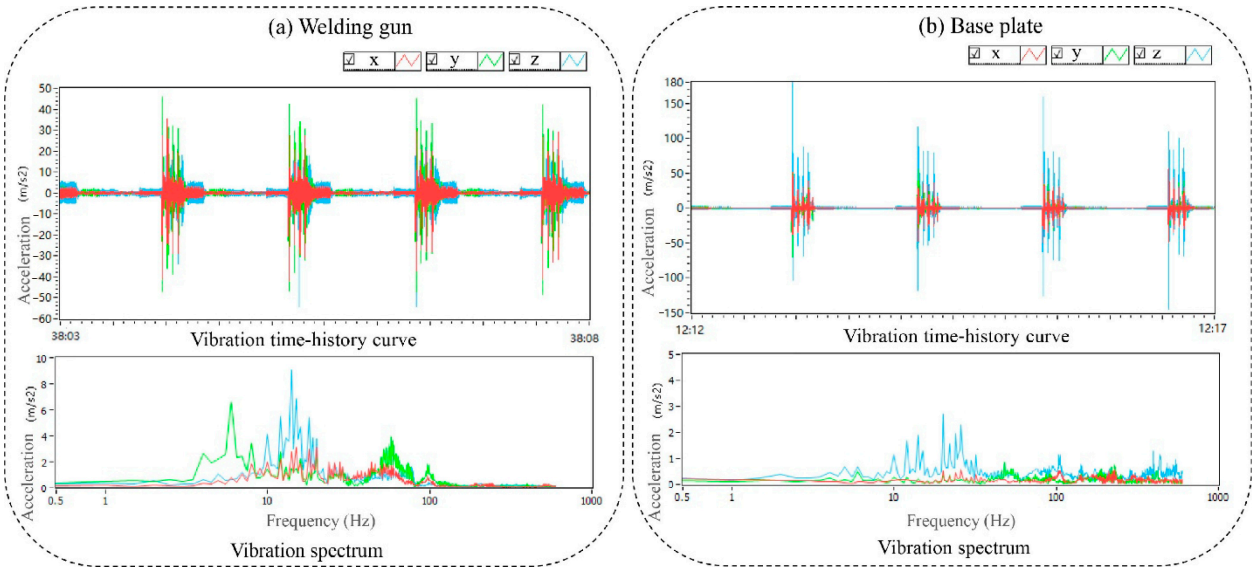


Figure 21. Acceleration curve based on time and frequency in (**a**) the welding gun and the (**b**) supporting (base) plate, which shows different behavior, subjected to externally applied vertical vibration [132].

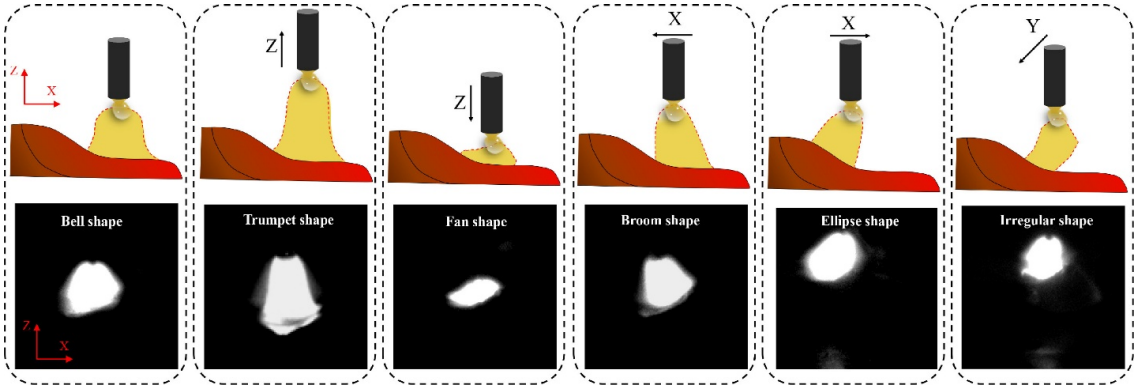


Figure 22. Different shapes of arc in steady and vibration conditions, showing the bell shape under steady conditions, and changing to trumpet, fan, broom, ellipse, and irregular shapes [54].

8. Multi-Sensor Fusion Approaches

The coordination of multiple sensors in advanced manufacturing systems enhances the capability to monitor process variables more effectively, resulting in decreased errors and improved precision of final products [133]. These individual measurements are then integrated into a unified representation of data through a signal processing algorithm [133], producing a comprehensive understanding of the fusion level [134,135]. The benefits of using data fusion over the measurement of a single criterion include increasing accuracy and reducing process-induced defects by evaluating multiple sources of information, as shown in Figure 23 [55]. Implementing multiple sensors in a real-time monitoring system improves process stability and overall reliability, as shown in Figure 24 [67,135]. To enhance the capability of precise measurement of the bead width in plasma arc welding, which is reduced by the deformation of the pool surface, an image processing technique is required to accurately reconstruct the molten pool [136]. One technique is to use a support vector machine (SVM) to predict the bead width with fewer experimental samples through kernel-based nonlinear mapping. Based on the analysis of information fusion data, three different levels of data fusion can be performed. Data layer fusion is based on using the weighted average method and other techniques, which provide detailed fusion data that require time-consuming computations and decrease performance [136]. With feature layer fusion, the amount of processed information is reduced, and in-situ monitoring performance is enhanced through using methods like the Kalman filter and neural network. Finally, the decision layer fusion offers greater flexibility and acceptable fault resistance, which increases computational costs [136]. The methods used in this data fusion level are the Dempster-Shafer (DS) evidence interface method and the Bayesian probabilistic interface method [136].

The three fusion levels operate at distinct levels, offering specific benefits and drawbacks for particular applications [67]. Raw sensor data must be processed first to extract features before different fusion methods can be applied for decision-making. The fundamental information needs to match regardless of the chosen method. The method of data-level fusion preserves the most original information, which yields detailed results, while decision-level fusion operates on processed conclusions rather than raw signals [137]. The selection of an appropriate fusion level requires careful consideration of multiple factors, including the system's objective, operational conditions, available computing power, sensor data characteristics, and system limitations [138]. Therefore, a closed-loop setup for multi-sensor real-time monitoring consists of a combination of sensors that act as a unified system to reduce defects during the deposition process in WAAM [67].

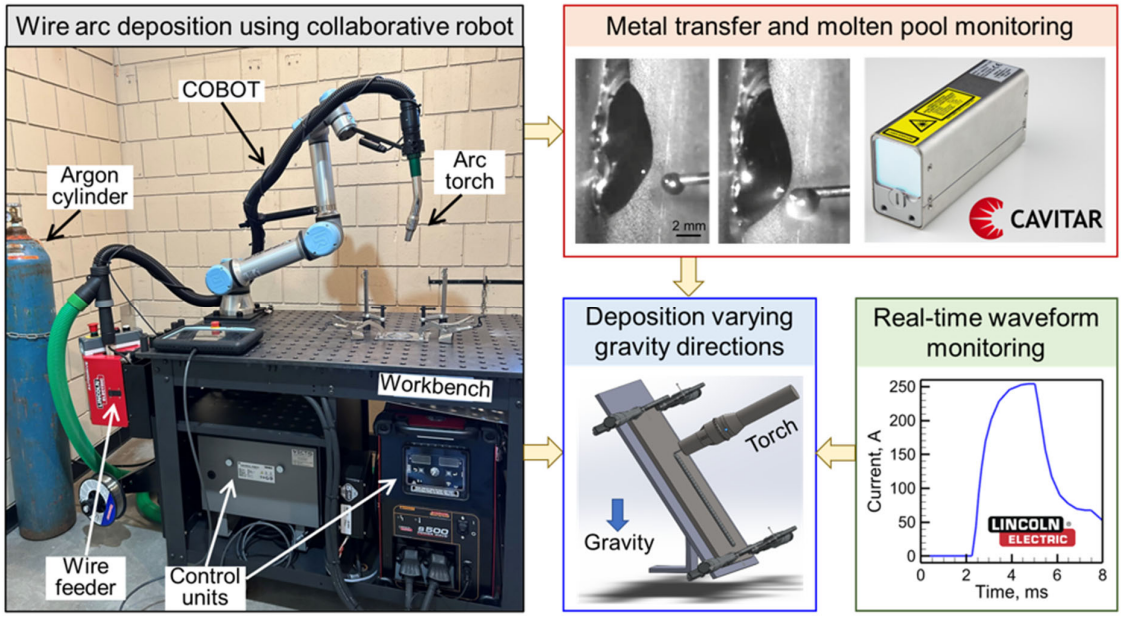


Figure 23. Using a waveform monitoring system with a high-speed camera in a collaborative robot (COBOT)-integrated WAAM system as a multi-sensor approach. This figure is owned by the authors.

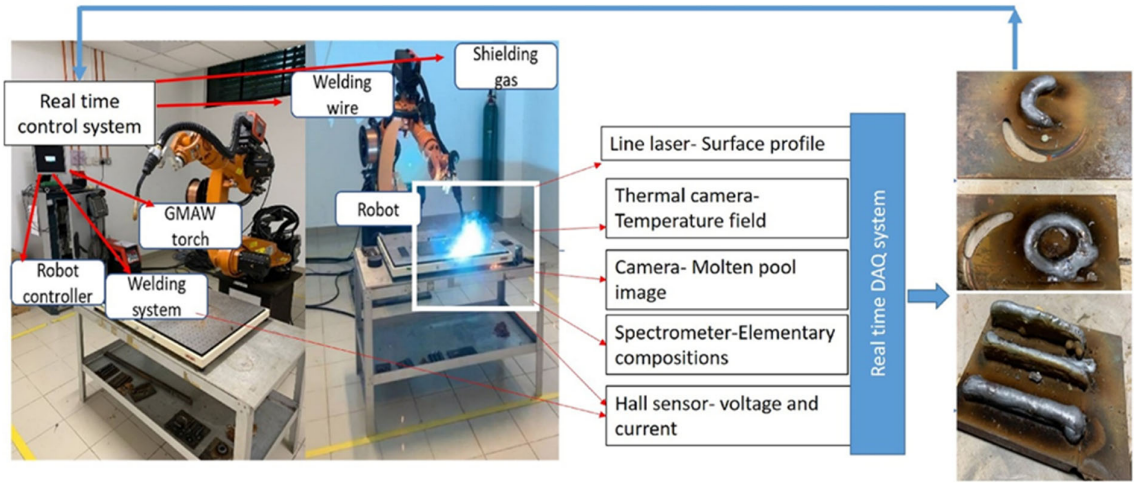


Figure 24. WAAM set up with various sensors for in-situ monitoring [67].

9. Applications of In-Situ Monitoring in WAAM

WAAM faces significant challenges related to thermal management and process stability that directly impact part quality and structural integrity. The primary source of deformation and elevated residual stresses in WAAM components stems from excessive heat accumulation caused by the process's relatively low energy density and continuous heat input during multi-layer deposition [139]. Compounding these thermal issues, the inherently non-linear and transient nature of the arc deposition process means that numerous interdependent factors, including shielding gas flow, wire feed dynamics, travel speed variations, and thermal boundary conditions, can destabilize the arc and adversely affect droplet transfer behavior, ultimately leading to defect formation and compromised deposition quality [140]. To effectively mitigate these detrimental effects and ensure consistent dimensional accuracy, mechanical properties, and surface finish in fabricated components, the implementation of robust online inspection and monitoring systems has become essential for meeting the stringent quality standards demanded in industrial WAAM applications [102].

The following sections explore specific applications (Table 2) where in-situ monitoring techniques have been deployed to address these challenges.

Table 2. Applications of monitoring in WAAM and corresponding sensors used along with their advantage and limitations.

Applications of In-Situ Monitoring in WAAM	Sensors Used	Explanation	Advantages and Limitations	Ref.
Defect detection and prevention	High speed camera, acoustic sensor, IR camera	• Real-time identification of porosity, lack of fusion, and geometric defects • Multi-sensor fusion captures complementary defect signatures • Enables immediate corrective action during deposition	**Advantages**: Early defect detection, reduced scrap rates, comprehensive coverage **Limitations**: Complex data processing, sensor integration challenges, computational demands	[70,73,141]
Process stability monitoring	CCD/CMOS sensors, high speed camera, IR camera	• Tracks arc behavior, melt pool dynamics, and droplet transfer consistency • Detects process deviations and instabilities in real-time • Provides feedback for maintaining optimal deposition conditions	**Advantages**: Continuous quality assurance, quantifiable stability metrics **Limitations**: Sensitivity to ambient conditions, arc brightness interference, calibration requirements	[54,55,75, 113,126,141]
Microstructure control	IR Thermal imaging and CCD camera	• Monitors thermal history and cooling rates affecting phase transformations • Controls inter-layer temperature to achieve desired microstructural properties • Correlates thermal profiles with grain size and mechanical properties	**Advantages**: Enhanced material properties, predictable microstructure, reduced heat-affected zones **Limitations**: Limited penetration depth measurement, surface-only observation, complex thermal data calibration	[142,143]
In-situ monitoring to reduce residual stress and distortion	Laser displacement sensors, digital image correlation (DIC)	• Measures real-time geometric deviations and surface displacements • Tracks accumulated distortion during build progression • Enables adaptive toolpath planning to compensate for warping	**Advantages**: Dimensional accuracy improvement, proactive distortion mitigation **Limitations**: Requires clear line-of-sight, sensitive to vibrations, data post-processing needed	[144,145]
Closed-loop control and adaptive process parameter adjustment	Voltage and current sensors, IR imaging sensor, optical sensors	• Continuously adjusts parameters based on real-time sensor feedback • Maintains consistent heat input and bead geometry across layers • Compensates for substrate variations and heat accumulation effects	**Advantages**: Autonomous quality control, process repeatability, reduced operator dependence **Limitations**: Control algorithm complexity, sensor lag time, system integration costs	[146]

9.1. Defect Detection and Prevention

Since WAAM commonly operates in an open-loop configuration, various process disturbances can destabilize the arc during deposition [73]. As shown in Figure 25, arc instabilities can cause defects like spatter, lack of fusion, and porosity. Porosity reduces the mechanical properties of the fabricated part by increasing stress concentration areas, which leads to a decrease in the potential benefits of using WAAM [73]. By using acoustic

sensors, the initiation of arc instability in the next layer can be prevented by optimizing the process parameters. The first step in acquiring accurate information is to use a wavelet transform, which filters out unwanted acoustic signals. The benefits of using wavelets over the Fourier related to non-stationary signals with sudden changes, like arc stability, and coping with sharp spikes that are common in WAAM. After wavelet denoising, the acoustic signal is converted into a graph representation and reduced to a single metric, the Fiedler number, which is used to detect flaw formation. This approach avoids computing multiple features and provides a computationally efficient monitoring method [73]. Arc instabilities are detected by tracking the Fiedler number on an exponentially weighted moving average (EWMA) control chart, providing a simple alternative to machine-learning-based flaw monitoring that is easy to implement in practice. Defect detection is performed through high-speed monitoring. The same high-speed imaging is also used for monitoring arc and process stability, as explained in the following section.

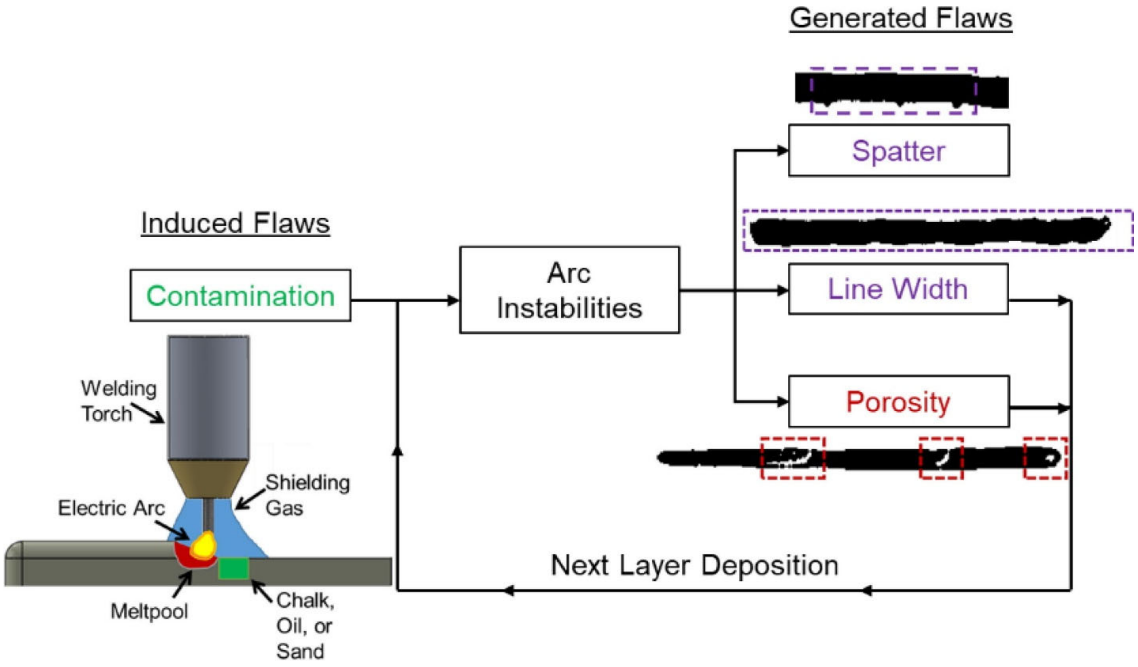


Figure 25. Flaws formed in one layer can influence the subsequent layer by inducing arc instabilities, which in turn promote the formation of additional defects [73].

9.2. Process Stability Monitoring

Although WAAM provides high deposition rates, the associated high heat input can lead to defect formation, often influenced by arc instability and unstable thermal conditions during the process [147,148]. Humping is one of the main defects caused by a lack of stability during the process. For identifying the onset of humping and porosity caused by humping in WAAM, high-speed pool imaging, integrated with machine learning, monitors the process in real-time [149]. Process optimization can identify suitable operating conditions for WAAM; however, the inherent stochasticity of WAAM can still amplify melt-pool instability [73]. Such instabilities can arise from a lack of shielding gas due to increased contact tip-to-work distance, surface contamination, or nozzle blockage by spatter [150]. Most WAAM monitoring methods rely on black box classifier defects, ignoring pool physics [151–153]. However, process dynamics-derived morphology features enable the detection of humping and humping-induced porosity [141]. As shown in Figure 26, the molten pool behavior in multi-layer thin-walled WAAM is monitored in real-time using a high-speed camera (Figure 26a). The captured image was then processed to determine the region of interest and extract the pool contour (Figure 26b,c). Four descriptive morphology

features were computed to serve as a process signature. In Figure 26d, the extracted melt-pool signatures serve as features for interpretable ML classifiers (e.g., shallow neural networks), which were trained in a supervised manner to categorize the deposition process into three states: nominal, humping, and humping-induced porosity [141]. This approach may not be suitable for conditions that require changes to melt-pool geometry, such as overhang structures or deposition against gravity. Process-stability monitoring provides critical information that enables the assessment of molten-pool behavior, as these factors directly affect the final microstructure and mechanical properties of the deposited materials.

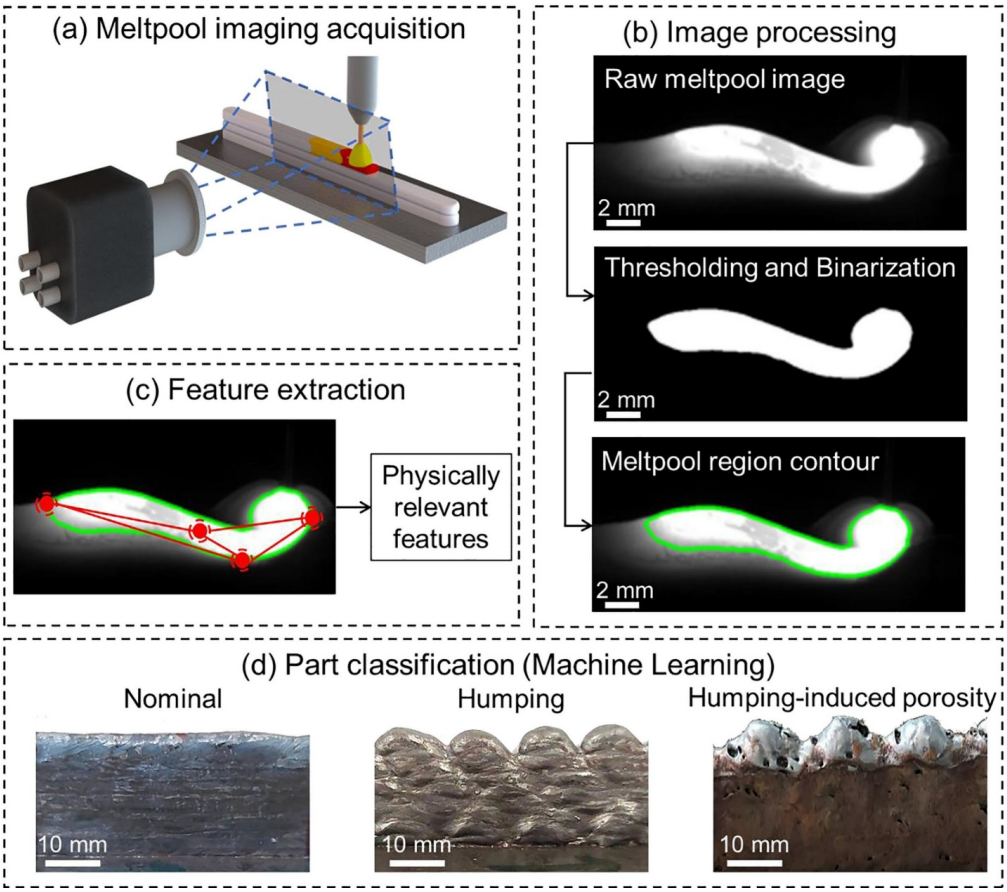


Figure 26. (**a**) A high-speed imaging of the melt-pool; (**b**) binarization/thresholding isolates the melt-pool contour; (**c**) morphology features (process signatures) are extracted from the contour; (**d**) these signatures classify the state as nominal, humping, or humping-induced porosity [141].

9.3. Microstructure and Mechanical Property Correlation

Achieving better mechanical properties during WAAM requires considering the microstructure of the fabricated part [154]. Improving the microstructure requires understanding the factors that impact deposition quality during production [155]. Tracking anomalies through online inspection of the molten pool provides indirect indicators of solidification conditions, enabling the prediction of the columnar-equiaxed tendency and grain size scale, both of which influence mechanical properties [156]. WAAM is a reliable method for producing aluminum alloy AA2024 [157]. The specific portion of Mg in this series makes the fabricated part through WAAM extremely brittle [142]. Therefore, improving the microstructure of the Al-alloy is required to decrease stress accumulation and thus prevent crack propagation in the material [155]. As shown in Figure 27 [142], the arc length and deposition are controlled and monitored during the process for defect detection using two CCD cameras. Moreover, using the STM32 microcontroller in the experimental system, with an ABB industrial robot and a GTAW machine, facilitates the real-time measurement

of waveform signals and wire feed rate. Based on Figure 28a in the solidification process in WAAM, columnar, dendritic crystals, and equiaxed are the main crystal morphologies that are formed in the fabricated part [142]. The red arrow shows the amount of dendritic crystal, which is larger than the other two, and the arm length is around 57.59 μm [142]. The yellow arrow indicates the columnar crystal, and the blue one indicates the cellular crystal. Coexistence of columnar, cellular, and dendritic zones reflects spatial changes in G/R (thermal gradient/solidification rate) and cooling rate during solidification (CET transition). Three different locations of the specimen, top, middle, and bottom, are shown in Figure 28b–d. In Figure 28b, speeding up the crystallization results in finer crystals, which is caused by the faster cooling rate due to the location of the top part [142]. As shown in Figure 28c, the cellular crystal shaped in the center of the part leads to increased material hardness. Finally, columnar structures in Figure 28d shows a high thermal gradient (G) aligned with the build direction, which reduces fatigue resistance.

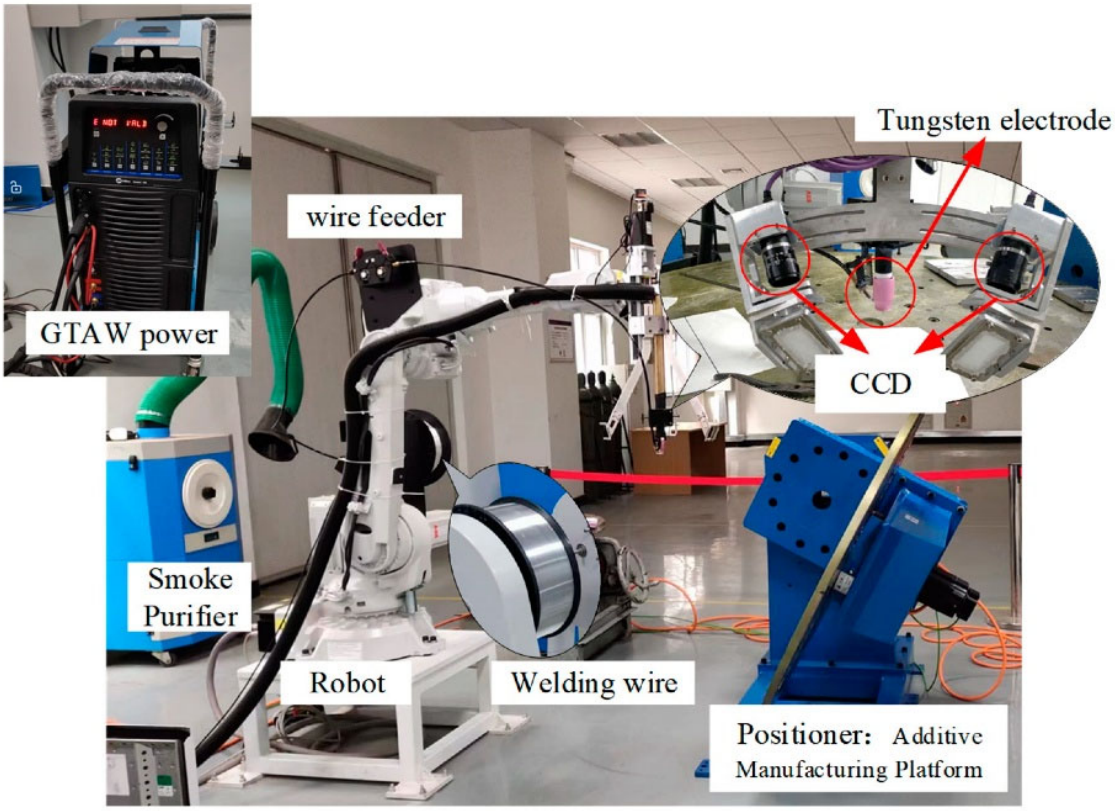


Figure 27. Experimental setup of the WAAM system using two CCD (Charge-Coupled Device) as an in-situ monitoring technique [142].

Adding each new layer during the WAAM process reheats the previously deposited material. The upper part of the wall becomes hot enough to alter the internal microstructure, causing some martensite to revert to austenite. The infrared images in Figure 29A show how the surface temperature varies across the wall [143], while Figure 29B illustrates temperature fluctuations over time during the first stage of deposition. The data indicates that section 1 cools through the austenite-to-martensite transformation range (FCC → BCC), remaining largely martensitic, as also confirmed in the IR temperature map (Figure 29E). During deposition of section 2 (Figure 29C,F), cyclic reheating raises the peak temperature above the austenite start temperature (As), producing localized reversion of martensite to austenite, which then transforms back to martensite on cooling. In section 3, as shown in Figure 29D,G, the newly deposited top region again cools through the austenite-to-

martensite range, while the middle portion of the wall experiences reheating above As [143]. The process of layer-by-layer deposition involves multiple heating and cooling cycles, resulting in intricate temperature and phase change patterns within the build. Apart from microstructure and track geometry, part quality also depends on residual stress and distortion, which in-situ monitoring often helps predict and control these factors.

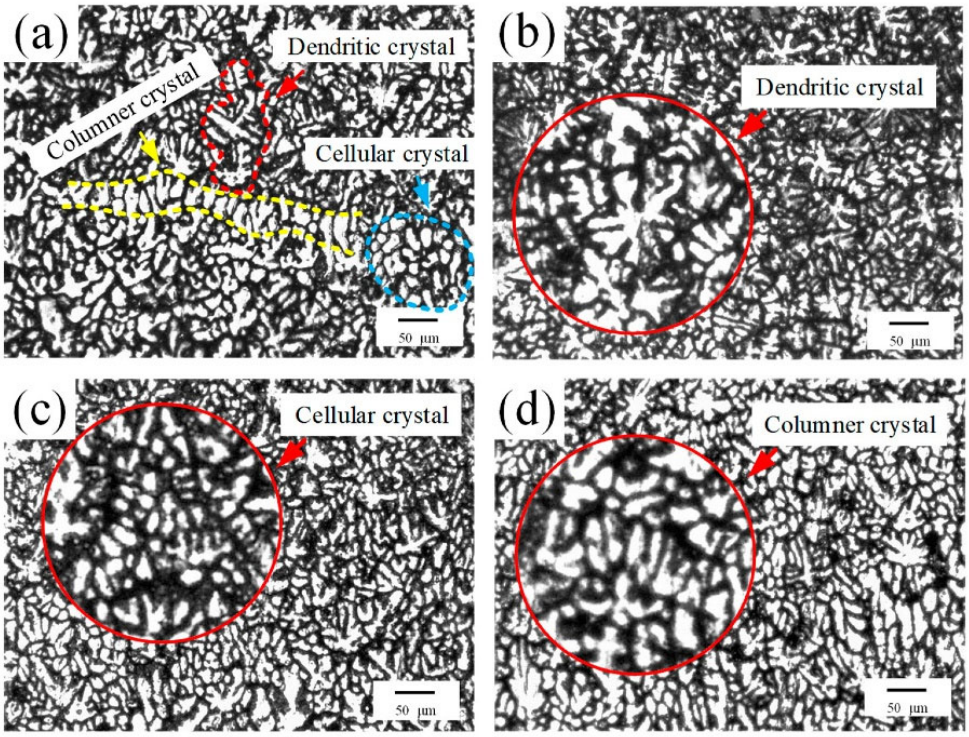


Figure 28. Super-depth-of-field images of the WAAM specimen illustrating (**a**) overall crystal morphology and detailed features from the (**b**) top, (**c**) middle, and (**d**) bottom regions [142].

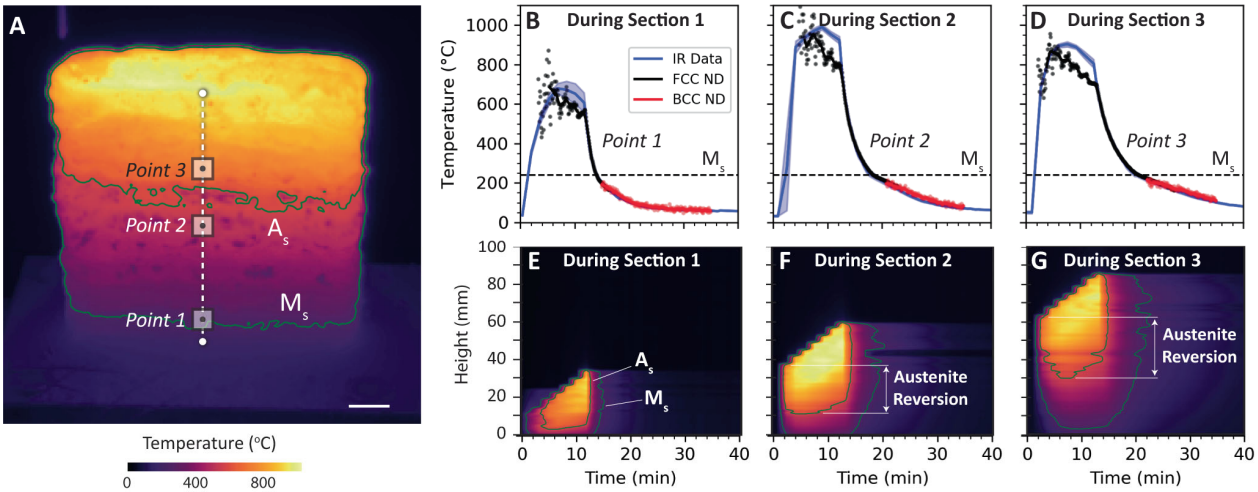


Figure 29. The thermal behavior and phase changes that occur during the multilayer WAAM fabrication process. Infrared (IR) thermography and operando neutron diffraction reveal the temperature evolution within different building sections. (**A**) Surface temperature map showing higher temperatures in the upper region of the wall, where reheating above the austenite start temperature (A_s) drives partial reversion of martensite (BCC) to austenite (FCC). (**B**–**D**) The IR and neutron data show temperature–time profiles at specific locations in sections 1–3, which demonstrate the periodic heating and cooling patterns that occurred during and after the deposition process. (**E**–**G**) The IR temperature maps display the step-by-step heating of the deposited layers and the development of thermal and phase transformation gradients that form throughout the build height [143].

9.4. In-Situ Monitoring to Reduce Residual Stress and Distortion

Residual stress and distortion are critical issues in WAAM, often leading to geometric inaccuracy, cracking, delamination between layers, and reduced mechanical performance of the final component [66,158,159]. These stresses arise from severe thermal gradients inherent to the localized heating process, repeated thermal cycles as new layers are deposited on previously solidified material, and non-uniform solidification during deposition caused by heat accumulation and variable cooling rates [160,161]. The magnitude of these stresses can exceed the material's yield strength, resulting in plastic deformation and dimensional deviation from the intended geometry. Real-time measurement and control are therefore essential to ensure dimensional accuracy, minimize part distortion, and reduce the need for extensive post-processing operations.

Digital Image Correlation (DIC) is a non-contact optical technique for in-situ measurement of strain and deformation fields [162,163]. By tracking the displacement of a stochastic pattern applied on the surface, DIC can capture real-time strain evolution with high spatial resolution. When synchronized with process parameters such as temperature or deposition rate, DIC enables quantitative mapping of transient deformation and strain accumulation between layers in WAAM. This information can be used to adjust interlayer dwell time, toolpath strategy, or heat input to minimize residual stresses and distortion. A recent study [145] demonstrated the capability of DIC to evaluate full-field residual stresses in WAAM-deposited steel walls by monitoring bending deformation (Figure 30). The DIC-measured strain fields were used to calculate residual stresses, which showed strong agreement with established techniques such as X-ray diffraction. These results highlight the potential of DIC not only for deformation tracking but also for quantitative stress analysis in WAAM builds. Laser displacement sensors provide another effective means for in-situ distortion monitoring by continuously measuring surface height variations or warping during the build [164].

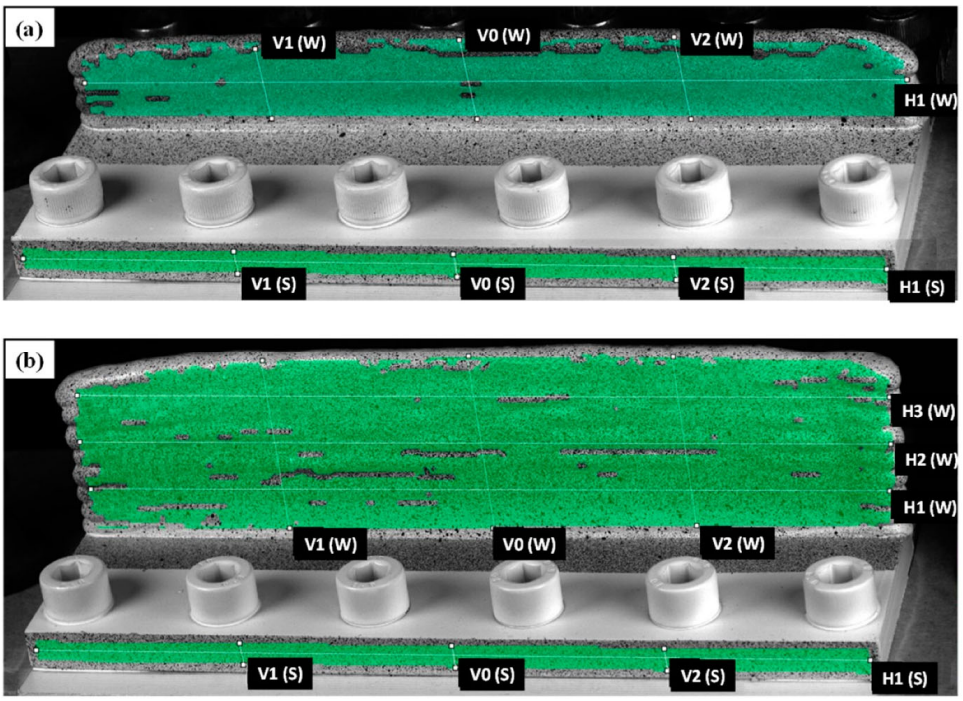


Figure 30. Digital Image Correlation (DIC) to evaluate full-field residual stresses in WAAM-deposited steel walls by monitoring bending deformation [145]. Regions of interest to extract results for comparing the (**a**) 24 mm wall and (**b**) 48 mm wall. V and H represent vertical and horizontal directions, respectively. Wall and substrate are indicated by W and S, respectively.

These sensors operate with high precision and can be easily integrated into robotic WAAM systems. Real-time displacement data allow for the detection of local distortion zones and provide feedback for the adaptive control of deposition parameters, such as current, travel speed, or wire feed rate. For example, Figure 31 shows the use of laser displacement sensors for in-situ monitoring of distortion during WAAM [144]. The schematic on the left illustrates the arrangement of laser displacement sensors placed beneath the substrate/support plate to measure vertical deformation in real time during deposition. The substrate is supported on a compliant rubber plate and fixed by a rigid support plate to simulate realistic boundary conditions while allowing measurable deflection. Laser speckles are positioned on the top surface for simultaneous surface tracking. The photograph on the right shows the actual experimental setup integrated with the WAAM torch, where the laser sensors continuously capture displacement data corresponding to layer-wise thermal distortion. This configuration enables high-precision, non-contact measurement of deformation behavior during metal deposition. While optical and laser-based approaches provide valuable surface-level insights, in-situ X-ray or synchrotron-based measurements [165,166] are needed to directly probe internal residual stresses during deposition. Such high-energy, real-time diagnostics can enable fundamental understanding and model validation for stress development mechanisms in WAAM.

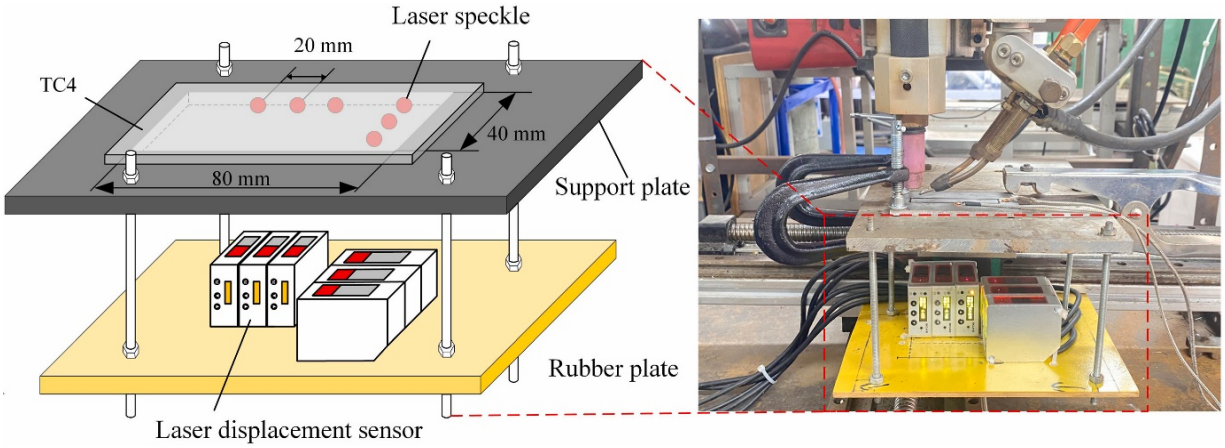


Figure 31. Experimental setup for in-situ distortion monitoring using laser displacement sensors during WAAM. Multiple sensors positioned beneath the substrate (support plate) measure real-time vertical deformation, while the compliant rubber plate allows measurable deflection. The setup enables precise, non-contact tracking of distortion evolution during deposition [144]. Sections 9.1– 9.4 discuss in-situ monitoring of important features of WAAM, which include process and product quality control. Often, this control is performed during the process, which is known as closed-loop control, as discussed.

9.5. Closed-Loop Control and Adaptive Process Parameter Adjustment

Closed-loop control refers to an automated control strategy in which process parameters are continuously adjusted based on real-time feedback from sensors to maintain desired output conditions. In this approach, measured signals are compared to target values, and corrective actions are applied to minimize deviations. Two primary types of control are feedback and feedforward. Feedback control works by continuously measuring the output of a system and adjusting the inputs based on the difference between the actual and desired output, much like a thermostat adjusting the heating based on the room temperature. Feed-forward control, on the other hand, anticipates and responds to known disturbances before they affect the system's output, similar to how a car's cruise control adjusts engine power when approaching a hill. Figure 32 schematically explains these two control models.

In WAAM, closed-loop feedback control plays a crucial role in achieving consistent bead geometry, stable arc behavior, and defect-free deposits. For instance, real-time thermal imaging data can be used to regulate the wire feed rate or welding current, thereby maintaining a constant melt pool temperature and controlling bead width and height. Similarly, optical sensors that track droplet transfer or arc length can feed back to the power supply controller to stabilize the metal transfer mode. In robotic WAAM systems, camera-based monitoring of layer height can inform motion control algorithms to automatically correct toolpath deviations caused by thermal distortion. Monitoring voltage and current signals allows dynamic adjustment of process parameters to prevent humping or internal defects. For example, a recent study [146] demonstrated the effectiveness of a closed-loop feedback approach for minimizing internal defects during short-circuit GMAW-based WAAM. In this work, the height of each deposited layer was dynamically controlled by calculating from real-time voltage and current measurements (Figure 33a) obtained during the short-circuit phase. This allowed for the automatic adjustment of height after each layer, eliminating the need for predefined height steps or empirical calibration experiments typically required in open-loop control. The closed-loop system successfully prevented the gradual accumulation of layer height errors, ensuring consistent bead geometry across multiple layers. Experimental comparisons revealed that the closed-loop method maintained stable interlayer spacing without generating internal defects (Figure 33b,c). Such adaptive feedback loops enable the system to respond instantly to variations in heat input, wire positioning, or environmental disturbances, resulting in improved dimensional accuracy, reduced defects, and reproducible microstructure.

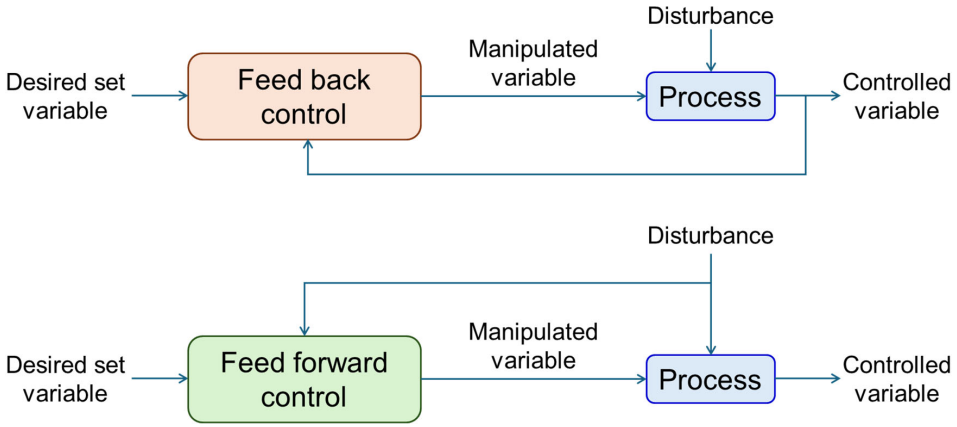


Figure 32. Schematic explanations of feedback and feed forward control models. This figure is owned by the authors.

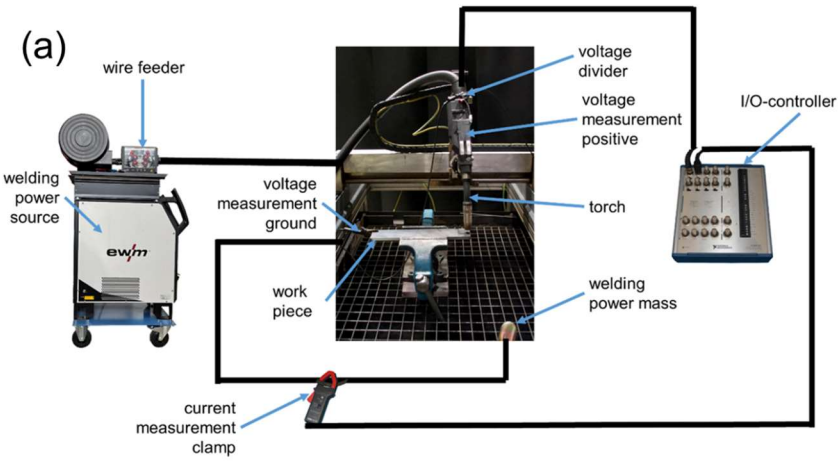


Figure 33. *Cont.*

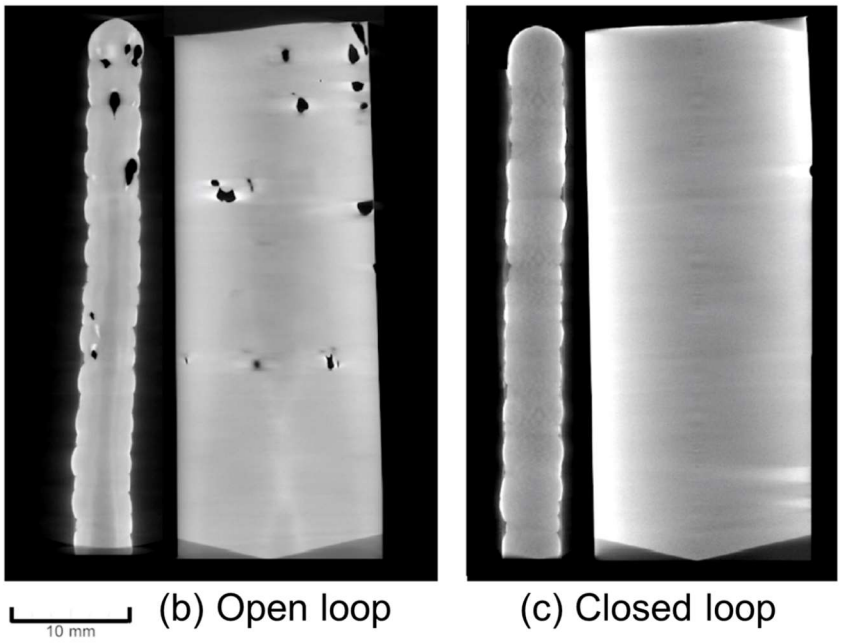


Figure 33. (**a**) Experimental setup of the closed-loop WAAM system with real-time control based on short-circuit current and voltage measurement, and corresponding microstructures of the deposited parts fabricated using (**b**) open-loop control showing internal defects and irregular bead geometry, and (**c**) closed-loop control exhibiting defect-free and uniform microstructure [146].

10. Current Challenges, Research Gaps, and Needs

Despite significant advancements in in-situ monitoring for WAAM, several critical research gaps remain that limit reliable, real-time control and industrial deployment. These gaps primarily originate from several scientific, technical, and standardization challenges. The following subsections discuss six major areas where further research and innovation are needed to strengthen the potential of in-situ monitoring in WAAM.

10.1. Standardization of Monitoring Methodologies and Protocols

Although a wide variety of sensing technologies have been applied in WAAM, the lack of standardized methodologies and data interpretation frameworks creates a major barrier to reproducibility and industrial adoption. Most studies are conducted under various system configurations, sensor setups, and process parameters, resulting in inconsistencies in measured data and performance metrics. Consequently, it becomes difficult to benchmark different monitoring approaches or compare their reliability across materials and deposition systems [167,168]. Establishing standardized protocols for monitoring device calibration, data acquisition frequency, sensor placement, and signal filtering is therefore crucial. Furthermore, there is a need for well-accepted metrics to evaluate monitoring performance in terms of sensitivity, temporal resolution, accuracy, and robustness. Standard test artifacts and controlled benchmark builds could also play an important role in validating sensor effectiveness and correlating measured signals with specific defect types or process deviations [169]. International standardization bodies such as ASTM and ISO are beginning to address AM monitoring frameworks [170,171], but WAAM-specific standards are still absent. Future research should focus on defining best practices for data labeling, documentation, and quantification of uncertainty. The establishment of open-access WAAM monitoring datasets would further accelerate comparative studies and facilitate community-driven validation.

10.2. Development of Robust, Cost-Effective, and Scalable Monitoring Systems

The harsh and dynamic WAAM environment, characterized by high thermal radiation, spatter, electromagnetic interference, and variable geometries, demands robust sensor systems capable of operating under extreme conditions [83]. Many laboratory-scale monitoring systems use high-end optical sensors or specialized instrumentation that are expensive, delicate, and not easily adaptable to industrial settings. There is thus a critical need to design durable, compact, and cost-effective sensors that can be easily integrated into robotic or multi-axis WAAM platforms without disrupting the process. Research should emphasize developing sensors with protective optics, active cooling, and real-time self-calibration features to ensure long-term stability [83]. Scalability also remains a concern, as monitoring large components or multi-material builds requires distributed sensing networks and synchronization among multiple sensors. Wireless or fiber-based sensor arrays [172] may provide a practical solution for large-scale WAAM operations. Moreover, developing modular, plug-and-play sensor architectures could significantly reduce setup time and complexity. From an economic standpoint, there is also a need to balance sensing accuracy with affordability to promote widespread adoption by small and medium manufacturers. Finally, integrating sensor health monitoring [173] and automated diagnostics will be essential for ensuring reliability during long-duration deposition.

10.3. Advanced Data Analytics and AI/ML Applications

The enormous volume and complexity of data generated during WAAM monitoring, encompassing optical, thermal, acoustic, and electrical signals, necessitate advanced data analytics and machine learning (ML) techniques for real-time interpretation. Current research primarily focuses on offline data correlation or supervised models trained on limited datasets. However, robust and generalizable AI frameworks are still lacking. Developing physics-informed ML models that combine data-driven learning with underlying process physics can enhance defect prediction accuracy and interpretability. Unsupervised ML techniques hold potential for adaptive process control, enabling real-time correction of process parameters such as current, voltage, and wire feed rate. For example, Figure 34 provides an example of the use of unsupervised ML for in-situ anomaly detection [174]. Arc current and voltage were monitored and analyzed using ML techniques for the detection of anomalies. While AI/ML techniques have demonstrated significant potential in laboratory settings for analyzing multi-modal in-situ monitoring data in WAAM, their industrial adoption remains limited due to challenges in model generalizability across different materials, equipment configurations, and operating conditions. Current industrial implementations primarily focus on simpler machine learning approaches for specific tasks such as bead geometry prediction and arc stability classification, while more sophisticated deep learning models require substantial training data, computational resources, and validation protocols that many manufacturing facilities are still developing to meet production reliability and traceability requirements.

Recently, an ML-based vision large model [175] was used to analyze in-situ images during WAAM. Several algorithms analyzed the monitored images of metal deposition (Figure 35). Another challenge lies in the fusion of multimodal data from disparate sensors, which requires synchronized data acquisition, dimensionality reduction, and feature extraction strategies. Explainable AI (XAI) methods [176] should also be explored in future WAAM monitoring systems to provide transparent, interpretable decision-making that enables operators to understand defect detection rationale and process adjustments, thereby building trust and facilitating regulatory acceptance in safety-critical industries. Additionally, establishing large annotated datasets, possibly through federated learning across institutions, can help overcome data scarcity and improve model robustness.

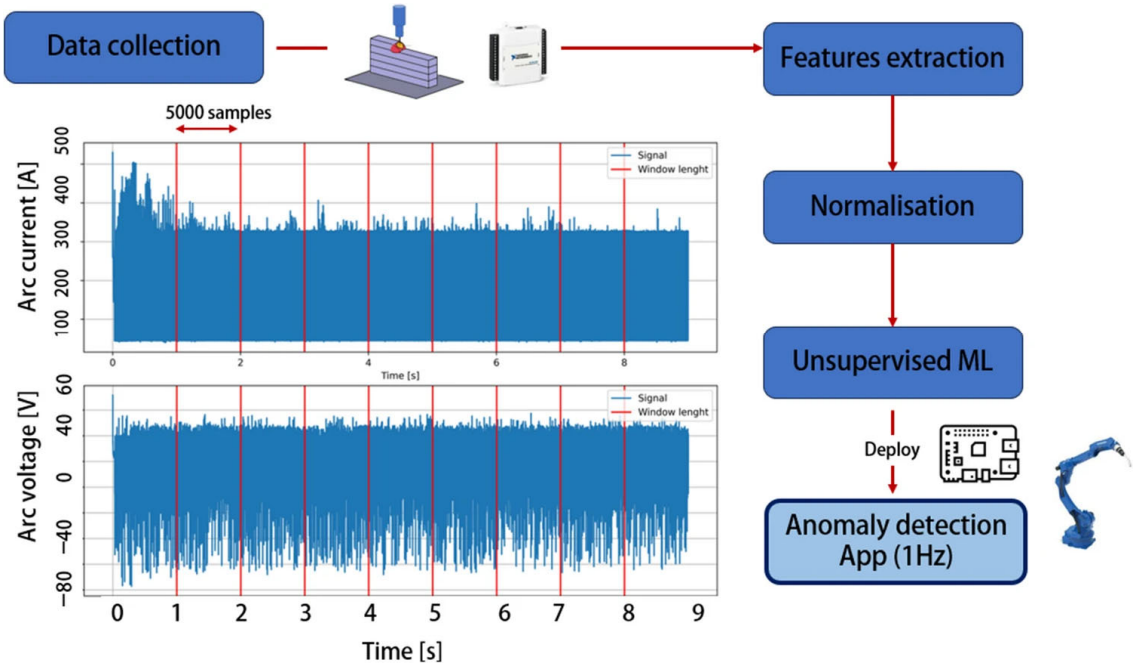


Figure 34. Anomaly detection during WAAM by analyzing the real time monitored arc current and voltage using unsupervised machine learning [174].

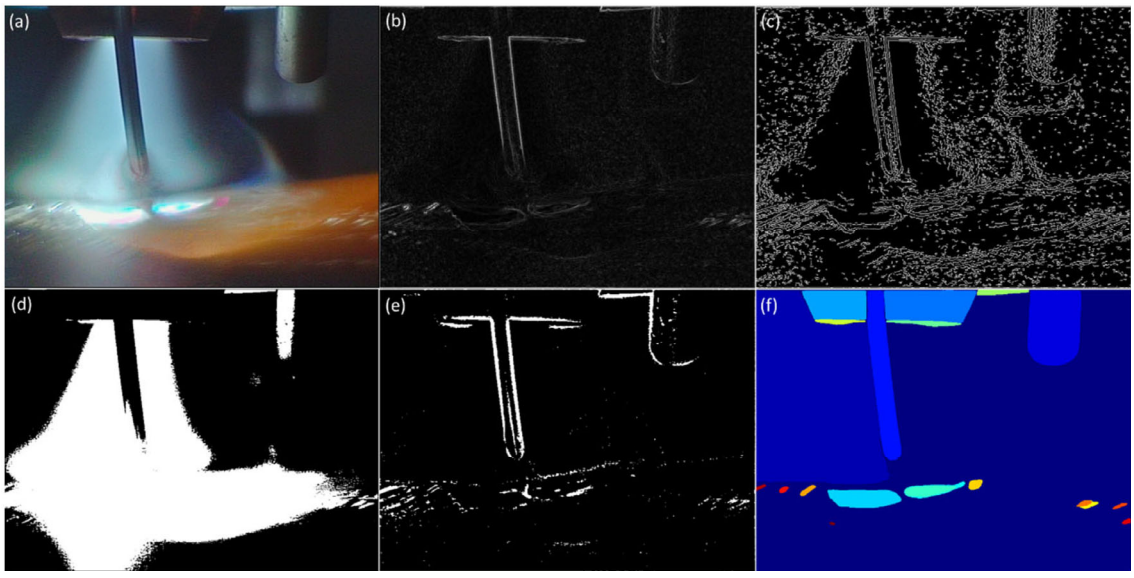


Figure 35. Applications of vision large models to analyze in-situ monitoring results in WAAM. (**a**) Image frame from a WAAM monitoring video, applying the (**b**) Sobel algorithm, (**c**) Canny algorithm, (**d**) Otsu thresh algorithm, (**e**) Adaptive thresh algorithm, and (**f**) Meta SAM (Segment Anything Model) to the frame [175].

10.4. Multi-Physics Modeling Coupled with Real-Time Monitoring

Current monitoring efforts often operate independently from process simulations, limiting their predictive power and interpretability. Integrating multi-physics modeling [177], encompassing heat transfer, fluid flow, electromagnetics, and solidification, with real-time monitoring can significantly enhance understanding of process dynamics and enable model-informed decision-making. Such integration allows the use of simulation outputs to predict trends in melt pool behavior, thermal gradients, and defect formation, which can then be validated or corrected through sensor feedback. For example, recently, a mechanistic model of WAAM was used to predict molten pool dimensions, which were

compared against high-speed imaging results [178]. Figure 36 shows both the computed and real-time monitored molten pool at two different scanning speeds. During WAAM, high-speed imaging is also often used to monitor the molten metal droplet transfer from the electrode wire to the substrate. Numerical models have been developed to simulate droplet transfer at various conditions [179]. Those models computed arc temperature and shielding gas flow fields, both of which directly influence droplet transfer [179]. Despite these recent progresses, coupling high-fidelity finite volume or finite element models with real-time monitoring remains computationally demanding. To bridge this gap, reduced-order models and surrogate modeling can provide efficient approximations that operate fast enough for on-the-fly corrections. Another emerging need is to establish two-way communication between simulations and monitoring systems, allowing models to adapt based on live sensor data while also predicting future process states. Moreover, uncertainty quantification and model calibration using real-time feedback can improve predictive accuracy.

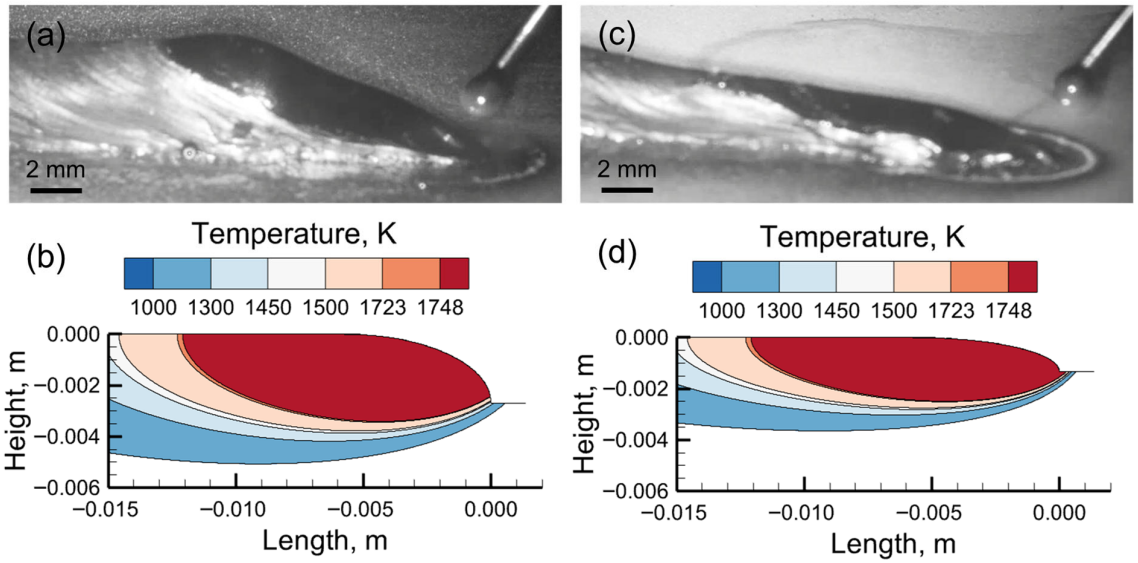


Figure 36. Experimental and computational molten pool dimensions at different scanning speeds. High-speed imaging of molten pool during wire arc deposition of ER308 stainless steel at scanning speeds of (**a**) 5 mm/s and (**c**) 10 mm/s. Computed temperature and pool geometry for the experimental cases in (**a**–**c**) at scanning speeds of (**b**) 5 mm/s and (**d**) 10 mm/s. This figure is owned by the authors.

10.5. Need for Quantum Sensing

Traditional sensors in WAAM often face limitations in resolution, response time, and stability under high electromagnetic noise and temperature fluctuations. Quantum sensing [180], based on quantum properties such as spin states or entanglement, offers a new pathway toward ultra-sensitive, noise-resilient, and high-bandwidth monitoring. Quantum magnetometers [181], for instance, can detect subtle magnetic field variations induced by current fluctuations. Table 3 provides selected examples of such quantum magnetometers and their capabilities. These magnetic field sensors have the potential to capture small variations in the magnetic field induced by the arc current in WAAM, providing new insights into arc stability and molten pool behavior. Similarly, quantum-based optical [182] and temperature [183] sensors could achieve nanoscale spatial resolution and sub-microsecond response times, providing a detailed understanding of transient phenomena such as droplet detachment or spatter formation. However, the translation of quantum sensing concepts from laboratory physics to industrial WAAM environments remains in its infancy. Future research should focus on developing robust calibration and

signal interpretation frameworks suitable for high-temperature, high-vibration conditions. Integrating quantum sensors with conventional sensors may further enhance data fidelity through the use of hybrid sensing architectures. Although currently expensive, the ongoing miniaturization and commercialization of quantum sensing technologies suggest a strong potential for their adoption in next-generation WAAM monitoring.

Table 3. Selected examples of quantum magnetic field sensors. T: Tesla. Adapted from [184].

Quantum Sensors	Sensitivity and Detection Bandwidth	Spatial Resolution	Working Temperature	Magnetic Shielding
SQUID magnetometers	2–5 fT $Hz^{-1/2}$ in the 1 Hz to 1 kHz	15 nm	Below 77 K	>100 nT
SERF atomic magnetometers	7–10 fT $Hz^{-1/2}$ in the 1–100 Hz	7–8 nm	373–423 K	<1.5 nT
Single NV-diamond magnetometers	0.5 μT $Hz^{-1/2}$ in the kHz	10 nm	Room temperature	Magnetic shielding is needed to shield the ambient magnetic field noise, when the target magnetic field is much smaller than the ambient magnetic noise.
NV ensembles diamond magnetometers	2–6 pT $Hz^{-1/2}$ in the 20–200 Hz	0.34 nm		

10.6. Transition from Lab-Scale Demonstrations to Industrial Implementation

While in-situ monitoring in WAAM has shown remarkable success in laboratory environments, industrial deployment remains limited due to challenges in system integration, reliability, and cost justification. Many current solutions rely on bulky instruments, manual calibration, and high data storage requirements that are often impractical for production lines. Bridging this gap demands collaborative efforts among academia, industry, and equipment manufacturers to develop monitoring systems compatible with commercial WAAM platforms. Scalability, interoperability, and ease of maintenance should be prioritized in system design. Industrial implementation also requires establishing robust communication protocols with robotic controllers [185]. Furthermore, the qualification and certification of monitored builds, especially for aerospace or defense applications, require traceable data documentation and compliance with manufacturing standards. Research should focus on long-duration experiments and validation under real conditions to assess system repeatability. Finally, workforce training and user-friendly visualization tools will be essential to translate monitoring data into actionable insights.

11. Outlook

In-situ monitoring in WAAM is steadily becoming an essential component of intelligent manufacturing systems, with the potential to fundamentally transform how complex metal components are fabricated. As the technology matures, three distinct yet interconnected future directions are emerging that will define the trajectory of WAAM development over the next decade: (1) the advancement toward fully autonomous, self-correcting manufacturing systems that leverage real-time sensing and adaptive control to eliminate human intervention while ensuring consistent quality; (2) the integration of WAAM into Industry 4.0 and 5.0 frameworks through smart manufacturing principles, cloud connectivity, and human-machine collaboration that enable distributed intelligence and continuous process improvement; and (3) the establishment of monitoring-enabled certification and qualification pathways that provide the traceability, transparency, and regulatory compliance required for adoption in safety-critical industries such as aerospace, defense, and automotive sectors. The following paragraphs highlight these future directions that are likely to define the research and development in this field.

The ultimate goal of in-situ monitoring research is to achieve fully autonomous and self-correcting WAAM systems capable of real-time decision-making without human inter-

vention. Achieving this objective requires integration of sensing, modeling, and control frameworks within a cyber-physical architecture [186]. Data-driven predictive models, reinforced by physics-based simulations, can anticipate process deviations before defects occur, while adaptive controllers can dynamically adjust parameters such as wire feed rate, travel speed, and current. The integration of AI algorithms with embedded control hardware will enable continuous learning and optimization during deposition. Furthermore, the development of digital twins [47,187,188] that replicate the evolving build in real time can provide a dynamic feedback loop between the physical and virtual systems, allowing not only defect detection but also autonomous correction. Such digital twins have been developed and implemented for other additive manufacturing processes (Figure 37) and can be developed and used for WAAM [188].

The convergence of in-situ monitoring with Industry 4.0 principles [189–191] will accelerate the digital transformation of WAAM. Smart manufacturing frameworks emphasize connectivity, interoperability, and real-time data exchange across sensors, machines, and cloud infrastructures. Within this system, WAAM is equipped with edge computing and IoT-enabled sensors [192] can perform distributed data analysis, enabling faster decision-making and remote supervision. Predictive maintenance [193] and quality tracking can be integrated into factory management systems, improving process reliability. Moreover, machine learning-driven analytics will support process optimization across multiple builds, contributing to a continuously improving manufacturing environment. The evolution toward Industry 5.0 [194] will further emphasize human–machine collaboration, where operators act as supervisors, aided by intelligent monitoring dashboards that visualize process health in real-time.

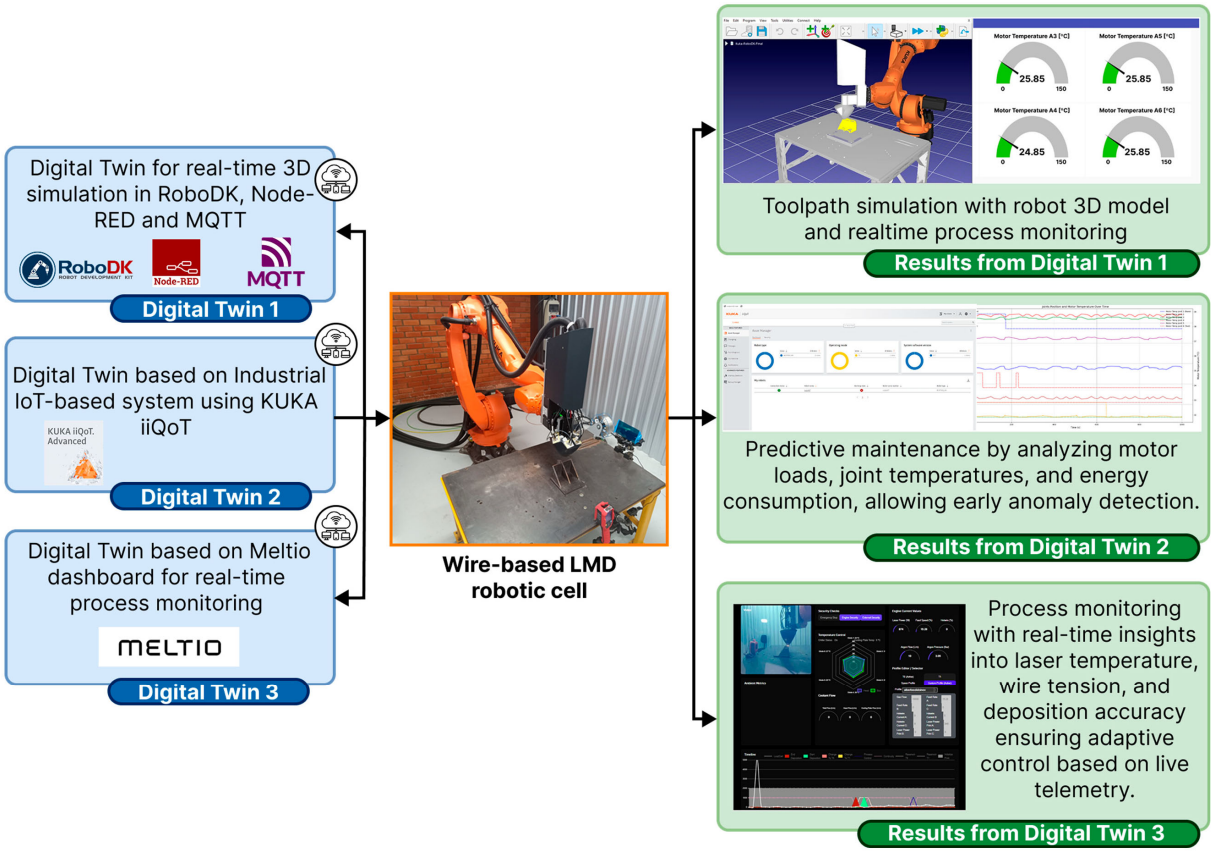


Figure 37. Various digital twins have been recently implemented for wire-based laser metal deposition (LMD) additive manufacturing [188]. A similar digital twin can be developed and used for WAAM in the future.

For WAAM to achieve widespread industrial adoption, in-situ monitoring must also support certification and qualification in critical sectors such as aerospace, automotive, and defense. These industries demand traceable, high-fidelity data to validate part integrity and ensure compliance with stringent safety and performance standards. Monitoring data can serve as a digital record for each build, supporting quality assurance, defect traceability, and life-cycle documentation. Standardizing such data streams through digital manufacturing certificates or blockchain-secured [195] process logs could enhance transparency and trust in additive production. Furthermore, collaboration between research institutions, standards organizations, and regulatory agencies will be essential to develop WAAM-specific qualification frameworks. In this context, in-situ monitoring will not only ensure process stability but also become a key enabler of digital certification, supporting fully verified, data-driven additive manufacturing ecosystems.

Author Contributions: Conceptualization: M.A., Q.N. and T.M.; Methodology: M.A. and J.M.; Formal analysis: M.A., J.M., Q.N., Y.A. and M.A.A.; Writing—original draft preparation: M.A., J.M., Q.N. and Y.A.; Writing—review and editing: M.A., J.M., Q.N., Y.A. and T.M.; Visualization: J.M., Q.N. and Y.A.; Supervision: T.M. All authors have read and agreed to the published version of the manuscript.

Funding: This research received no external funding.

Data Availability Statement: No new data was created.

Conflicts of Interest: The authors declare no conflicts of interest.

References

1. DebRoy, T.; Mukherjee, T.; Wei, H.L.; Elmer, J.W.; Milewski, J.O. Metallurgy, mechanistic models and machine learning in metal printing. *Nat. Rev. Mater.* **2021**, *6*, 48–68. [CrossRef]
2. DebRoy, T.; Wei, H.L.; Zuback, J.S.; Mukherjee, T.; Elmer, J.W.; Milewski, J.O.; Beese, A.M.; Wilson-Heid, A.; De, A.; Zhang, W. Additive manufacturing of metallic components–process, structure and properties. *Prog. Mater. Sci.* **2018**, *92*, 112–224. [CrossRef]
3. Mukherjee, T. Recent progress in process, structure, properties, and performance in additive manufacturing. *Sci. Technol. Weld. Join.* **2023**, *28*, 941–945. [CrossRef]
4. Mukherjee, T.; DebRoy, T. *Theory and Practice of Additive Manufacturing*; John Wiley & Sons: Hoboken, NJ, USA, 2023.
5. Chaturvedi, M.; Scutelnicu, E.; Rusu, C.C.; Mistodie, L.R.; Mihailescu, D.; Subbiah, A.V. Wire arc additive manufacturing: Review on recent findings and challenges in industrial applications and materials characterization. *Metals* **2021**, *11*, 939. [CrossRef]
6. Omiyale, B.O.; Olugbade, T.O.; Abioye, T.E.; Farayibi, P.K. Wire arc additive manufacturing of aluminium alloys for aerospace and automotive applications: A review. *Mater. Sci. Technol.* **2022**, *38*, 391–408. [CrossRef]
7. Pant, H.; Arora, A.; Gopakumar, G.S.; Chadha, U.; Saeidi, A.; Patterson, A.E. Applications of wire arc additive manufacturing (WAAM) for aerospace component manufacturing. *Int. J. Adv. Manuf. Technol.* **2023**, *127*, 4995–5011. [CrossRef]
8. Raut, L.P.; Taiwade, R.V. Wire arc additive manufacturing: A comprehensive review and research directions. *J. Mater. Eng. Perform.* **2021**, *30*, 4768–4791. [CrossRef]
9. Shah, A.; Aliyev, R.; Zeidler, H.; Krinke, S. A review of the recent developments and challenges in wire arc additive manufacturing (WAAM) process. *J. Manuf. Mater. Process.* **2023**, *7*, 97. [CrossRef]
10. Treutler, K.; Wesling, V. The current state of research of wire arc additive manufacturing (WAAM): A review. *Appl. Sci.* **2021**, *11*, 8619. [CrossRef]
11. Terzakis, M.A.; Papaioannou, C.; Sainz, I.; Vazquez, J.R.; Lagios, P.; Gil Illescas, E.; Stavropoulos, P. Layout Optimization of Multi-Robot Manufacturing Processing Systems: Applications in Directed Energy Deposition–Arc Additive Manufacturing and Jig-Less Welding. *Machines* **2025**, *13*, 172. [CrossRef]
12. Zarei, M.A.; Shabestari, M.G.; Shabestari, S.G.; Abedi, H. Microstructural heterogeneity and anisotropic mechanical propertiers of titanium alloys manufactured by wire arc additive manufacturing: A review. *J. Mater. Res. Technol.* **2025**, *36*, 8381–8409. [CrossRef]
13. Vijayan, V.; Panneerselvam, K.; Sathiya, P. Advancements in biocompatibility and mechanical behaviour of wire arc additive manufacturing for biomedical applications. *Multiscale Multidiscip. Model. Exp. Des.* **2025**, *8*, 190. [CrossRef]
14. Treutler, K.; Wesling, V. New Developments in the Field of Production and Application of Multi-Material Wire Arc Additive Manufacturing Components: A Review. *Adv. Eng. Mater.* **2025**, *27*, 2500578. [CrossRef]

15. Raspall, F.; Araya, S.; Pazols, M.; Valenzuela, E.; Castillo, M.; Benavides, P. Wire Arc Additive Manufacturing for Widespread Architectural Application: A Review Informed by Large-Scale Prototypes. *Buildings* **2025**, *15*, 906. [CrossRef]
16. Omiyale, B.O.; Ogedengbe, I.I.; Olugbade, T.O.; Rasheed, A.A.; Ogbeyemi, A.; Farayibi, P.K. Cold metal transfer WAAM of aluminum alloys: Influence of processing parameters. *Int. J. Adv. Manuf. Technol.* **2025**, *136*, 1967–1987. [CrossRef]
17. Omiyale, B.O.; Ogedengbe, I.I.; Ogbeyemi, A.; Olugbade, T.O.; Zhang, W.C.; Farayibi, P.K. Influence of heat input and uniform temperature distribution during wire arc additive manufacturing process: A critical review. *Int. J. Adv. Manuf. Technol.* **2025**, *138*, 2673–2695. [CrossRef]
18. Omiyale, B.O.; Ogedengbe, I.I.; Ogbeyemi, A.; Akinfolarin, J.F.; Adewole, K.A.; Zhang, W.C. Defects in Wire Arc Additive Manufacturing of Stainless Steel: A Brief Critical Review. *Lasers Manuf. Mater. Process.* **2025**, *12*, 1061–1105. [CrossRef]
19. Omiyale, B.O.; Jack, T.A.; Ogedengbe, I.I.; Odeyemi, J.; Mishra, D.; Ogbeyemi, A.; Zhang, W.C. Impact of cold metal transfer variants on the mechanical and microstructural properties of aluminum alloys in wire arc additive manufacturing: A critical review. *Int. J. Adv. Manuf. Technol.* **2025**, *140*, 1183–1210. [CrossRef]
20. Nagalingam, A.P.; Shamir, M.; Tureyen, E.B.; Sharman, A.R.C.; Poyraz, O.; Yasa, E.; Hughes, J. Recent progress in wire-arc and wire-laser directed energy deposition (DED) of titanium and aluminium alloys. *Int. J. Adv. Manuf. Technol.* **2025**, *136*, 2035–2073. [CrossRef]
21. Mishra, S.K.; R, S.P.; Jose, S.S.S.; Upadhyay, R.K. Wire arc additive manufacturing: Materials, processes and its constraints. *Mater. Manuf. Process.* **2025**, *40*, 723–740. [CrossRef]
22. Lambiase, F.; Yanala, P.B.; Pace, F.; Andreucci, E.; Paoletti, A. A state of the art review of wire arc additive manufacturing (WAAM)-part 1: Process fundamentals, parameters and materials. *Int. J. Adv. Manuf. Technol.* **2025**, *138*, 4965–4993. [CrossRef]
23. Kishor, G.; Mugada, K.K.; Mahto, R.P. Wire Arc Additive Manufacturing of Titanium Alloys for Enhancing Mechanical Properties and Grain-Refinement. *Met. Mater. Int.* **2025**, 1–31. [CrossRef]
24. Kim, Y.H.; Gunasegaram, D.R.; Cleary, P.W.; Murphy, A.B. Numerical modelling of wire arc additive manufacturing: Methods, status, trends, and opportunities. *J. Phys. D Appl. Phys.* **2025**, *58*, 143001. [CrossRef]
25. Jadhav, S.; Kusekar, S.; Belure, A.; Digole, S.; Mali, A.; Cheepu, M.; Mugale, M.; Alkunte, S.; Kim, D. Recent Progress and Scientific Challenges in Wire-Arc Additive Manufacturing of Metallic Multi-Material Structures. *J. Manuf. Mater. Process.* **2025**, *9*, 284. [CrossRef]
26. Guo, C.; Lin, Q.; Hu, R.; Wu, S. Research Progress and Application Scenarios of Wire plus Arc Additive Manufacturing: From Process Control to Performance Evaluation. *Micromachines* **2025**, *16*, 749. [CrossRef]
27. Gerashi, E.; Duan, X.; Alidokht, S.A. Functionally Graded Materials Fabrication Using Wire Arc Additive Manufacturing: A Review of Recent Research Progress. *J. Mater. Eng. Perform.* **2025**, *34*, 29062–29093. [CrossRef]
28. Gain, S.; Veeman, D. A review on advances and challenges in wire arc additive manufacturing: Process parameters, microstructural evolution and material performance across alloys. *J. Alloys Compd.* **2025**, *1029*, 180735. [CrossRef]
29. Dekis, M.; Tawfik, M.; Egiza, M.; Dewidar, M. Challenges and developments in wire arc additive manufacturing of steel: A review. *Results Eng.* **2025**, *26*, 104657. [CrossRef]
30. Chen, Z.; Yuan, L.; Pan, Z.; Zhu, H.; Ma, N.; Ding, D.; Li, H. A comprehensive review and future perspectives of simulation approaches in wire arc additive manufacturing (WAAM). *Int. J. Extrem. Manuf.* **2025**, *7*, 022016. [CrossRef]
31. Zhang, H.; Li, R.; Liu, J.; Wang, K.; Weijian, Q.; Shi, L.; Lei, L.; He, W.; Wu, S. State-of-art review on the process-structure-properties-performance linkage in wire arc additive manufacturing. *Virtual Phys. Prototyp.* **2024**, *19*, e2390495. [CrossRef]
32. Yadav, S.; Mukherjee, M.; Singh, D. Review of current challenges in the implementation of WAAM for Ti-6Al-4 V alloys. *Int. J. Adv. Manuf. Technol.* **2024**, *133*, 2103–2130. [CrossRef]
33. Wani, Z.K.; Abdullah, A.B. Bead Geometry Control in Wire Arc Additive Manufactured Profile—A Review. *Pertanika J. Sci. Technol.* **2024**, *32*, 917–942. [CrossRef]
34. AbouelNour, Y.; Gupta, N. In-situ monitoring of sub-surface and internal defects in additive manufacturing: A review. *Mater. Des.* **2022**, *222*, 111063. [CrossRef]
35. Everton, S.K.; Hirsch, M.; Stravroulakis, P.; Leach, R.K.; Clare, A.T. Review of in-situ process monitoring and in-situ metrology for metal additive manufacturing. *Mater. Des.* **2016**, *95*, 431–445. [CrossRef]
36. Tapia, G.; Elwany, A. A Review on Process Monitoring and Control in Metal-Based Additive Manufacturing. *J. Manuf. Sci. Eng.* **2014**, *136*, 060801. [CrossRef]
37. Herzog, T.; Brandt, M.; Trinchi, A.; Sola, A.; Molotnikov, A. Process monitoring and machine learning for defect detection in laser-based metal additive manufacturing. *J. Intell. Manuf.* **2024**, *35*, 1407–1437. [CrossRef]
38. Hou, Z.-J.; Wang, Q.; Zhao, C.-G.; Zheng, J.; Tian, J.-M.; Ge, X.-H.; Liu, Y.-G. Online monitoring technology of metal powder bed fusion processes: A review. *Materials* **2022**, *15*, 7598. [CrossRef]

39. McCann, R.; Obeidi, M.A.; Hughes, C.; McCarthy, É.; Egan, D.S.; Vijayaraghavan, R.K.; Joshi, A.M.; Garzon, V.A.; Dowling, D.P.; McNally, P.J.; et al. In-situ sensing, process monitoring and machine control in Laser Powder Bed Fusion: A review. *Addit. Manuf.* **2021**, *45*, 102058. [CrossRef]
40. Papatheodorou, A.; Papadimitriou, N.; Stathatos, E.; Benardos, P.; Vosniakos, G.-C. Recent Advances in Sensor Fusion Monitoring and Control Strategies in Laser Powder Bed Fusion: A Review. *Machines* **2025**, *13*, 820. [CrossRef]
41. Taherkhani, K.; Ero, O.; Liravi, F.; Toorandaz, S.; Toyserkani, E. On the application of in-situ monitoring systems and machine learning algorithms for developing quality assurance platforms in laser powder bed fusion: A review. *J. Manuf. Process.* **2023**, *99*, 848–897. [CrossRef]
42. Ansari, M.J.; Roccisano, A.; Arcondoulis, E.J.; Schulz, C.; Schläfer, T.; Hall, C. Advancements in In-Situ Monitoring Technologies for Detecting Process-Induced Defects in the Directed Energy Deposition Process: A Comprehensive Review. *Materials* **2025**, *18*, 4304. [CrossRef]
43. Haley, J.; Karandikar, J.; Herberger, C.; MacDonald, E.; Feldhausen, T.; Lee, Y. Review of in situ process monitoring for metal hybrid directed energy deposition. *J. Manuf. Process.* **2024**, *109*, 128–139. [CrossRef]
44. Imran, M.M.; Idris, A.C.; De Silva, L.C.; Kim, Y.-B.; Abas, P.E. Advancements in 3D printing: Directed energy deposition techniques, defect analysis, and quality monitoring. *Technologies* **2024**, *12*, 86. [CrossRef]
45. Liu, W.; Wang, T.; Liu, B.; Li, W.; Hu, G.; Lyu, Z. Research of on-line monitoring technology and control strategy for laser-directed energy deposition: A review. *Int. J. Adv. Manuf. Technol.* **2024**, *133*, 3105–3132. [CrossRef]
46. Fan, H.; Liu, C.; Bian, S.; Ma, C.; Huang, J.; Liu, X.; Doyle, M.; Lu, T.; Chow, E.; Chen, L.; et al. New era towards autonomous additive manufacturing: A review of recent trends and future perspectives. *Int. J. Extrem. Manuf.* **2025**, *7*, 032006. [CrossRef]
47. Kim, C.J.; Han, S.B.; Seo, B.W.; Bae, I.; Kim, D.; Kim, S.; Cho, Y.T. Architecture Development of Digital Twin-Based Wire Arc Directed Energy Deposition. *Int. J. Precis. Eng. Manuf. Green Technol.* **2025**, *12*, 885–904. [CrossRef]
48. Kim, K.W.; Kamerkar, A.; Chiu, T.E.; Abdi, I.; Qin, J.; Suder, W.; Asif, S. WAAM-ViD: Towards universal vision-based monitoring for wire arc additive manufacturing. *Front. Manuf. Technol.* **2025**, *5*, 1676365. [CrossRef]
49. Mattera, G.; Chozaki, S.P.; Norrish, J. Advances in machine learning for parameters optimisation and in-situ monitoring of wire arc additive manufacturing. *Weld. World* **2025**, 1–30. [CrossRef]
50. Sell, S.; Villani, K.; Stautner, M. Reducing Delivery Times by Utilising On-Site Wire Arc Additive Manufacturing with Digital-Twin Methods. *Computers* **2025**, *14*, 221. [CrossRef]
51. Cai, Y.; Xiong, J.; Chen, H.; Zhang, G. A review of in-situ monitoring and process control system in metal-based laser additive manufacturing. *J. Manuf. Syst.* **2023**, *70*, 309–326. [CrossRef]
52. Jorge, V.L.; Teixeira, F.R.; Scotti, A. Pyrometrical interlayer temperature measurement in WAAM of thin wall: Strategies, limitations and functionality. *Metals* **2022**, *12*, 765. [CrossRef]
53. Keshmiri, M.; Dehgahi, S.; Mohiuddin, A.; Qureshi, A.J. Transformer based spatially resolved prediction of mechanical properties in wire arc additive manufacturing. *Sci. Rep.* **2025**, *15*, 21662. [CrossRef] [PubMed]
54. Shi, X.; Cai, C.; Bao, P.; Li, Z. Influence of ship-based vibration on characteristics of arc and droplet and morphology in wire arc additive manufacturing. *Chin. J. Mech. Eng. Addit. Manuf. Front.* **2023**, *2*, 100067. [CrossRef]
55. Arjomandi, M.; Ngo, Q.; Mukherjee, T. Effects of gravity on track integrity during collaborative robot assisted wire arc deposition. *SFF*, 2025; *in press*.
56. Singh, S.; Sharma, S.K.; Rathod, D.W. A review on process planning strategies and challenges of WAAM. *Mater. Today Proc.* **2021**, *47*, 6564–6575. [CrossRef]
57. Chabot, A.; Laroche, N.; Carcreff, E.; Rauch, M.; Hascoët, J.-Y. Towards defect monitoring for metallic additive manufacturing components using phased array ultrasonic testing. *J. Intell. Manuf.* **2020**, *31*, 1191–1201. [CrossRef]
58. Franke, J.; Heinrich, F.; Reisch, R.T. Vision based process monitoring in wire arc additive manufacturing (WAAM). *J. Intell. Manuf.* **2025**, *36*, 1711–1721. [CrossRef]
59. Guo, Y.; Zhang, Y.; Pan, Z.; Zhou, W. Recent progress of sensing and machine learning technologies for process monitoring and defects detection in wire arc additive manufacturing. *J. Manuf. Process.* **2024**, *125*, 489–511. [CrossRef]
60. Li, Y.; Mu, H.; Polden, J.; Li, H.; Wang, L.; Xia, C.; Pan, Z. Towards intelligent monitoring system in wire arc additive manufacturing: A surface anomaly detector on a small dataset. *Int. J. Adv. Manuf. Technol.* **2022**, *120*, 5225–5242. [CrossRef]
61. Xia, C.; Pan, Z.; Polden, J.; Li, H.; Xu, Y.; Chen, S.; Zhang, Y. A review on wire arc additive manufacturing: Monitoring, control and a framework of automated system. *J. Manuf. Syst.* **2020**, *57*, 31–45. [CrossRef]
62. Zimermann, R.; Mohseni, E.; Vasilev, M.; Loukas, C.; Vithanage, R.K.W.; Macleod, C.N.; Lines, D.; Javadi, Y.; E Silva, M.P.E.; Fitzpatrick, S.; et al. Collaborative robotic wire+ arc additive manufacture and sensor-enabled in-process ultrasonic non-destructive evaluation. *Sensors* **2022**, *22*, 4203. [CrossRef]

63. Artaza, T.; Alberdi, A.; Murua, M.; Gorrotxategi, J.; Frías, J.; Puertas, G.; Melchor, M.; Mugica, D.; Suárez, A. Design and integration of WAAM technology and in situ monitoring system in a gantry machine. *Procedia Manuf.* **2017**, *13*, 778–785. [CrossRef]
64. Yang, D.; Wang, G.; Zhang, G. Thermal analysis for single-pass multi-layer GMAW based additive manufacturing using infrared thermography. *J. Mater. Process. Technol.* **2017**, *244*, 215–224. [CrossRef]
65. Lockett, H.; Ding, J.; Williams, S.; Martina, F. Design for Wire+ Arc Additive Manufacture: Design rules and build orientation selection. *J. Eng. Des.* **2017**, *28*, 568–598. [CrossRef]
66. Arjomandi, M.; Sanvelly, R.R.; Mukherjee, T. Variations in temperature, residual stress, and distortion in collaborative robot-assisted patterned additive manufacturing. *Manuf. Lett.* **2025**, *43*, 64–69. [CrossRef]
67. Zahidin, M.R.; Yusof, F.; Rashid, S.H.A.; Mansor, S.; Raja, S.; Jamaludin, M.F.; Manurung, Y.H.; Adenan, M.S.; Hussein, N.I.S. Research challenges, quality control and monitoring strategy for Wire Arc Additive Manufacturing. *J. Mater. Res. Technol.* **2023**, *24*, 2769–2794. [CrossRef]
68. Rosli, N.A.; Alkahari, M.R.; Ramli, F.R.; Sudin, M.N.; Maidin, S. Influence of process parameters in wire and arc additive manufacturing (WAAM) process. *J. Mech. Eng. (JMechE)* **2020**, *17*, 69–78. [CrossRef]
69. He, H.; Wen, J.T. Wire Arc Additive Manufacturing With Infrared Image Feedback. *ASME Lett. Transl. Robot.* **2025**, *1*, 011004. [CrossRef]
70. Luo, L.; Qian, E.; Lu, T.; Pan, J.; Liu, M.; Liu, C.; Guo, Y.; Bi, L. Vision-based estimation of force balance of near-suspended melt pool for drooping and collapsing prediction. *Sensors* **2024**, *24*, 3270. [CrossRef]
71. Wang, Y.; Zhang, D.; Zhang, C. Metal Transfer Behavior and Molten Pool Dynamics in Cold Metal Transfer Pulse Advanced Additive Manufacturing of 7075 Aluminum Alloy. *Micromachines* **2024**, *15*, 1489. [CrossRef]
72. Pal, K.; Bhattacharya, S.; Pal, S.K. Prediction of metal deposition from arc sound and weld temperature signatures in pulsed MIG welding. *Int. J. Adv. Manuf. Technol.* **2009**, *45*, 1113. [CrossRef]
73. Bevans, B.; Ramalho, A.; Smoqi, Z.; Gaikwad, A.; Santos, T.G.; Rao, P.; Oliveira, J. Monitoring and flaw detection during wire-based directed energy deposition using in-situ acoustic sensing and wavelet graph signal analysis. *Mater. Des.* **2023**, *225*, 111480. [CrossRef]
74. Bhattacharya, S.; Pal, K.; Pal, S.K. Multi-sensor based prediction of metal deposition in pulsed gas metal arc welding using various soft computing models. *Appl. Soft Comput.* **2012**, *12*, 498–505. [CrossRef]
75. Gao, Q.; Lyu, F.; Wang, L.; Zhan, X. Investigation of Arc Stability in Wire Arc Additive Manufacturing of 2319 Aluminum Alloy. *Materials* **2024**, *17*, 5160. [CrossRef] [PubMed]
76. Sreedhar, U.; Krishnamurthy, C.; Balasubramaniam, K.; Raghupathy, V.; Ravisankar, S. Automatic defect identification using thermal image analysis for online weld quality monitoring. *J. Mater. Process. Technol.* **2012**, *212*, 1557–1566. [CrossRef]
77. Xiong, J.; Li, Y.-J.; Yin, Z.-Q.; Chen, H. Determination of surface roughness in wire and arc additive manufacturing based on laser vision sensing. *Chin. J. Mech. Eng.* **2018**, *31*, 74. [CrossRef]
78. Xiong, J.; Zhang, Y.; Pi, Y. Control of deposition height in WAAM using visual inspection of previous and current layers. *J. Intell. Manuf.* **2021**, *32*, 2209. [CrossRef]
79. Serrati, D.S.M.; Machado, M.A.; Oliveira, J.P.; Santos, T.G. Non-Destructive Testing Inspection for Metal Components Produced Using Wire and Arc Additive Manufacturing. *Metals* **2023**, *13*, 648. [CrossRef]
80. Hossain, M.S.; Gonzalez, J.A.; Hernandez, R.M.; Shuvo, M.A.I.; Mireles, J.; Choudhuri, A.; Lin, Y.; Wicker, R.B. Fabrication of smart parts using powder bed fusion additive manufacturing technology. *Addit. Manuf.* **2016**, *10*, 58–66. [CrossRef]
81. Li, X. Embedded Sensors in Layered Manufacturing. Ph.D. Thesis, Stanford University, Stanford, CA, USA, 2001.
82. Pixner, F.; Buzolin, R.; Schönfelder, S.; Theuermann, D.; Warchomicka, F.; Enzinger, N. Contactless temperature measurement in wire-based electron beam additive manufacturing Ti-6Al-4V. *Weld. World* **2021**, *65*, 1307–1322. [CrossRef]
83. Sivakumar, M.; Karthikeyan, R.; Balaji, N.S.; Kannan, G.R. Advanced Techniques in Wire Arc Additive Manufacturing: Monitoring, Control, and Automation. *Adv. Addit. Manuf.* **2024**, 443–466. [CrossRef]
84. Dong, K.; Wu, Q.; Qin, X.; Hu, Z.; Hua, L. In-situ optical monitoring and analysis of weld pool based on machine vision for wire and arc additive manufacturing. *Int. J. Adv. Manuf. Technol.* **2024**, *133*, 4865–4878. [CrossRef]
85. Leung, C.L.A.; Marussi, S.; Towrie, M.; Atwood, R.C.; Withers, P.J.; Lee, P.D. The effect of powder oxidation on defect formation in laser additive manufacturing. *Acta Mater.* **2019**, *166*, 294–305. [CrossRef]
86. Qin, J.; Wang, Y.; Ding, J.; Williams, S. Optimal droplet transfer mode maintenance for wire+ arc additive manufacturing (WAAM) based on deep learning. *J. Intell. Manuf.* **2022**, *33*, 2179–2191. [CrossRef]
87. Varela, J.; Merino, J.; Pickett, C.; Abu-Issa, A.; Arrieta, E.; Murr, L.E.; Wicker, R.B.; Ahlfors, M.; Godfrey, D.; Medina, F. Performance characterization of laser powder bed fusion fabricated Inconel 718 treated with experimental hot isostatic processing cycles. *J. Manuf. Mater. Process.* **2020**, *4*, 73. [CrossRef]
88. Zhang, Y.; Shen, S.; Li, H.; Hu, Y. Review of in situ and real-time monitoring of metal additive manufacturing based on image processing. *Int. J. Adv. Manuf. Technol.* **2022**, *123*, 1–20. [CrossRef]

89. He, K.; Zhang, X.; Ren, S.; Sun, J. Deep residual learning for image recognition. In Proceedings of the IEEE Conference on Computer Vision and Pattern Recognition, Las Vegas, NV, USA, 27–30 June 2016.
90. Sarid, O.; Huss, E. Image formation and image transformation. *Arts Psychother.* **2011**, *38*, 252–255. [CrossRef]
91. Cheng, H.; Jiang, X.; Sun, Y.; Wang, J. Color image segmentation: Advances and prospects. *Pattern Recognit.* **2001**, *34*, 2259–2281. [CrossRef]
92. Wang, D.C.; Vagnucci, A.H.; Li, C. Digital image enhancement: A survey. *Comput. Vis. Graph. Image Process.* **1983**, *24*, 363–381. [CrossRef]
93. Ronneberger, O.; Fischer, P.; Brox, T. U-net: Convolutional networks for biomedical image segmentation. In *International Conference on Medical Image Computing and Computer-Assisted Intervention*; Springer International Publishing: Cham, Switzerland, 2015.
94. Wu, Q.; Qin, X.; Dong, K.; Shi, A.; Hu, Z. A learning-based crack defect detection and 3D localization framework for automated fluorescent magnetic particle inspection. *Expert Syst. Appl.* **2023**, *214*, 118966. [CrossRef]
95. Cunha, F.G.; Santos, T.G.; Xavier, J. In situ monitoring of additive manufacturing using digital image correlation: A review. *Materials* **2021**, *14*, 1511. [CrossRef]
96. Tang, S.; Wang, G.; Huang, C.; Li, R.; Zhou, S.; Zhang, H. Investigation, modeling and optimization of abnormal areas of weld beads in wire and arc additive manufacturing. *Rapid Prototyp. J.* **2020**, *26*, 1183–1195. [CrossRef]
97. Shen, B.; Lu, J.; Wang, Y.; Chen, D.; Han, J.; Zhang, Y.; Zhao, Z. Multimodal-based weld reinforcement monitoring system for wire arc additive manufacturing. *J. Mater. Res. Technol.* **2022**, *20*, 561–571. [CrossRef]
98. Nagarajan, S.; Chen, W.H.; Chin, B.A. Infrared sensing for adaptive arc welding. *Weld. J.* **1989**, *68*, 462–466.
99. Yousef, S.G.; Sperfeld, P.; Metzdorf, J. Measurement and calculation of the emissivity of a high-temperature black body. *Metrologia* **2000**, *37*, 365. [CrossRef]
100. Reis, D.; Kupec, J.; Hong, J.; Daoudi, A. Real-time flying object detection with YOLOv8. *arXiv* **2023**, arXiv:2305.09972. [CrossRef]
101. Wu, B.; Pan, Z.; Ding, D.; Cuiuri, D.; Li, H.; Xu, J.; Norrish, J. A review of the wire arc additive manufacturing of metals: Properties, defects and quality improvement. *J. Manuf. Process.* **2018**, *35*, 127–139. [CrossRef]
102. Jafari, D.; Vaneker, T.H.; Gibson, I. Wire and arc additive manufacturing: Opportunities and challenges to control the quality and accuracy of manufactured parts. *Mater. Des.* **2021**, *202*, 109471. [CrossRef]
103. Li, Y.; Su, C.; Zhu, J. Comprehensive review of wire arc additive manufacturing: Hardware system, physical process, monitoring, property characterization, application and future prospects. *Results Eng.* **2022**, *13*, 100330. [CrossRef]
104. Yu, R.; Li, W.; Wu, M.; Wang, J.; Han, Q.; Wang, J.; Bing, S. Advanced visual sensing and control in CMT-based WAAM processes. *Front. Mater.* **2025**, *12*, 1499635. [CrossRef]
105. Pal, K.; Bhattacharya, S.; Pal, S.K. Investigation on arc sound and metal transfer modes for on-line monitoring in pulsed gas metal arc welding. *J. Mater. Process. Technol.* **2010**, *210*, 1397–1410. [CrossRef]
106. Ramalho, A.; Santos, T.G.; Bevans, B.; Smoqi, Z.; Rao, P.; Oliveira, J. Effect of contaminations on the acoustic emissions during wire and arc additive manufacturing of 316L stainless steel. *Addit. Manuf.* **2022**, *51*, 102585. [CrossRef]
107. Čudina, M.; Prezelj, J. Evaluation of the sound signal based on the welding current in the gas—Metal arc welding process. *Proc. Inst. Mech. Eng. Part C J. Mech. Eng. Sci.* **2003**, *217*, 483–494. [CrossRef]
108. Arata, Y.; Inoue, K.; Futamata, M.; Toh, T. INVESTIGATION ON WELDING ARC SOUND. II: EVALUATION BY HEARING ACUITY AND SOME CHARACTERISTICS OF ARC SOUND. *Trans. JWRI* **1979**, *8*, 193–198.
109. Doumanidis, C.; Kwak, Y.-M. Multivariable adaptive control of the bead profile geometry in gas metal arc welding with thermal scanning. *Int. J. Press. Vessel. Pip.* **2002**, *79*, 251–262. [CrossRef]
110. Müller, J.; Hensel, J.; Dilger, K. Mechanical properties of wire and arc additively manufactured high-strength steel structures. *Weld. World* **2022**, *66*, 395–407. [CrossRef]
111. Yang, J.; Sun, S.; Brandt, M.; Yan, W. Experimental investigation and 3D finite element prediction of the heat affected zone during laser assisted machining of Ti6Al4V alloy. *J. Mater. Process. Technol.* **2010**, *210*, 2215–2222. [CrossRef]
112. Machado, M.A.; Silva, M.I.; Martins, A.P.; Carvalho, M.S.; Santos, T.G. Double active transient thermography. *NDT E Int.* **2022**, *125*, 102566. [CrossRef]
113. Gurmesa, F.D.; Lemu, H.G. Literature review on thermomechanical modelling and analysis of residual stress effects in wire arc additive manufacturing. *Metals* **2023**, *13*, 526. [CrossRef]
114. da Silva, L.J.; Souza, D.M.; de Araújo, D.B.; Reis, R.P.; Scotti, A. Concept and validation of an active cooling technique to mitigate heat accumulation in WAAM. *Int. J. Adv. Manuf. Technol.* **2020**, *107*, 2513–2523. [CrossRef]
115. Geng, H.; Li, J.; Xiong, J.; Lin, X. Optimisation of interpass temperature and heat input for wire and arc additive manufacturing 5A06 aluminium alloy. *Sci. Technol. Weld. Join.* **2017**, *22*, 472–483. [CrossRef]
116. Vollmer, M.; Möllmann, K.P. *Infrared Thermal Imaging: Fundamentals, Research and Applications*; John Wiley & Sons: Hoboken, NJ, USA, 2018.
117. Bradshaw, F.J. The optical emissivity of titanium and zirconium. *Proc. Phys. Soc. Sect. B* **1950**, *63*, 573. [CrossRef]

118. Li, L.; Yu, K.; Zhang, K.; Liu, Y. Study of Ti–6Al–4V alloy spectral emissivity characteristics during thermal oxidation process. *Int. J. Heat Mass Transf.* **2016**, *101*, 699–706. [CrossRef]
119. Scotti, F.M.; Teixeira, F.R.; da Silva, L.J.; de Araújo, D.B.; Reis, R.P.; Scotti, A. Thermal management in WAAM through the CMT Advanced process and an active cooling technique. *J. Manuf. Process.* **2020**, *57*, 23–35. [CrossRef]
120. Halisch, C.; Radel, T.; Tyralla, D.; Seefeld, T. Online Monitoring in WAAM: Using a two colored pyrometric camera for temperature field monitoring in wire arc additive manufacturing. *PhotonicsViews* **2021**, *18*, 2–3. [CrossRef]
121. Richter, A.; Rembe, C.; Gehling, T.; Treutler, K.; Wesling, V. Echtzeittemperaturmessung bei additivem Lichtbogenschweißen/Real-time temperature measurement at wire arc additive welding. *Tech. Mess.* **2019**, *86*, 112. [CrossRef]
122. Baier, D.; Weckenmann, T.; Wolf, F.; Wimmer, A.; Zaeh, M.F. Underlying methodology for a thermal process monitoring system for wire and arc additive manufacturing. *J. Manuf. Mater. Process.* **2022**, *7*, 10. [CrossRef]
123. Coppa, P.; Consorti, A. Normal emissivity of samples surrounded by surfaces at diverse temperatures. *Measurement* **2005**, *38*, 124–131. [CrossRef]
124. Derekar, K.; Lawrence, J.; Melton, G.; Addison, A.; Zhang, X.; Xu, L. Influence of interpass temperature on wire arc additive manufacturing (WAAM) of aluminium alloy components. In *MATEC Web of Conferences*; EDP Sciences: Les Ulis, France, 2019.
125. Knezović, N.; Garašić, I.; Jurić, I. Influence of the interlayer temperature on structure and properties of wire and arc additive manufactured duplex stainless steel product. *Materials* **2020**, *13*, 5795. [CrossRef]
126. Richter, A.; Gehling, T.; Treutler, K.; Wesling, V.; Rembe, C. Real-time measurement of temperature and volume of the weld pool in wire-arc additive manufacturing. *Meas. Sens.* **2021**, *17*, 100060. [CrossRef]
127. Kurz, W.; Fisher, D.; Rappaz, M. Fundamentals of Solidification. 2023. Available online: https://www.torrossa.com/it/resources/an/5482726 (accessed on 17 December 2025).
128. Jegede, O.E.; Haque, N.; Mullis, A.M.; Cochrane, R.F. Relationship between cooling rate and SDAS in liquid phase separated metastable Cu–Co alloys. *J. Alloys Compd.* **2021**, *883*, 160823. [CrossRef]
129. Peng, X.; Kong, L.; An, H.; Dong, G. A review of in situ defect detection and monitoring technologies in selective laser melting. *3D Print. Addit. Manuf.* **2023**, *10*, 438–466. [CrossRef] [PubMed]
130. Ramirez-Vidaurri, L.E.; Castro-Román, M.; Herrera-Trejo, M.; Fraga-Chavez, K.-L. Secondary dendritic arm spacing and cooling rate relationship for an ASTM F75 alloy. *J. Mater. Res. Technol.* **2022**, *19*, 5049–5065. [CrossRef]
131. Reinhart, G.; Nguyen-Thi, H.; Gastaldi, J.; Billia, B.; Mangelinck-Noël, N.; Schenk, T.; Härtwig, J.; Baruchel, J. In situ and real time investigation of directional solidification of Al-Ni alloys by synchrotron imaging. *Mater. Sci. Forum* **2006**, *508*, 75–80. [CrossRef]
132. Petro, P.; Shi, X.; Wang, J.; Li, Z.; Yin, B.; Zhou, H.; Zhou, Y.; Yu, B.; Wang, Z. Enhancing Wire Arc Additive Manufacturing for Maritime Applications: Overcoming Operational Challenges in Marine and Offshore Environments. *Appl. Sci.* **2025**, *15*, 9070. [CrossRef]
133. Hackett, J.K.; Shah, M. Multi-sensor fusion: A perspective. In Proceedings of the IEEE International Conference on Robotics and Automation, Cincinnati, OH, USA, 13–18 May 1990; IEEE: New York, NY, USA, 1990.
134. Abdulhafiz, W.A.; Khamis, A. Bayesian approach to multisensor data fusion with Pre-and Post-Filtering. In Proceedings of the 2013 10th IEEE International Conference on Networking, Sensing and Control (ICNSC), Evry, France, 10–12 April 2013; IEEE: New York, NY, USA, 2013.
135. Luo, R.; Su, K. A review of high-level multisensor fusion: Approaches and applications. In Proceedings of the 1999 IEEE/SICE/RSJ International Conference on Multisensor Fusion and Integration for Intelligent Systems, MFI'99, Taipei, Taiwan, 18 August 1999; IEEE: New York, NY, USA, 1999.
136. Kong, L.; Peng, X.; Chen, Y.; Wang, P.; Xu, M. Multi-sensor measurement and data fusion technology for manufacturing process monitoring: A literature review. *Int. J. Extrem. Manuf.* **2020**, *2*, 022001. [CrossRef]
137. Yan, L.; Cui, M.; Prasad, S. Joint Euclidean and angular distance-based embeddings for multisource image analysis. *IEEE Geosci. Remote Sens. Lett.* **2018**, *15*, 1110–1114. [CrossRef]
138. Xing, Z.; Xia, Y.; Yan, L.; Lu, K.; Gong, Q. Multisensor distributed weighted Kalman filter fusion with network delays, stochastic uncertainties, autocorrelated, and cross-correlated noises. *IEEE Trans. Syst. Man Cybern. Syst.* **2016**, *48*, 716–726. [CrossRef]
139. Williams, S.W.; Martina, F.; Addison, A.C.; Ding, J.; Pardal, G.; Colegrove, P. Wire+ arc additive manufacturing. *Mater. Sci. Technol.* **2016**, *32*, 641–647. [CrossRef]
140. Ding, D.; Pan, Z.; Cuiuri, D.; Li, H. Wire-feed additive manufacturing of metal components: Technologies, developments and future interests. *Int. J. Adv. Manuf. Technol.* **2015**, *81*, 465–481. [CrossRef]
141. Ramalho, A.; Neto, A.A.; Bevans, B.; Deschamps, F.; Santos, T.G.; Oliveira, J.P.; Rao, P. Understanding and detection of process instabilities in wire arc directed energy deposition additive manufacturing using meltpool imaging and machine learning. *Mater. Des.* **2025**, *258*, 114598. [CrossRef]
142. Yang, J.; Wang, A. Microstructure evolution and performance of AA2024 alloy through wire-arc additive manufacturing under different heat inputs. *Metals* **2024**, *14*, 1265. [CrossRef]

143. Plotkowski, A.; Saleeby, K.; Fancher, C.M.; Haley, J.; Madireddy, G.; An, K.; Kannan, R.; Feldhausen, T.; Lee, Y.; Yu, D.; et al. Operando neutron diffraction reveals mechanisms for controlled strain evolution in 3D printing. *Nat. Commun.* **2023**, *14*, 4950. [CrossRef] [PubMed]
144. Xiang, R.; Huang, J.; Yu, X.; Zhao, H.; Song, X.; Fan, D. The effect of Ni/Ti atomic ratios on residual stress and deformation in WAAM of dissimilar filler wire NiTi alloys. *J. Mater. Res. Technol.* **2025**, *35*, 1813–1828. [CrossRef]
145. Boruah, D.; Dewagtere, N.; Ahmad, B.; Nunes, R.; Tacq, J.; Zhang, X.; Guo, H.; Verlinde, W.; De Waele, W. Digital image correlation for measuring full-field residual stresses in wire and arc additive manufactured components. *Materials* **2023**, *16*, 1702. [CrossRef] [PubMed]
146. Hölscher, L.V.; Hassel, T.; Maier, H.J. Development and evaluation of a closed-loop z-axis control strategy for wire-and-arc-additive manufacturing using the process signal. *Int. J. Adv. Manuf. Technol.* **2023**, *128*, 1725–1739. [CrossRef]
147. Albannai, A.I. A brief review on the common defects in wire arc additive manufacturing. *Int. J. Curr. Sci. Res. Rev.* **2022**, *5*, 4556–4576. [CrossRef]
148. Rodrigues, T.A.; Duarte, V.; Miranda, R.M.; Santos, T.G.; Oliveira, J.P. Current status and perspectives on wire and arc additive manufacturing (WAAM). *Materials* **2019**, *12*, 1121. [CrossRef]
149. Tammas-Williams, S.; Withers, P.J.; Todd, I.; Prangnell, P.B. The influence of porosity on fatigue crack initiation in additively manufactured titanium components. *Sci. Rep.* **2017**, *7*, 7308. [CrossRef]
150. Bitharas, I.; McPherson, N.A.; McGhie, W.; Roy, D.; Moore, A.J. Visualisation and optimisation of shielding gas coverage during gas metal arc welding. *J. Mater. Process. Technol.* **2018**, *255*, 451–462. [CrossRef]
151. Adebayo, A.; Mehnen, J.; Tonnellier, X. Limiting travel speed in additive layer manufacturing. In Proceedings of the 9th International Conference on Trends in Welding Research, Chicago, IL, USA, 4–8 June 2012.
152. Gu, Y.; Hua, X.; Ye, D.; Li, F.; Ma, X.; Xu, C. Numerical simulation of hump suppression in high-speed triple-wire GMAW. *Int. J. Adv. Manuf. Technol.* **2017**, *89*, 727–734. [CrossRef]
153. Wu, D.; Hua, X.; Ye, D.; Li, F. Understanding of humping formation and suppression mechanisms using the numerical simulation. *Int. J. Heat Mass Transf.* **2017**, *104*, 634–643. [CrossRef]
154. Dai, H.; Zhao, H.; Xia, Y.; Cai, X.; Dong, B.; Lin, S.; Zhao, Y. Wire arc additive manufacturing of ZL205A: Heat input effect on the forming quality, pore defects and mechanical properties. *J. Alloys Compd.* **2024**, *1005*, 175777. [CrossRef]
155. Seow, C.E.; Zhang, J.; Coules, H.E.; Wu, G.; Jones, C.; Ding, J.; Williams, S. Effect of crack-like defects on the fracture behaviour of Wire+ Arc Additively Manufactured nickel-base Alloy 718. *Addit. Manuf.* **2020**, *36*, 101578. [CrossRef]
156. Wen, W.; Qi, H.; Liao, Z.; Jiang, L.; Huang, M.; Yang, B.; Wu, Z.; Zhou, S. In-situ study of crack propagation mechanisms in wire arc additive manufactured Al-Mg alloys: Multiple strategies involving microdefects and microstructures. *Mater. Sci. Eng. A* **2025**, *924*, 147802. [CrossRef]
157. Wang, Z.; Lin, X.; Wang, L.; Cao, Y.; Zhou, Y.; Huang, W. Microstructure evolution and mechanical properties of the wire+ arc additive manufacturing Al-Cu alloy. *Addit. Manuf.* **2021**, *47*, 102298. [CrossRef]
158. Wu, Q.; Mukherjee, T.; De, A.; DebRoy, T. Residual stresses in wire-arc additive manufacturing–Hierarchy of influential variables. *Addit. Manuf.* **2020**, *35*, 101355. [CrossRef]
159. Wu, Q.; Mukherjee, T.; Liu, C.; Lu, J.; DebRoy, T. Residual stresses and distortion in the patterned printing of titanium and nickel alloys. *Addit. Manuf.* **2019**, *29*, 100808. [CrossRef]
160. Mukherjee, T.; Zhang, W.; DebRoy, T. An improved prediction of residual stresses and distortion in additive manufacturing. *Comput. Mater. Sci.* **2017**, *126*, 360–372. [CrossRef]
161. Mukherjee, T.; Zuback, J.; Zhang, W.; DebRoy, T. Residual stresses and distortion in additively manufactured compositionally graded and dissimilar joints. *Comput. Mater. Sci.* **2018**, *143*, 325–337. [CrossRef]
162. Bartlett, J.L.; Croom, B.P.; Burdick, J.; Henkel, D.; Li, X. Revealing mechanisms of residual stress development in additive manufacturing via digital image correlation. *Addit. Manuf.* **2018**, *22*, 1–12. [CrossRef]
163. Nasajpour-Esfahani, N.; Karimi, S.; Nasseri, S.; Borna, H.; Boostani, A.F.; Gao, R.; Huang, W.; Garmestani, H.; Liang, S.Y. Advancements and applications of digital image correlation to characterize residual stress: A review. *Mater. Charact.* **2025**, *228*, 115416. [CrossRef]
164. He, B.; Bi, C.; Li, X.; Wang, W.; Yang, G. Residual stresses and deformations of laser additive manufactured metal parts: A review. *Int. J. Mater. Form.* **2023**, *16*, 7. [CrossRef]
165. Laurence, R.C.; Canelo-Yubero, D.; Maawad, E.; Faria, G.A.; Staron, P.; Schell, N.; Ramadhan, R.S.; Cabeza, S.; Paecklar, A.; Pirling, T.; et al. Determination of Residual Stress in Additively Manufactured 316L Stainless Steel Benchmark Parts Through Synchrotron X-Ray Diffraction and Neutron Diffraction. *Strain* **2025**, *61*, e70005. [CrossRef]
166. Rahimi, A.; Coduri, M.; Fitch, A.; Vedani, M.; Schröder, J.; Bruno, G.; Casati, R. Synchrotron investigation of heat treatment effects on the 3D residual stress distribution in laser powder bed fused AlSi7Mg alloys. *Mater. Lett.* **2025**, *396*, 138742. [CrossRef]
167. Cambon, C.; Bendaoud, I.; Rouquette, S.; Soulié, F. A WAAM benchmark: From process parameters to thermal effects on weld pool shape, microstructure and residual stresses. *Mater. Today Commun.* **2022**, *33*, 104235. [CrossRef]

168. Nunes, R.; Vandermeiren, N.; Verlinde, W.; Boruah, D.; Motte, R.; De Waele, W. A benchmark of mechanical properties and operational parameters of different steel filler metals for wire arc additive manufacturing. *Int. J. Adv. Manuf. Technol.* **2023**, *127*, 599–613. [CrossRef]
169. Chen, X.; Kong, F.; Fu, Y.; Zhao, X.; Li, R.; Wang, G.; Zhang, H. A review on wire-arc additive manufacturing: Typical defects, detection approaches, and multisensor data fusion-based model. *Int. J. Adv. Manuf. Technol.* **2021**, *117*, 707–727. [CrossRef]
170. Kawalkar, R.; Dubey, H.K.; Lokhande, S.P. A review for advancements in standardization for additive manufacturing. *Mater. Today Proc.* **2022**, *50*, 1983–1990. [CrossRef]
171. Martínez-García, A.; Monzón, M.; Paz, R. Standards for additive manufacturing technologies: Structure and impact. In *Additive Manufacturing*; Elsevier: Amsterdam, The Netherlands, 2021; pp. 395–408.
172. Kopitzke, S.; Geissinger, P. An optical fiber-based sensor array for the monitoring of zinc and copper ions in aqueous environments. *Sensors* **2014**, *14*, 3077–3094. [CrossRef]
173. Tulsyan, A.; Garvin, C.; Undey, C. Condition-based sensor-health monitoring and maintenance in biomanufacturing. *IFAC-PapersOnLine* **2020**, *53*, 170–175. [CrossRef]
174. Mattera, G.; Polden, J.; Norrish, J. Monitoring the gas metal arc additive manufacturing process using unsupervised machine learning. *Weld. World* **2024**, *68*, 2853–2867. [CrossRef]
175. Feng, S.; Wainwright, J.; Wang, C.; Wang, J.; Pardal, G.R.; Qin, J.; Yin, Y.; Lasisi, S.; Ding, J.; Williams, S. Video Segmentation of Wire+ Arc Additive Manufacturing (WAAM) Using Visual Large Model. *Sensors* **2025**, *25*, 4346. [CrossRef] [PubMed]
176. Ukwaththa, J.; Herath, S.; Meddage, D. A review of machine learning (ML) and explainable artificial intelligence (XAI) methods in additive manufacturing (3D Printing). *Mater. Today Commun.* **2024**, *41*, 110294. [CrossRef]
177. Wei, H.; Mukherjee, T.; Zhang, W.; Zuback, J.; Knapp, G.; De, A.; DebRoy, T. Mechanistic models for additive manufacturing of metallic components. *Prog. Mater. Sci.* **2021**, *116*, 100703. [CrossRef]
178. Sanvelly, R.R.; Arjomandi, M.; Mukherjee, T. Controlling molten pool instability-induced humping in wire arc deposition using mechanistic augmented learning. *Manuf. Lett.* 2026; *unpublished*..
179. Xing, C.; Jia, C.; Han, Y.; Dong, S.; Yang, J.; Wu, C. Numerical analysis of the metal transfer and welding arc behaviors in underwater flux-cored arc welding. *Int. J. Heat Mass Transf.* **2020**, *153*, 119570. [CrossRef]
180. Degen, C.L.; Reinhard, F.; Cappellaro, P. Quantum sensing. *Rev. Mod. Phys.* **2017**, *89*, 035002. [CrossRef]
181. Bonavolontà, C.; Vettoliere, A.; Sorrentino, P.; Granata, C. Superconducting Quantum Magnetometers for Brain Investigations. *Sensors* **2025**, *25*, 4625. [CrossRef]
182. Wicht, A.; Bawamia, A.; Krüger, M.; Kürbis, C.; Schiemangk, M.; Smol, R.; Peters, A.; Tränkle, G. Narrow linewidth diode laser modules for quantum optical sensor applications in the field and in space. In *Components and Packaging for Laser Systems III*; SPIE: Cergy-Pontoise, France, 2017.
183. Chen, J.; Luo, Y.; Luo, J.; Huang, H.; Cheng, H.; Liu, G.-S.; Chen, L.; Chen, Z.; Chen, Y. Magnetic-field-assisted optical fiber quantum temperature sensor with enhanced sensitivity. *Opt. Lett.* **2024**, *49*, 1421–1424. [CrossRef]
184. Bao, B.; Hua, Y.; Wang, R.; Li, D. Quantum-Based Magnetic Field Sensors for Biosensing. *Adv. Quantum Technol.* **2023**, *6*, 2200146. [CrossRef]
185. Coutinho, F.; Lizarralde, N.; Mendes, M.; Bostrom, R.; Silva, T.; Couto, M.; Lizarralde, F. iWAAM: An automated system for monitoring and control of wire-arc additive manufacturing. *IFAC-PapersOnLine* **2023**, *56*, 6576–6581. [CrossRef]
186. Reisch, R.T.; Janisch, L.; Tresselt, J.; Kamps, T.; Knoll, A. Prescriptive analytics-a smart manufacturing system for first-time-right printing in wire arc additive manufacturing using a digital twin. *Procedia CIRP* **2023**, *118*, 759–764. [CrossRef]
187. Ahmmed, M.S.; Khan, L.; Mahmood, M.A.; Liou, F. Digital Twins, AI, and cybersecurity in additive manufacturing: A comprehensive review of current trends and challenges. *Machines* **2025**, *13*, 691. [CrossRef]
188. Alvares, A.J.; Rodriguez, E.; Figueroa, B. Digital-Twin-Enabled Process Monitoring for a Robotic Additive Manufacturing Cell Using Wire-Based Laser Metal Deposition. *Processes* **2025**, *13*, 2335. [CrossRef]
189. Azarian, M.; Yu, H.; Solvang, W.D. Integrating additive manufacturing into a virtual Industry 4.0 factory. In *International Workshop of Advanced Manufacturing and Automation*; Springer: Singapore, 2020.
190. Tamir, T.S.; Xiong, G.; Shen, Z.; Leng, J.; Fang, Q.; Yang, Y.; Jiang, J.; Lodhi, E.; Wang, F.-Y. 3D printing in materials manufacturing industry: A realm of Industry 4.0. *Heliyon* **2023**, *9*, e19689. [CrossRef]
191. Wankhede, V.A.; Vinodh, S. Analysis of challenges of wire-arc additive manufacturing process in the context of Industry 4.0 using graph theory approach. *Int. J. Adv. Manuf. Technol.* **2022**, *123*, 1059–1078. [CrossRef]
192. Mattera, G.; Yap, E.W.; Polden, J.; Brown, E.; Nele, L.; Van Duin, S. Utilising unsupervised machine learning and IoT for cost-effective anomaly detection in multi-layer wire arc additive manufacturing. *Int. J. Adv. Manuf. Technol.* **2024**, *135*, 2957–2974. [CrossRef]
193. Fernández-Zabalza, A.; Rodríguez-Díaz, Á.; Veiga, F.; Suárez, A.; Uralde, V.; Ballesteros, T.; Alfaro, J.R. AI-driven predictive modeling of homogeneous bead geometry for WAAM processes. *Int. J. Adv. Manuf. Technol.* **2025**, 1–12. [CrossRef]

194. Kumar, A.; Rajeshwari, P. The Role of Additive Manufacturing in the Era of Industry 5.0. *Assoc. J. Interdiscip. Tech. Eng. Mech.* **2024**, *2*, 17–24.
195. Ghimire, T.; Joshi, A.; Sen, S.; Kapruan, C.; Chadha, U.; Selvaraj, S.K. Blockchain in additive manufacturing processes: Recent trends & its future possibilities. *Mater. Today Proc.* **2022**, *50*, 2170–2180.

Disclaimer/Publisher's Note: The statements, opinions and data contained in all publications are solely those of the individual author(s) and contributor(s) and not of MDPI and/or the editor(s). MDPI and/or the editor(s) disclaim responsibility for any injury to people or property resulting from any ideas, methods, instructions or products referred to in the content.